NOTE TO USERS

Université d'Ottawa · University of Ottawa

Université d'Ottawa · University of Ottawa

FACULTÉ DES ÉTUDES SUPÉRIEURES ET POSTDOCTORALES

FACULTY OF GRADUATE AND POSTDOCTORAL STUDIES

Frédéric ARPIN

AUTEUR DE LA THÈSE - AUTHOR OF THESIS

M. A. Sc. (Electrical Engineering)

GRADE - DEGREE

School of Information Technology and Engineering

FACULTÉ, ÉCOLE, DÉPARTEMENT - FACULTY, SCHOOL, DEPARTMENT

TITRE DE LA THÈSE - TITLE OF THE THESIS

Multi-Feed Spatial Power Combining Reflectarrays

D. McNamara

DIRECTEUR DE LA THÈSE - THESIS SUPERVISOR

CO-DIRECTEUR DE LA THÈSE - THESIS CO-SUPERVISOR

EXAMINATEURS DE LA THÈSE - THESIS EXAMINERS

E. Gad

A. Petosa

J.-M. De Koninck, Ph.D.

LE DOYEN DE LA FACULTÉ DES ÉTUDES SUPÉRIEURES ET POSTDOCTORALES

DEAN OF THE FACULTY OF GRADUATE AND POSTDOCTORAL STUDIES

Multi-Feed Spatial Power Combining Reflectarrays

by

Frédéric N. Arpin, B. A. Sc.

A thesis submitted to the
Faculty of Graduate and Postdoctoral Studies
in partial fulfillment of the requirements for the degree of

Master of Applied Science
in Electrical Engineering

Ottawa-Carleton Institute for Electrical and Computer Engineering
School of Information Technology and Engineering
Faculty of Engineering
University of Ottawa

November 13, 2004

Your file Votre référence
ISBN: 0-494-01401-6
Our file Notre référence
ISBN: 0-494-01401-6

Abstract

In order to have increased bandwidth, future wireless communications systems will use millimeter-wave frequencies. Such systems will require antennas with relatively high gain and sources with sufficient power. Reflectarrays using printed circuit technology represent an attractive option for such antennas, because they are low-cost, high-gain, low-profile antennas. However, at millimeter-wave frequencies solid-state devices have limited power-handling capabilities and traditional multi-stage circuit-power combiners are inefficient. Spatial power combining provides an attractive alternative to these issues. This thesis develops a means of combining the antenna and spatial power-combining functions in a single device. We formulate a design procedure that allows multiple feeds to illuminate a reflectarray that will give a single-beam. The reflectarray acts both as a spatial-power combiner and as the antenna. Unlike previous work that has been done on spatial power-combining reflectarrays, the proposed design does not involve the integration of any active devices. The new design procedure for a multi-feed spatial power-combining reflectarray was first applied to a two-feed reflectarray which was fabricated and tested as a proof of concept. This design showed that the reflectarray combined the power of the two feeds into a single-beam. Finally the design procedure was then applied to a four-feed reflectarray, which was fabricated and whose performance was analyzed. The four-feed reflectarray was found to have a combining efficiency of 87.3%; existing configurations of spatial power combiners have combining efficiencies ranging from 70-90%. The aperture efficiency was 36.82% at 30Ghz, which is consistent with existing reflectarray antennas having aperture efficiencies ranging from 25-50%.

Publications

F. Arpin, D.A. McNamara, J. Shaker & A. Ittipiboon, "A Receive-Mode Analysis of Reflectarray Antennas", Proceedings of the ANTEM Symposium, Ottawa, Canada, July 2004

F. Arpin, J. Shaker & D.A. McNamara, "Multi-Feed Single-Beam Power-Combining Reflectarray Antenna", Electronics Letters, Volume 40, Number 17, August 2004, pp. 1035-1037

F. Arpin, D.A. McNamara & P. Cowles, "Scanning of an Offset Dual-Reflector Antenna Pattern Through Sub-Reflector Movement: Translation Versus Rotation", To Appear in Microwave & Optical Technology Letters, February 2005.

Acknowledgements

The author wishes to acknowledge many different individuals that contributed to this work. First I would like to thank my thesis supervisor, Dr. Derek McNamara, whose guidance and insight was invaluable throughout the last two years.

I would also like to thank the entire antenna research group at the Communication Research Center (CRC). Specifically Dr. Jafar Shaker for proposing the idea of this reflectarray configuration for spatial power combining and his guidance on this subject. I would like to thank David Lee and John Bradley for their help with the hardware and measurement setup relating to this work. Thank you to Dr. Apisak Ittipiboon, Dr. Reza Charharmir and Dr. Aldo Petosa for always being available to help with technical problems, their expertise was greatly appreciated. I am indebted to Michel Cuhaci, the Research Project Manager at the CRC, for contributing financially for the hardware and test facilities used for this work.

Finally, I would like to acknowledge support of my fiancé, Marie-Josée, my parents and my entire family who's love, understanding and encouragement provided the necessary motivation to complete this work.

Contents

Chapter 1

INTRODUCTION

1.1 Introductory Remarks

The reflectarray, often called a flat reflector,works much like a traditional reflector antenna. The traditional reflector works by making use of its geometry to, in the transmit mode, convert the wave transmitted by a feed with a spherical phase front into a wave with a planar phase front at the reflector aperture. From the receive-mode viewpoint the reflector works in the opposite manner. It converts a wave that is incident, with a planar phase front, into a wave with a spherical phase front, and hence focuses the energy to the geometrical focal point of the reflector. This concept is demonstrated schematically in Figure 1.1. The reflectarray works in

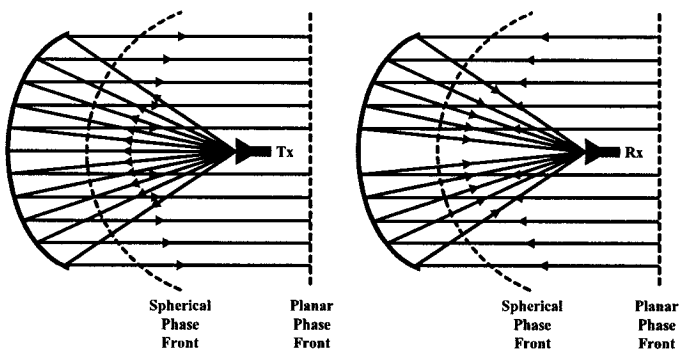

Figure 1.1: Traditional Reflector Geometry

much the same way. The reflectarray is made up of an array of elements, each of the elements designed in such a way as to correct the phase of the incident wave,

be it in transmit-mode or in the receive-mode, as is done in the traditional reflector. The concept of reflectarray antennas dates back to 1963 [1], where the elements of the reflectarray were made up of different lengths of terminated rectangular waveguides. By changing the lengths at which point the waveguides were terminated it was possible to control the phase of the reflected wave, and by proper design, the phase transformation would replicate the operation of a traditional reflector. This type of reflectarray was very bulky and the technology was apparently not pursued. However, with the rapid development of microstrip technology in the early 80's, and the need for high gain, low cost antennas, the microstrip reflectarray was conceived [2]. The microstrip reflectarray is made up of an array of microstrip patches on a grounded dielectric substrate, each element of the reflectarray being designed in such a way as to provide the proper phase correction upon reflection to achieve the same wave transformation as in traditional reflectors. Throughout this work when we make reference to reflectarrays we will assume that we are refereing to microstrip reflectarrays.

1.2 Thesis Overview

Future wireless communications (terrestrial or satellite) will likely provide increased bandwidth. This can be achieved by operating at millimeter-wave frequencies (in order to achieve the increased bandwidth) and ensuring sufficient signal-to-noise ratio at the receiver. The reason we have increased bandwidth as we go to higher millimeter-wave frequencies is that as we go higher in frequency the bandwidth achieved increases for the same fractional bandwidth. For example a fractional bandwidth of 5% at 10GHz represents a bandwidth of 500MHz, while the same fractional bandwidth at 1GHz translates to a bandwidth of only 50MHz. This can be seen in Figure 1.2. To ensure sufficient signal-to-noise ratio at the receiver one

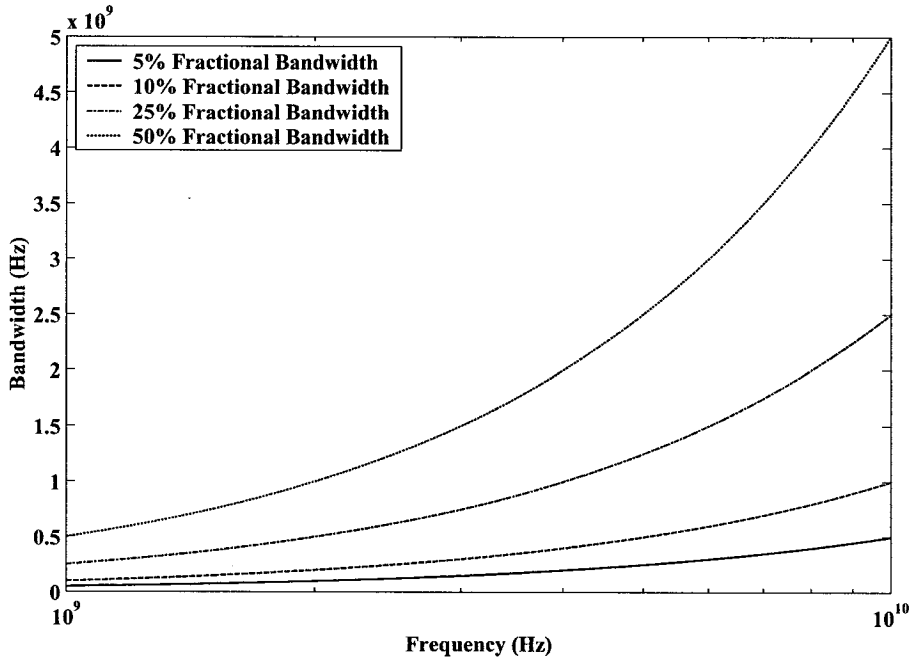

Figure 1.2: Bandwidth versus Frequency

requires antennas of sufficiently high gain and transmitters with sufficient power. At the same time, for such commercial applications, the cost of the antenna and the source of RF power need to be reasonably inexpensive, lest they adversely affect the total cost of the complete terminal. Reflectarray antennas offer a viable alternative to conventional reflectors in such instances since they can exploit printed technology and yet do not suffer from the same feed network losses observed in conventional microstrip antenna arrays. Furthermore, solid state sources are a must because of their smaller size, lower weight, increased reliability and lower cost of production, when compared to vacuum devices. However, the output power of solid state devices at millimeter-wave frequencies is limited, and some sort of combining of the output from several such devices is necessary. Power combining using circuit-type power combiners reaches a point of diminishing returns at millimeter-wave frequencies since the combiner losses become excessive and hence the combining efficiency is low. Spatial power combining has been under development as an alternative, and

can indeed be a very efficient method at millimeter-wave frequencies. Unfortunately this can add significant cost to a commercial terminal. One way around this dilemma would be the use of the reflectarray antenna itself, illuminated by several feeds (each with its own solid state source, and all sources operated coherently), to achieve the power combining action. This possibility is investigated in the present thesis.

Chapter 2 provides a brief overview of existing spatial power combining methods. It also gives a fairly complete summary of all the various reflectarray configurations that have been described in the literature, in so doing also providing a useful bibliography of work on reflectarrays. A procedure for designing existing forms of the reflectarray is also explained in this chapter. This procedure will also be used in later chapters (with the necessary added generalizations) to design the new types of reflectarray developed in this thesis.

This thesis will consider reflectarray antennas which have several feeds but a single main lobe (this is the power combining action), and the design procedure for such cases is considered in detail in Chapter 4. It was expected that new ways of interpreting the operation of reflectarrays would be needed during the research on such unconventional multi-feed single-beam types. Therefore, as preparation for the work in Chapters 4, electromagnetic modeling of reflectarray operation in the receive mode, which does not appear to have been done before, forms the subject of Chapter 3. This provides increased understanding of the reflectarray operation. Chapter 3 considers the receive mode operation of a conventional single-feed single-beam reflectarray (designed using the procedure from Section 2.5) and experimental validation is given. Although not the major contribution of this thesis such results are not available elsewhere. Use of the receive mode analysis for the multi-feed case is used in Chapter 4 as a means of validating the generalization of the design procedure to

the multi-feed case developed in that chapter.

The principal contributions of this thesis are described in Chapter 4. The mathematical analysis that allows the design procedure of Chapter 2 to be applied to multi-feed single-beam reflectarray antennas is first described. A complete description of the implementation of the procedure to the two-feed case is then described and experimentally validated. This is immediately followed by a description of the design, implementation, predicted performance, and measured performance of a four-feed single-beam reflectarray antenna/power combiner.

Finally, some general conclusions are reached in Chapter 5, and the research reported herein put into perspective.

Chapter 2

A REVIEW OF REFLECTARRAYS AND SPATIAL POWER COMBINING

2.1 Preliminaries

In this chapter we will first look at existing spatial power combining methods, which is presented in Section 2.2. In Section 2.3 a thorough review of all the reflectarray configurations will be given. Section 2.4 will deal with work that has been done on reflectarrays which perform spatial power combining (albeit in a manner different to that developed in this thesis). Finally in Section 2.5 we will look at a general design procedure for a single-feed, single-beam, reflectarray with rectangular patches of varying size.

2.2 Review of Spatial Power Combining Methodologies

As the demand for high frequency, high power antennas increases, there is an increasing need for semiconductor solid-state devices that operate in these millimeter-wave regions. At these high frequencies such solid-state semiconductor devices have limited

power-handling capacities. Figure 2.1 shows the power-handling capacities of several devices that operate in the millimeter-wave region. In Figure 2.1 the shaded area

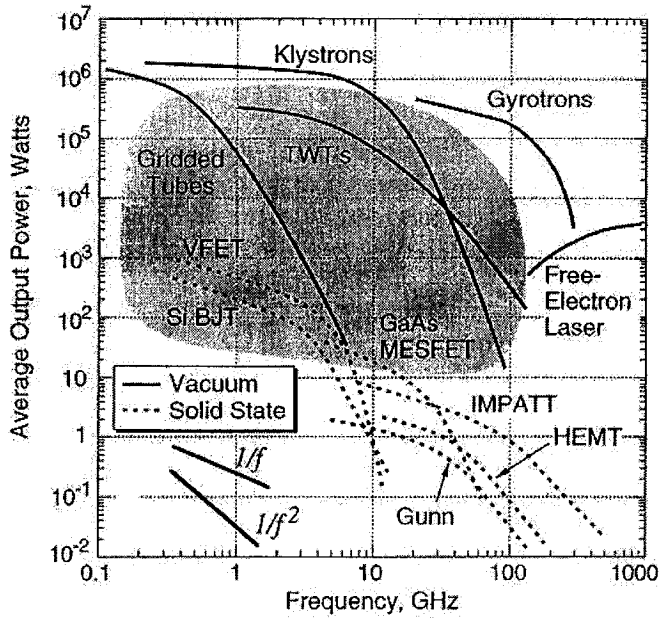

Figure 2.1: Power-Handling Capacities of Millimeter-Wave Devices (After [3])

corresponds to the current and future applications requirements for commercial and military systems [3]. We can also see that vacuum devices would be the most likely choice for application in this frequency range. However, solid-state devices are preferred for their size, weight, reliability and the lower cost of production. We can therefore see the problem of having a single high powered device at millimeter-wave frequencies. An alternative to using a single high powered device is to use several devices and a power-combining circuit. To date, this type of circuit based power combining has been the easiest and the most popular way of combining the power from several devices. In Figure 2.2 we see a schematic diagram of a corporate power combiner which is commonly used in planar circuits and in feeds for arrays. Ideally this type of corporate power combining could be used to combine any number of sources to achieve the desired power capabilities at millimeter-wave frequencies. However, there is a problem with this type of combining circuit, namely that there

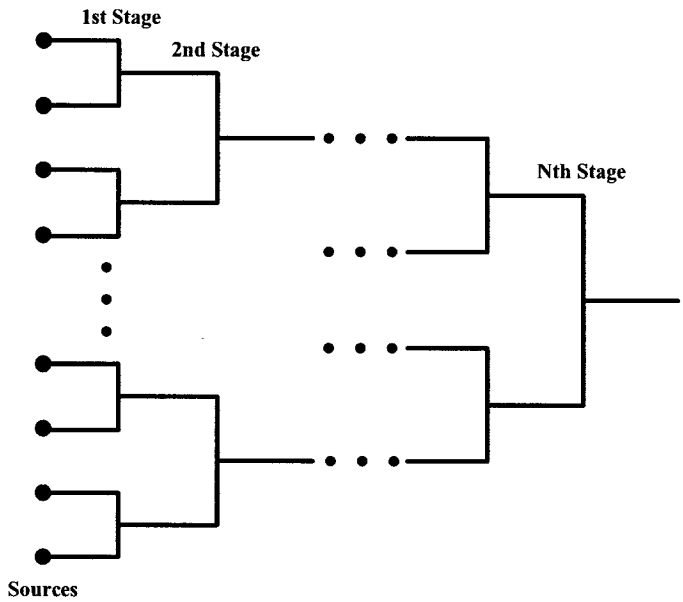

Figure 2.2: Corporate Power Combiner

are losses present in the transmission lines that make up the combining circuit itself. After adding a certain number of sources one reaches the point of diminishing returns; in other words the increase in power that you get by adding a device at a certain point is less than the losses of the additional transmission lines required to do so. Figure 2.3 demonstrates this point graphically. Spatial or quasi-optical power combining is a viable alternative to circuit based power combiners. These spatial power combining techniques have been explored for some time [3–6]. The interest in spatial power combining is based on the fact that the losses in free-space are much lower than in planar circuits or waveguide. Figure 2.4 shows a comparison between the propagation losses of several transmission-line structures and the losses in free-space. We can clearly see from Figure 2.4 the advantages of combining power in free-space; the losses are significantly lower than any traditional transmission-line structure. Figure 2.5 shows three configurations for spatial power combining [4]. In these schemes the power from the feed horn is distributed spatially (due to spreading) to each of the smaller receive antennas of the quasi-optical (or spatial) amplifier. The

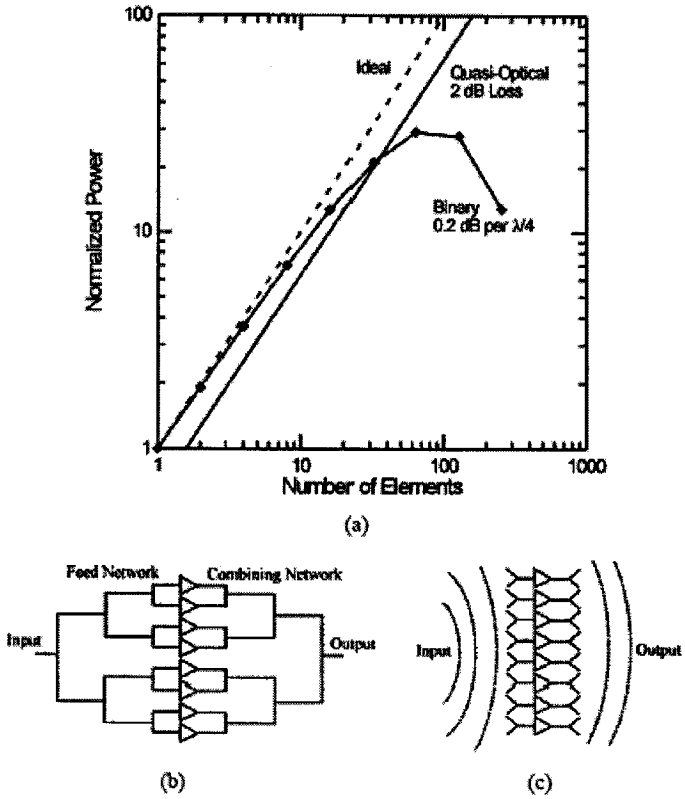

Figure 2.3: (a) Output power available from (b) corporate and (c) quasi-optical power combiners as a function of the number of sources (After [4])

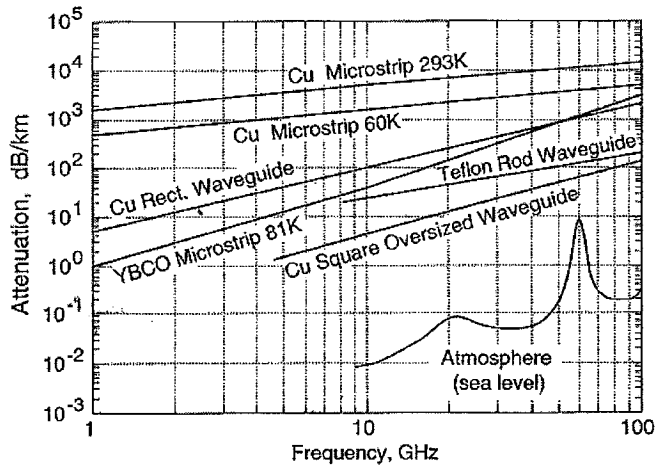

Figure 2.4: Propagation Losses versus Frequency for Various Media

received signal at each of the antenna elements of the array is amplified by its own amplifier circuit and then immediately re-radiated. The "re-radiating array" fields

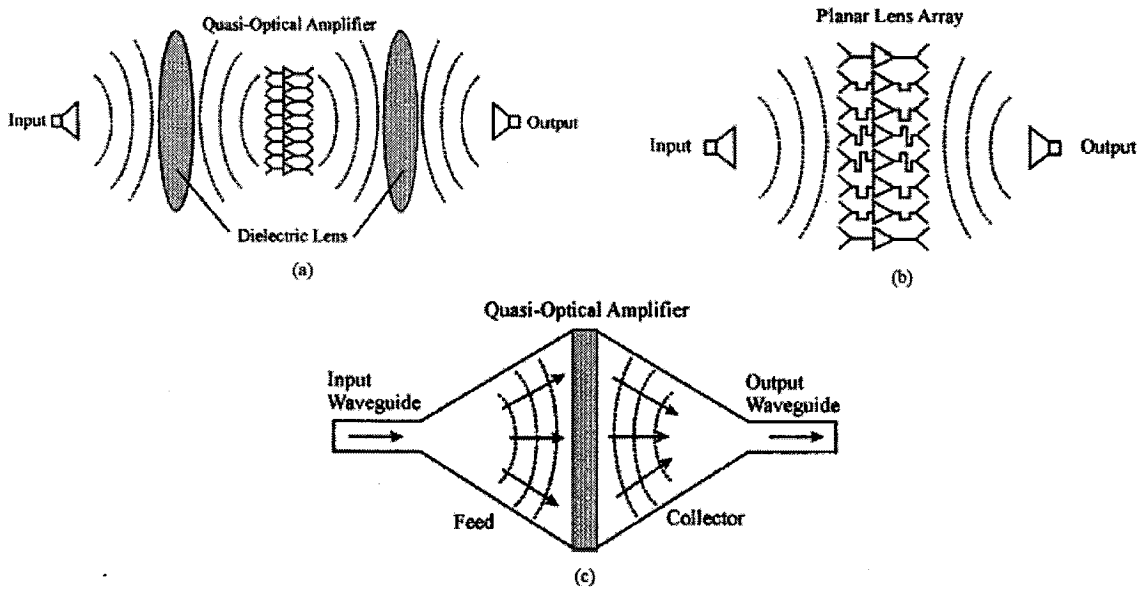

Figure 2.5: (a) Lens-focused quasi-optical system: The focusing will cause a nonuniform power distribution at the plane of the amplifier. (b) Planar lens amplifier: The amplifier works as a planar Rotman lens, with transmission-line delays providing the proper phase shift. (c) Quasi-optical amplifier in a waveguide fixture. (After [4])

are caused to converge on the collecting horn either by appropriate phasing of the re-radiating array elements (i.e. Figure 2.5(b)), or by using some other form of focusing device (i.e. Figure 2.5(a) and (c)).

2.3 Review of Reflectarray Antennas

2.3.1 Introductory Remarks

As is the case with antennas generally, there are many ways in which reflectarrays could be classified. We noted in Section 1.1 that reflectarrays consist of conducting patches printed on dielectric substrates that are backed by a conducting groundplane, the whole structure being illuminated by a primary radiator. Thus reflectarrays could be classified in terms of their configuration:

- *Conducting Patch Shape* - Different patch shapes may be used for specific

performance-related reasons.

- *Number of Substrate Layers* - There may be a single dielectric layer or several such layers (usually for bandwidth related reasons).

- *Feed Type* - Although the majority of reflectarrays reported in the literature use a horn antenna feed, other less conventional possibilities have been described (i.e. for reasons of compactness).

- *Feed Position* - As in the case of conventional reflector antennas, some reflectarrays use on-axis feeds while others use offset feeds.

However, reflectarrays could also be classified according to the radiation pattern requirements which they have been designed to satisfy:

- *Beam Shape* - While most reflectarrays discussed in the literature have been required to provide pencil beams, successful designs have been reported that yield shaped beams.

- *Polarisation* - In certain instances patch shapes have been selected so that the resulting reflectarray is capable of supporting dual polarisation.

- *Bandwidth of Operation* - The conducting patches required to provide the correct phase shift on reflection will usually only do so over a restricted frequency range. However, it has been shown by some authors that multiple band reflectarrays are possible.

In Section 2.3.2 that follows, we will group some of the more than one hundred references that were reviewed according to their configuration. In Section 2.3.3 we will group the reflectarray references according to the pattern performance characteristics described, those which provide details on analysis or synthesis techniques which have been applied to such antennas, those which contain parametric studies, and those

which have been designed as active antennas. We will also separately highlight work that has been done on issues not covered under the above-mentioned headings. Since the classifications overlap we will purposefully mention certain of the references more than once.

2.3.2 Review of Reflectarray Antennas According to Configuration

A. Conducting Patch Shape

Although the 1987 patent by Munson et al. [2] is often quoted as the first reference to reflectarrrays that use printed patches, it is clear from the references in the earlier 1977 paper by Montgommery [7] that others had already utilized the idea, albeit adopting the more complicated approach of integrating diodes with each circular patch to obtain the required phase shift. The use of rectangular patches all of the same size, with stubs of varying length providing the different reflection phase required of each patch, has been reported by Huang et al. [8, 9], and in [10]. In [8] each patch has a single stub, and is used for linear polarisation operation. In [9] the rectangular patches are rotated with respect to each other, and each has two stubs attached (one on each of two orthogonal sides) in order to allow circular polarisation operation. The use of rectangular patches without stubs, but whose size is varied to obtain the required phase distribution, is the subject of the work by Pozar et al. [11–14]. Spiral type patch elements are treated in [15] and reported to be less sensitive to etching errors than other types; but the elements are geometrically more complicated. Split ring elements are discussed in [16] for circular polarisation operation, the ring size being the variable used to adjust the reflection phase. The advantage of ring elements is that, at frequencies away from the designed center-frequency, the reflectarrays composed of such elements allow electromagnetic fields to pass through them. Thus they have been used in reflectarrays composed of

multilayers for multi-frequency operation [17, 18]. Hat-shaped patches (specifically for line-source-fed reflectarrrays) have been used by Shafai et al. [19]. A comparison of several patch shapes (in addition to those already mentioned above) has been given in [20, 21], where the authors compare the slope of the reflection phase versus adjustable parameter (eg. patch length in the case of rectangular patch elements). Crossed dipole elements are discussed in [22]; the reason for their use is that there was a requirement for the reflectarray elements to be interleaved with devices on a spacecraft solar panel. The bandwidth of these crossed dipole elements is less than that of rectangular patches. Finally, aperture-coupled patches were used in [23]. These consist of rectangular patches which couple through slots in the reflectarray groundplane to stubs in a lower plane. It is not clear that this added complexity offers any advantage over other reflectarray element shapes.

B. Number of Substrate Layers

Single-layer reflectarrays are obviously preferable to multi-layer ones from the point of view of fabrication complexity, and the majority of such antennas described in the literature have been single-layer. Multi-layer reflectarrays have principally been used (and quite successfully so) in attempts to increase antenna bandwidth. Two-layer reflectarrays were apparently described for the first time in 1995 by Huang et al. [24]. The most detailed studies of two-layer reflectarrays were performed by Encinar et al. [18, 25], who describes a two-layer antenna composed of variable size rectangular patches for dual frequency operation over two widely separated narrow bands. The antenna is able to support two orthogonal linear polarizations over these bands. Subsequent work by the same author [26] discusses a two-layer reflectarray design that achieves dual linear polarization over a single 16% bandwidth from a 16λ diameter antenna. In order to combat the decreasing bandwidth that results

with increasing reflectarray size, Encinar et al. [27] devised three-layer reflectarrays for dual polarization operation over single 10% bandwidths in spite of the fact that these are as large as $40\lambda \times 40\lambda$ in size. The increased degrees of freedom (albeit with a significant increase in fabrication complexity) offered by three-layer designs has allowed reflectarrays to be designed to provide contoured beams over the bandwidths required for satellite applications [28–30], although it is not certain if these have actually been used in practice yet. Two-layer reflectarrays composed of ring elements have been described in [31], also for increased bandwidth.

C. Feed Position

As with conventional reflector antennas, on-axis feeds cause aperture blockage and its resulting effects, such as a decrease in gain, and increased sidelobe level because of scattering off the feeding structure. It is similarly possible, with reflectarrays, to use offset feeds and design the reflectarray appropriately. References [32, 33] discuss reflectarrays composed of stub-loaded rectangular patches, illuminated by offset feeds. It appears that the aim in these references was to experimentally verify the possibility of such configurations. Reference [34] considers reflectarrays that have main beams in directions other than broadside, and shows that offset feeds are able to provide slightly higher aperture efficiencies than on-axis feeds in such instances. Reflectarrays designed to have such off-broadside main beams apparently exhibit beam squint, and [35] points out that offset feeds can be used to achieve a lower squint than on-axis feeds.

D. Feed Type

Most of the references on reflectarray design and realization use feeds that are either pyramidal or conical (eg. corrugated) horns. Of course one can use other types of feeds too (as is the case with conventional reflectors), and the use if such alternatives would not be considered to be novel. A completely different type of feed system for reflectarrays, devised to make the geometry more compact, is the so-called "folded" reflectarray [36–38]. While it is certainly novel, it also represents an increase in fabrication complexity that could be considered to negate the advantage of fabrication simplicity offered by reflectarrays.

2.3.3 Alternative Groupings of Reflectarray Antenna References

The devising of ways to obtain increased bandwidth is a topic pursued for virtually all antenna types. The reflectarray is no exception. References [39, 40] attempt to establish the bandwidth of conventional single-layer reflectarrays. Multiple-layer reflectarrays with wider bandwidths than single-layer ones are described in [18,24,27]. Reference [41] uses unequal spacing in order to achieve increased bandwidth.

The standard variable rectangular patch reflectarray is intended for linear polarisation. Circularly polarized reflectarrays are discussed in [42–45] and dual-polarisation cases in [46–48].

The customised electromagnetic modeling of reflectarray elements is the subject of references [14, 49–60].

Synthesis methods for reflectarrays with shaped or (more generally) contoured beams

are considered in [28–30, 60–67].

Useful parametric studies of reflectarray design (eg. the effect of element size) can be found in [68–70], as well as some of the papers listed above as containing the description of customized analysis methods.

The effect of altering the groundplane of a reflectarray forms the subject of references [71–76].

Reflectarrays which incorporate active elements, some of which are discussed in the next section, form the topic of discussion in [77–85].

Examination of reflectarrays in terms of their radar cross sections is discussed in [2,86,87]. Virtually all the reflectarrays (except the first [1]) that have been referenced utilize printed circuit technology for their fabrication. The other exceptions are the inflatable reflectarrays which might possibly be used in future space applications, and which have been discussed in [88–94]. The latter possibly represents more exposure in the literature than such antennas deserve.

2.4 Existing Methods of Integrating Reflectarrays and Spatial Power Combining

The use of reflectarrays in spatial power combining was first proposed by Zaman et. al. [95]. The proposed application of the reflectarray in this spatial power combining system is to eliminate the use of lenses in spatial amplifier arrays. Lenses are used in spatial amplifiers as a means of performing the phase correction to turn a wave with a spherical phase front into one with a planar phase front. In a typical spatial

power combining scheme, often called a beam waveguide system, a spatial amplifier is placed between two lenses and each lens is "fed" by a horn. This configuration can be seen in Figure 2.6. The author of [95] investigates the feasibility of using a

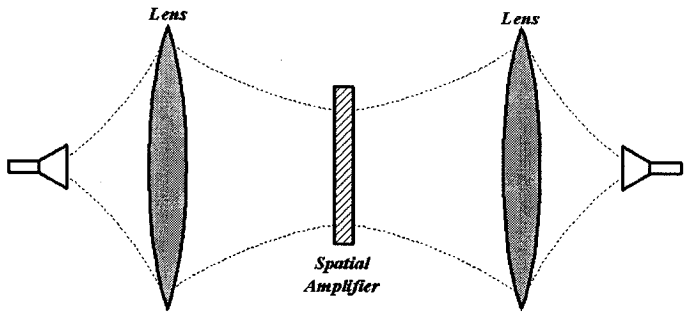

Figure 2.6: Spatial Amplifier Array -Beam Waveguide System

reflectarray to provide the necessary phase correction. To do this he uses a horn with an orthomode transducer as the feed of the reflectarray. The horn transmits a vertically polarized field. The elements of the reflectarray are stub loaded microstrip patches with a feedback loop, as shown in Figure 2.7. The reradiated field from this

Figure 2.7: Reflectarray Element Proposed in [95]

reflectarray would now be horizontally polarized with a planar phase front. The test setup utilized is shown in Figure 2.8. In this setup the output power would be lower

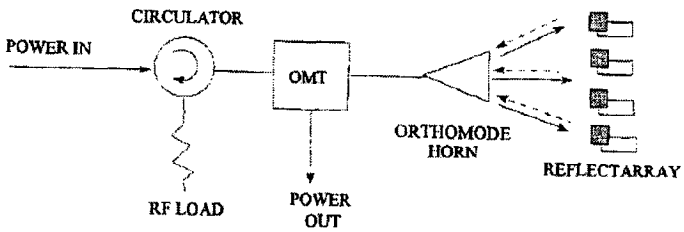

Figure 2.8: Conceptual Layout of a Horn/Planar Array Power Combining Arrangement (After [95])

then that of the input power but, the results of [95] showed that a reflectarray could be used for spatial power combining applications by integrating an active element in the feedback loop of the reflectarray element to amplify the signal.

All further advances in the use of reflectarrays for spatial power combining have involved the integration of active elements within the reflectarray elements [77–81, 83, 84, 96, 97]. The first proposed element [83] is shown in Figure 2.9. This is a

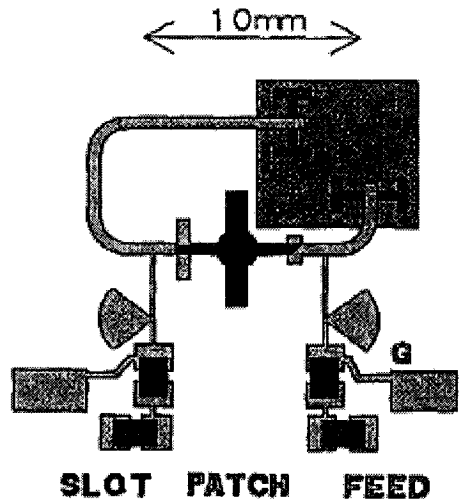

Figure 2.9: Single Reflection Amplifier Element (After [83])

multi-layer element which is made up of an aperture coupled microstrip patch as the radiator. On the trace layer there is a feedback loop; by varying its length one can control the phase of the reradiated field. Embedded in each element on the trace layer is a general purpose MESFET which, with its bias network, acts as an amplifier. This reflectarray element works much like that described by Zaman et. al. [95]. The element is meant to receive a vertically or horizontally polarized field, the energy is coupled into the feedback loop, in which it is amplified and then re-coupled to the radiating patch and the field is re-radiated in the orthogonal polarization. The feeding method of these reflectarrays has also been investigated. As described earlier in [95], an orthomode horn is used to both transmit and receive

in both linear polarizations (i.e. horizontal and vertical).

In [77, 81] the authors propose a microstrip patch element with a slot, in order to integrate the active elements within the footprint and on the same layer as the microstrip patch. This configuration would reduce the size necessary for each element of the reflectarray. The ability to place the elements of the reflectarray closer to one another will help in suppressing the higher order Floquet modes which are the cause of grating lobes.

It should be noted that none of the authors of the papers that deal with reflectarrays in spatial power combining configurations [77–81, 83, 84, 95–97] state the combining efficiency of their devices.

2.5 Existing Design Procedure for a Single-Feed Microstrip Reflectarray with Variable Size Rectangular Patches

The design of a single-feed microstrip reflectarray with variable size rectangular patches was first described by Pozar et al. [11]. The following steps outline the design of such a reflectarray:

1. Select design parameters.
2. Perform full-wave analysis to generate data of the reflected phase versus patch length.
3. Select required patch sizes.

We will now go through these steps to detail the design of this type of reflectarray.

1. Select design parameters.

   There are several design parameters that must be selected in the design of this type of reflectarray. To help in the description of these parameters we will make reference to Figure 2.10 which describes the geometry of this type of reflectarray. The first of these parameters is the aperture shape and size.

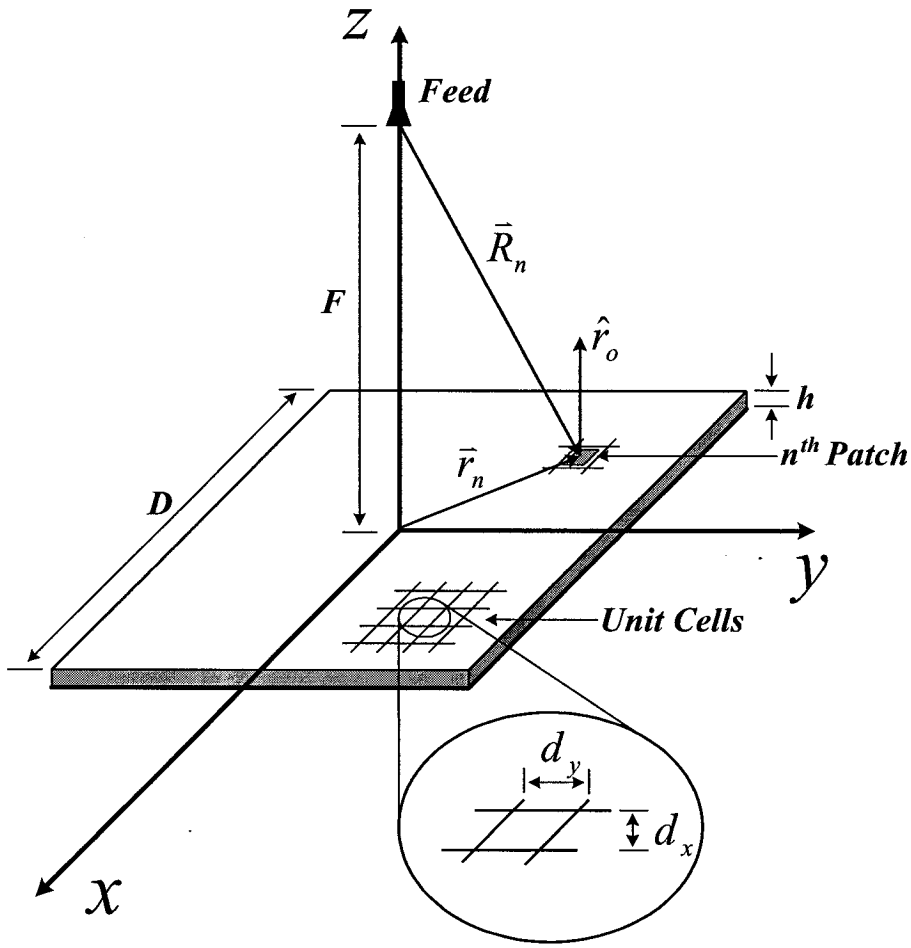

Figure 2.10: Reflectarray Geometry

For this description we will consider a square aperture. The required size of the aperture D is governed by the required gain of the antenna. The next parameter to consider is the unit cell size d_x and d_y. The size of the unit cell will determine the center to center distance between each element; this is critical in suppressing the higher order Floquet modes [98]. The cell size must

be selected so that only the lowest order Floquet mode is allowed to propagate. If the cell size is selected too large (i.e. large element spacing) higher order Floquet modes will propagate causing gratting lobes. However, the cell size must still be large enough so that the width of a microstrip patch contained inside the cell can be varied from its resonant size to achieve the full 360° range of reflected phases. The next design parameter is the feed location, be it center-fed or offset-fed. One must also select the height of the feed over the reflectarray, given by F. The spillover and taper efficiencies will be governed by the selection of the feed location. Typically the feed location is selected to have -10dB illumination, due to the feed pattern, at the edges of the reflectarray. Finally one must select a substrate and its thickness. The selection of the substrate will affect the bandwidth of the reflectarray and the slope of the reflected phase versus patch size design curves which will be discussed next.

2. Perform full-wave analysis to generate data of the reflected phase versus patch length.

   In order to select the patch sizes that will generate the desired reflected phase, one must generate a set of data for the phase of the reflected field of a uniform infinite array of identical patches versus patch size. This analysis can be done because it has been shown [11] that the mutual coupling between elements is quite low for thin microstrip substrates, and therefore the size of the surrounding patches has very little effect. Nevertheless, this approach will have the same limitations as the so-called infinite array method [99] widely used in the design of large conventional array antennas. This full-wave analysis was done using a commercial moment method code EmPicasso [100]. With this code one is able to model a single unit cell with periodic boundary conditions to simulate the unit cell in an infinite array of identical elements. The unit cell is then excited by an incident plane wave and the phase of the reflected field is obtained.

Figure 2.11 shows an example curve of the phase of the reflected field of an infinite array of identical microstrip patches, versus patch size. It should be

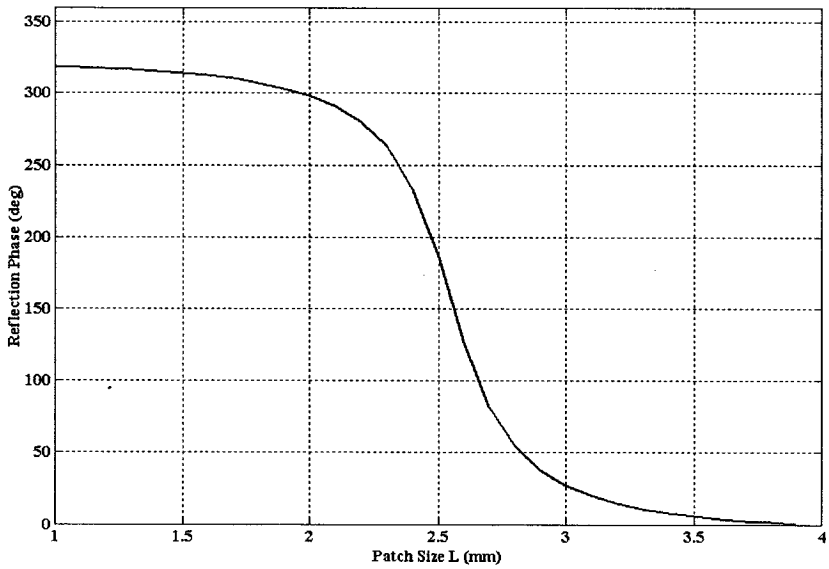

Figure 2.11: Reflected Phase from an Infinite Array of Identical Microstrip Patches versus Patch Size

noted that if the E-field is x-directed, then the dimension of the patch along the y-axis (width) is selected (and remains fixed) and the dimension of the patch along the x-axis (length) is varied, which is the independent variable (patch size) in Figure 2.11. The selection of the width of the patch is also important. As shown in Figure 2.12, the slope of the design curve is affected by the width of the patch. Ideally the curve with the most gradual slope is more desirable, in order to have more refinement when selecting the patch sizes.

3. Select required patch sizes.

   The selection of the patch sizes is done, based on the requirement that the phase at the aperture of the antenna must be uniform. To accomplish this, the required phase correction at each unit cell must be determined. To do this we

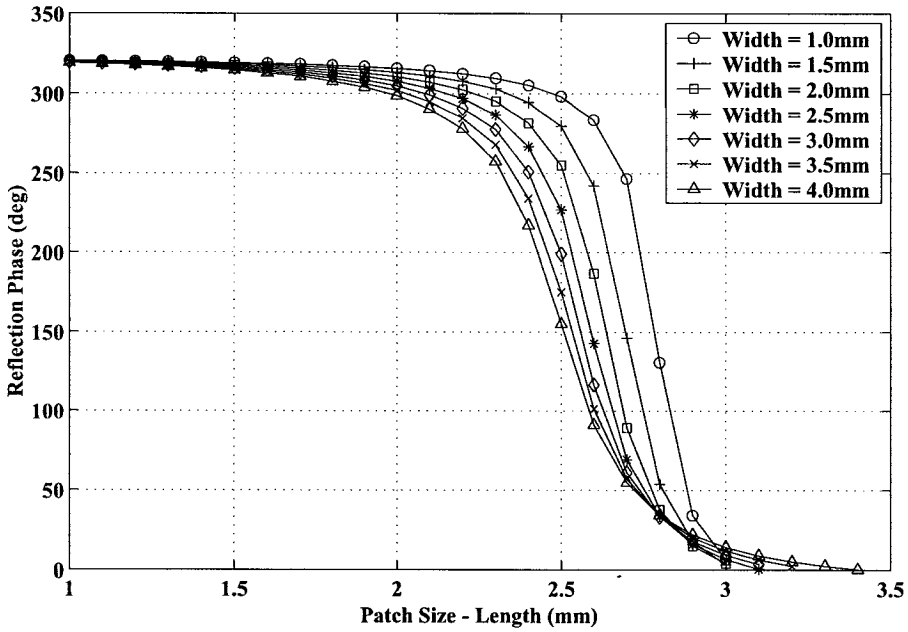

Figure 2.12: Reflected Phase from an Infinite Array of Identical Microstrip Patches versus Patch Size for Various Widths

make use of the following equation [11]

$$k_o(|\vec{R_n}| - \vec{r_n} \cdot \hat{r_o}) - \phi_n = 2\pi N \tag{2.1}$$

The quantity ϕ_n in Equation (2.1) is the required phase in order to obtain the appropriate phase correction in order to have a uniform phase across the aperture of the antenna. In other words ϕ_n must be chosen in such a way that the phase delay from the feed to an aperture in front of the reflectarray be the same for all the elements. The quantities $\vec{R_n}$, $\vec{r_n}$ and $\hat{r_o}$ are described in Figure 2.10. Once ϕ_n is determined for all the elements you can then use the design curve (the reflected phase versus patch size) described in the previous step to select the patch size that will give you the required phase correction ϕ_n. This can be done using an interpolation technique. For the designs of this research we used a cubic spline data interpolation routine.

These steps outline the design of a single-feed single-beam microstrip reflectarray with variable sized rectangular patches. Some alterations will need to be done to the design procedure to accommodate the multi-feed single-beam case.

2.6 Concluding Remarks

Section 2.2 provided a brief overview of spatial power combining methods. Section 2.3 gave a fairly complete summary of all the various reflectarray configurations that have been described in the literature. The references used at once also provide a useful comprehensive bibliography of work that has been described on reflectarray antennas. Section 2.4 reviewed the work done by others on incorporating power-combining into reflectarray antennas. These methods are different from that developed in Chapter 4 of the present thesis. Section 2.5 describes a design procedure for reflectarrays that can be used for the design of the existing forms of these antennas, but which will also be used in Chapter 4 to design the new type of reflectarray developed there.

Chapter 3

ELECTROMAGNETIC SIMULATION CONSIDERATIONS FOR REFLECTARRAYS: RECEIVE-MODE ANALYSIS

3.1 Description of the Receive-Mode Analysis Approach

In order to test the validity of a reflectarray design we consider performing a receive-mode analysis. This analysis entails simulating the complete reflectarray structure, that is, microstrip patches on a grounded dielectric substrate, with an incident plane wave, and then examining the reflected near-field along lines of interest. For the purpose of the description of this technique we will consider a single, center fed reflectarray with patches of variable size, as described by Pozar et al. in [11]. Figure 3.1 shows a ray-picture of the receive-mode operation of a reflectarray antenna. The reflectarray is designed using the design procedure that was outlined in Section 2.5. For this design we have a square aperture with D = 150mm, unit cell size d_x = 6mm and d_y = 6mm, F/D = 1 and the single main beam at broadside. The reflectarray was made using a 20mil or 0.508mm Rogers RT3003 substrate with $\epsilon_r = 3$. This yields a 625 cell reflectarray. Figure 3.2 shows the resulting distribution

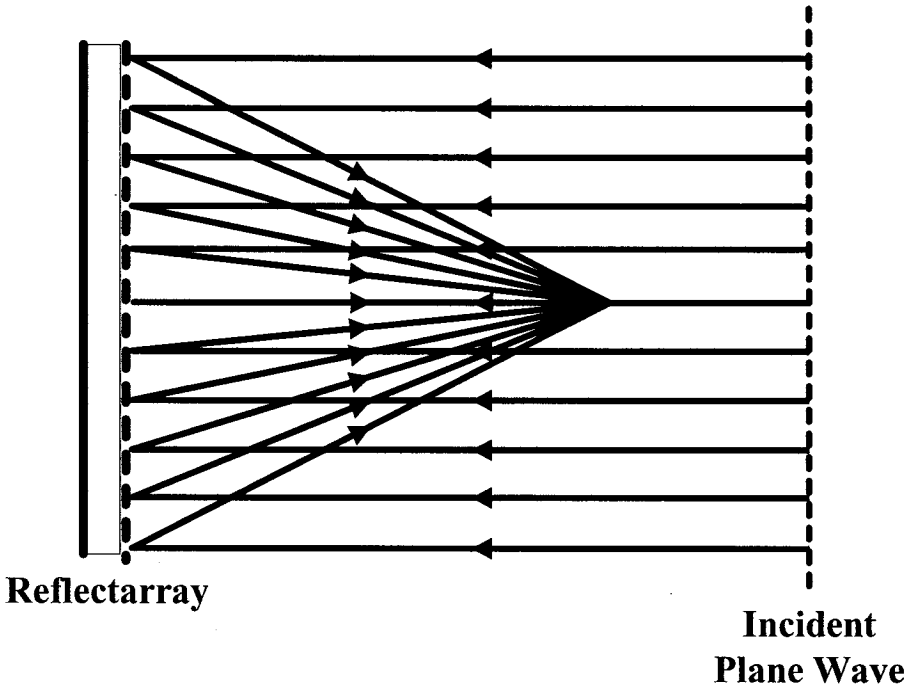

Figure 3.1: The Receive-Mode of a Reflectarray Antenna

of relative patch sizes for this reflectarray.

We now want to perform a receive-mode analysis on this finite reflectarray structure. To do this we will make use of the finite element method based code HFSS [101]. The patch distribution as well as the dielectric and ground plane must all be included in the design. To input this reflectarray design into HFSS we made use of HFSS's macro language. A MATLAB code that was written to determine the patch sizes has a subroutine that writes a macro that can be executed inside HFSS to automate the entry of the reflectarray structure. The macro also assigns all the material properties, boundary conditions, excitation, and sets up the solution properties. The use of such macros drastically reduces the time necessary to input a large structure, as is the case with the reflectarray we are currently considering, into HFSS. Once this has been done the reflectarray structure can be analysed. However, there is an issue with the electrical size of the problem. At 30GHz we have a 10mm wavelength (i.e.

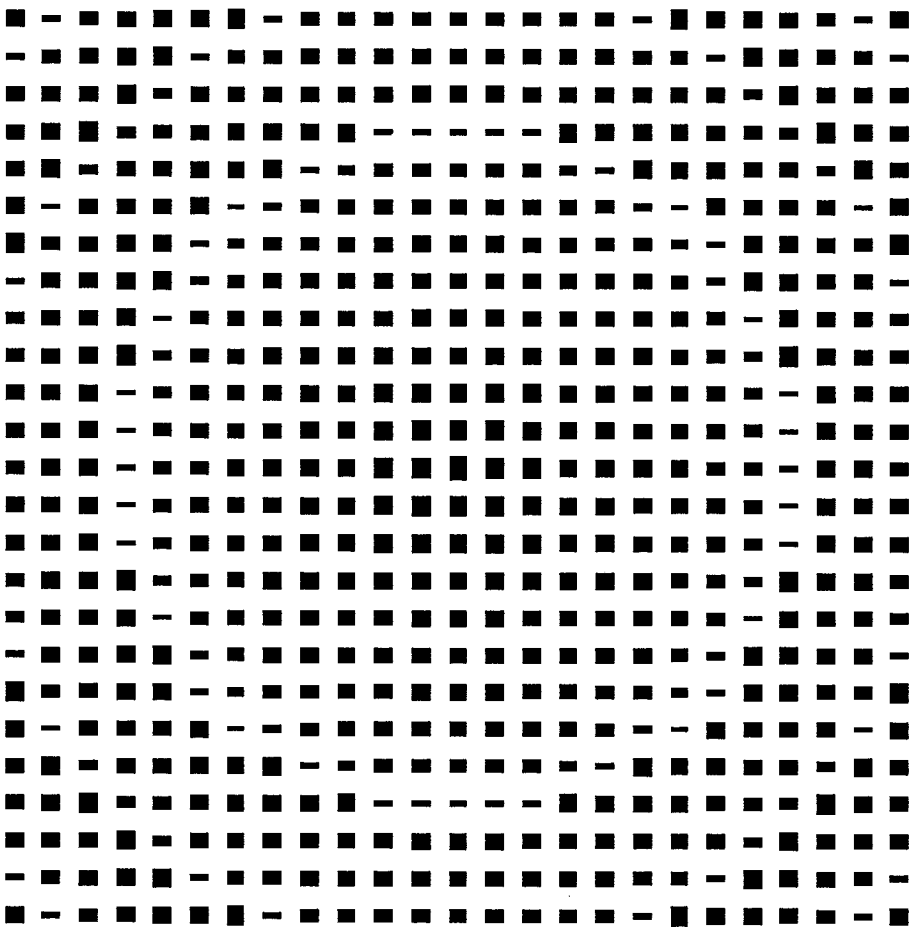

Figure 3.2: Reflectarray Patch Distribution (625 Cells)

$\lambda = 10mm$). We here have a structure that occupies a volume 150mm x 150mm x 6.508mm. The height of the structure includes the dielectric thickness, of 0.508mm, and the height of the radiation boundary (which is $\lambda/6$), giving us the total height of 6.508mm. This represents a structure that has a volume of $146.43\lambda^3$. A structure with this volume is too large to be analysed in HFSS on a standard PC. However, if we refer to Figure 3.3, we can see that we can exploit the symmetry of the structure. If we input only the dark patches into HFSS and use symmetry boundaries we can greatly reduce the solution region size. By making use of the symmetry of the structure, we reduce the volume of the solution region to $36.61\lambda^3$, which is much more manageable.

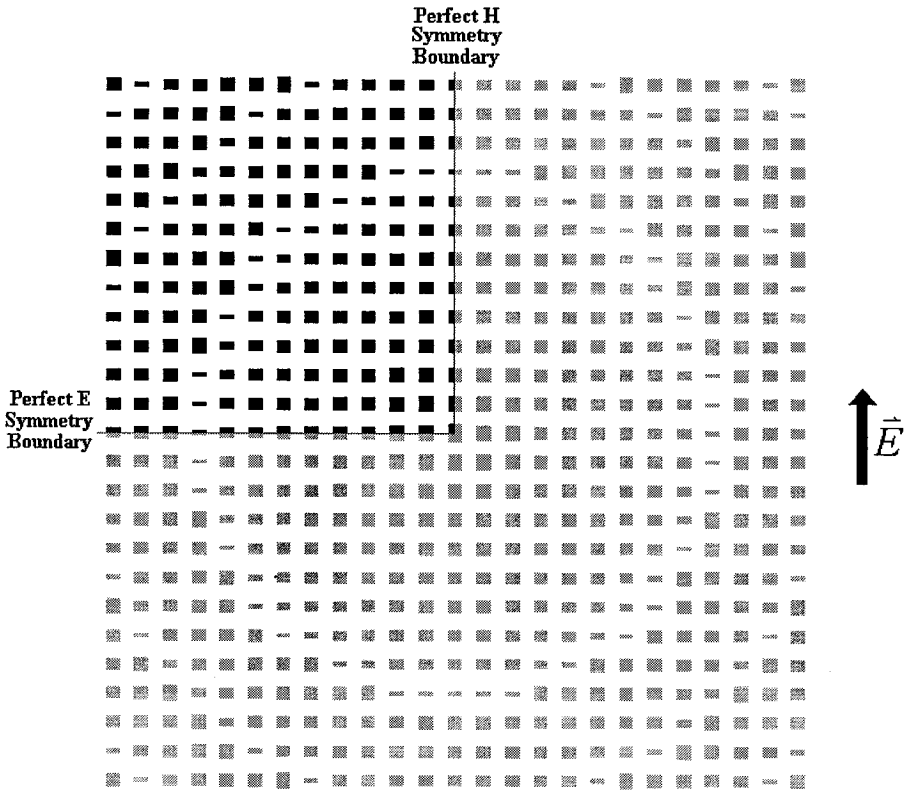

Figure 3.3: Symmetry of Reflectarray Patch Distribution (625 cell)

We are now able to use HFSS to solve this problem. The solution is carried out using an adaptive mesh to ensure that we have converged results. The convergence criterion, in HFSS, is based on the change in a computed energy term and is called "$DeltaE$". For the purpose of this simulation we have set the convergence criterion to $DeltaE < 0.05$. Once the simulation is completed and we are assured of having converged results, we can then use HFSS's post processing ability to look at the near field of the reflectarray. For this receive-mode analysis we are interested in the near field along the feed axis. Figure 3.4 shows the computed near field along the feed axis, namely a line beginning at the point (0,0,50mm) and terminated at (0,0,250mm). For this reflectarray design, with $F/D = 1$ and $D = 150$mm we expect to see the near field to be maximum at z $= F$ or z $= 150$mm. We can see from Figure 3.4 that

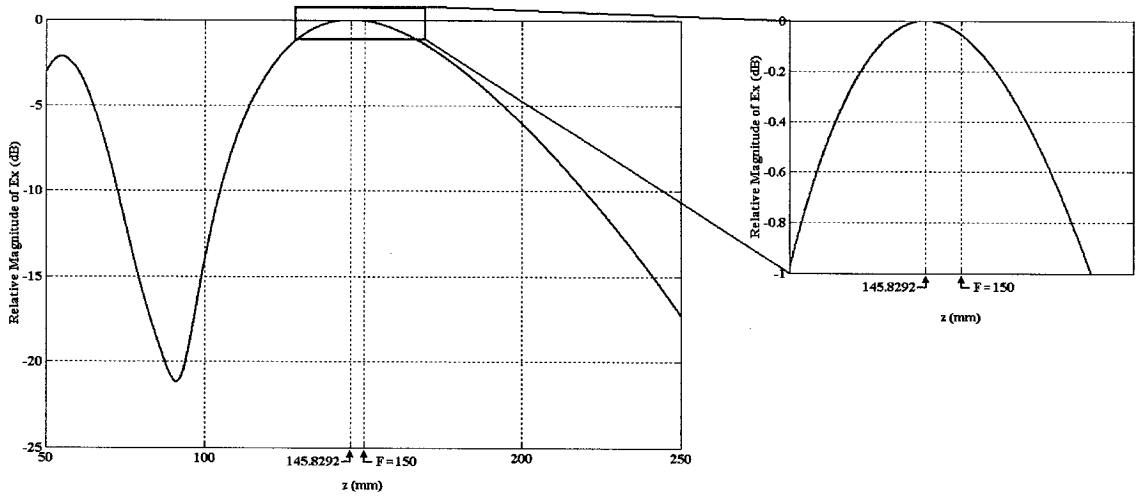

Figure 3.4: Near Field along Feed Axis (625 cell Reflectarray)

the near field is at its maximum near the design focal point of z = 150mm. However, we notice also from Figure 3.4 that the maximum near field does not occur exactly at the design focal point. The near field is maximum at z = 145.8292mm, which is about 0.42λ towards the reflectarray. This focal shift will be the topic of the next section.

To further test the validity of this type of analysis, let us apply the receive-mode analysis to another reflectarray design. For this second reflectarray we have the following design criteria: square aperture with $D = 198$mm, unit cell size $d_x = 6$mm and $d_y = 6$mm, $F/D = 0.6$, and the single main beam at broadside. All other design criteria are the same as the previous design. We then have a reflectarray with 1089 cells. Using the same procedure as described above, we can examine the near field along the feed axis for this reflectarray. Figure 3.5 shows the computed near field along the feed axis, namely a line beginning at the point (0,0,50mm) and terminated at (0,0,300mm). For a reflectarray of this size with $F/D = 0.6$, we have the design focal point at $F = 118$mm. We can see from Figure 3.5 that the near field is at a maximum near z = 118mm, but again we have that the maximum occurs at z

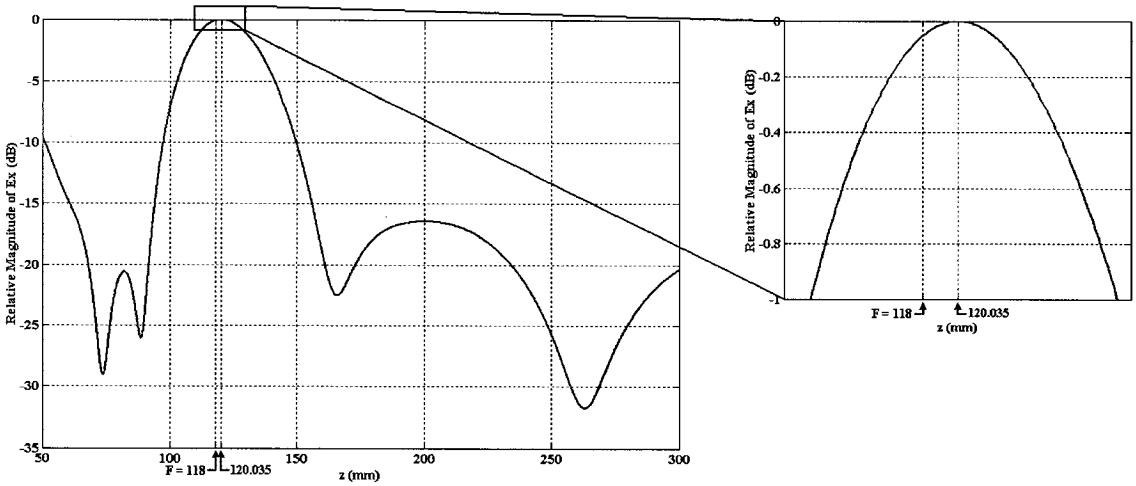

Figure 3.5: Near Field along Feed Axis (1089 cell Reflectarray)

= 120.0350. We again have a focal shift, in this case about 0.2λ away from the reflectarray.

Finally, to ensure that this receive-mode analysis gives accurate results we will apply it to a simple flat conducting plate. The conducting plate will be modeled in the same way as the 625 cell reflectarray, described earlier, but here we will remove the square patches and the dielectric. We are then left with a square ground plane with D = 150mm. To stay consistent with the previous analysis we will also apply symmetry boundaries to this structure; however it is not required due to the simplicity of the structure. Figure 3.6 shows the computed near field along the feed axis. Note in this case of the conducting plat we are assuming that the feed would be located same location of the 625 cell reflectarray described previously, namely (0,0,150mm). With a plane wave incident on a simple conducting plate we expect to have a reflected plane wave, but the conducting plate will not perform any focusing, as is the case with a reflectarray. In Figure 3.6 we can see that the near field along the feed axis is almost constant and there is indeed no evident focusing. We can also see that the relative magnitude of E_x for the conducting plate is much lower than for the

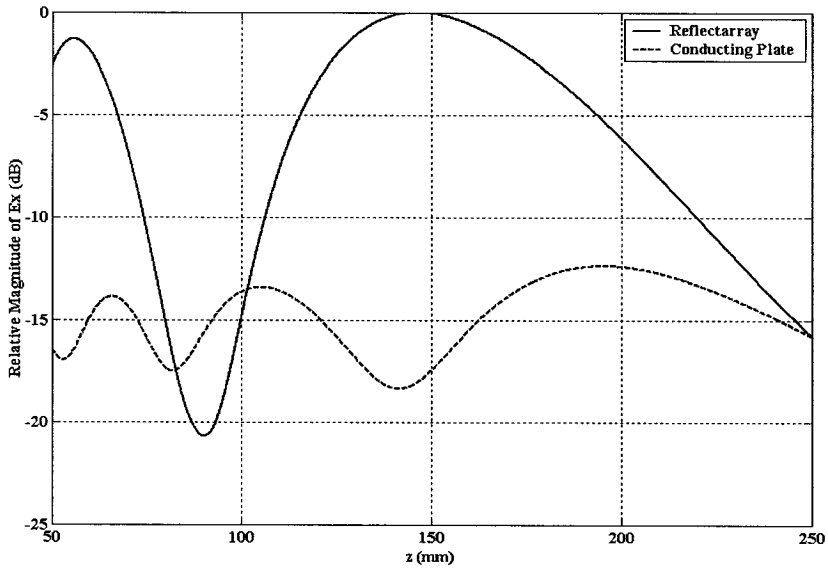

Figure 3.6: Near Field along Feed Axis (Reflectarray vs. Conducting Plate)

reflectarray. We do however see a ripple in the computed near field, most likely due to diffraction from the edges of the conducting plate. If we had an infinite conducting plate we would not see this ripple.

3.2 Investigation into the Focal Shift in Reflectarrays

In the previous section, we briefly discussed the phenomenon of a focal shift in reflectarrays. The focal shift in traditional reflectors has been previously investigated [102, 103]. If we consider a parabolic reflector the focal point of this reflector is simply the focus of the parent paraboloid; this is the geometrical optics focal point. Based on this one would expect that if a feed is placed at the focal point we can expect to have the maximum received power. However, this is not precisely the case [103]. It has been shown that you can sometimes get maximum received power when the feed is moved away from the geometrical optics focal point. This

movement of the feed to achieve maximum received power is called the focal shift. The main factor that contributes to this focal shift in parabolic reflectors is the finite size of the paraboloid. When designing the reflector the focal point is selected based on the parent paraboloid which is theoretically infinite. Having a finite sized reflector introduces diffractions from the edges, causing extra contributions to the reflected field that will shift the optimal feed position. As seen in [103], when the reflector size gets larger the focal shift decreases because the reflector is looking more like an infinite paraboloid and the diffraction off the edges has less effect on the reflected field. Using the receive-mode analysis described in the previous section, we have noticed this focal shift phenomenon in reflectarray antennas. We will next investigate whether the focal shift in reflectarrays is consistent with what is observed for traditional reflectors [103].

In order to examine the phenomenon of focal shift in reflectarrays we will analyse, using the receive-mode analysis, several different size reflectarrays, namely $D = 10.2\lambda$, $D = 15\lambda$ and $D = 19.8\lambda$. Each of the different size reflectarrays will also be analysed with different F/D ratios, namely $F/D = 0.6$, $F/D = 0.8$, $F/D = 1.0$ and $F/D = 1.2$. This combination of sizes and F/D ratios gives us 12 different reflectarrays to simulate. With this data, we will be able to compare the effect of focal shift in reflectarrays versus traditional reflectors. Figure 3.7, Figure 3.8 and Figure 3.9 show the near field computed along the feed axis for the three different reflectarray sizes $D = 10.2\lambda$, $D = 15\lambda$ and $D = 19.8\lambda$, respectively. We can see from these figures that for different sized reflectarrays we have different amounts of focal shift. Table 3.1 summarizes the amount of focal shift for each of these cases. To more easily understand how the amount of focal shift varies with different sized reflectarrays and different F/D ratios, we can look at the results of the above table in graphical form. Figure 3.10 shows the amount of focal shift, for different sized

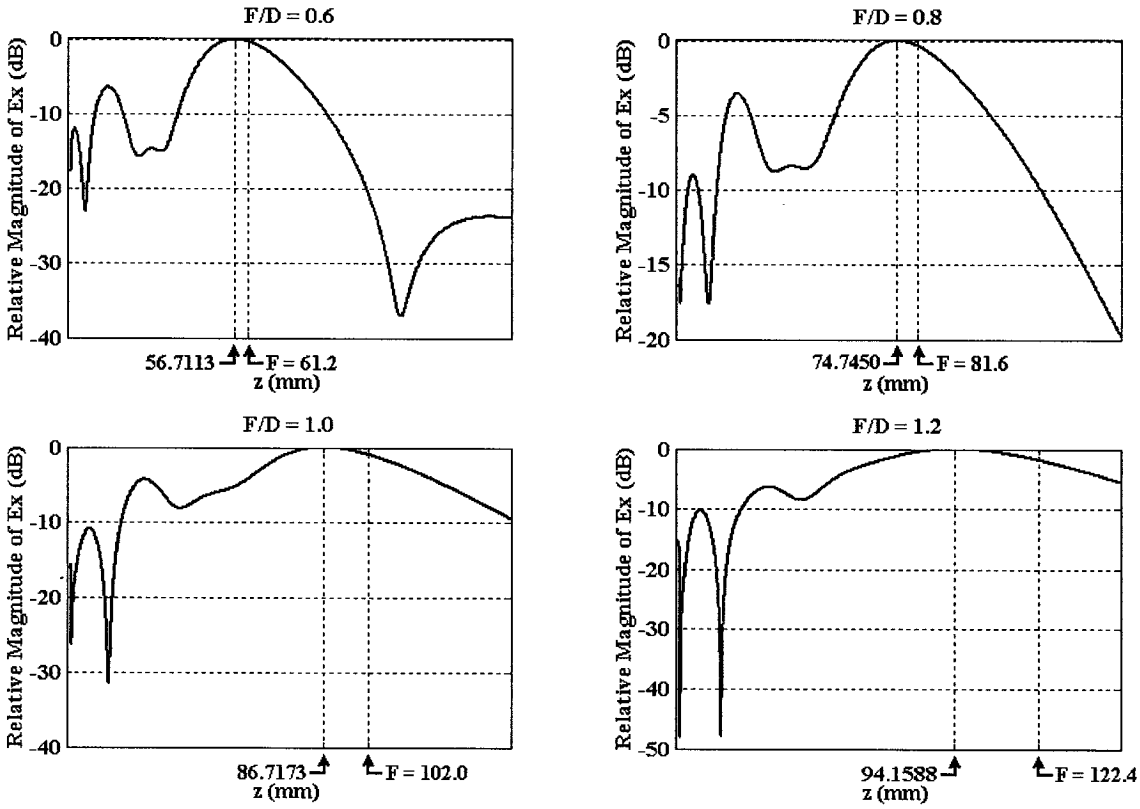

Figure 3.7: Near Field along Feed Axis ($D = 10.2\lambda$)

reflectarrays, versus F/D ratio. In Figure 3.10, we can clearly see the trends in the amount of focal shift based on the size of the reflectarray and the selected F/D ratio. It should be noted that for larger reflectarrays (i.e. 15λ,20λ) there is very little focal shift as is the case in traditional reflectors discussed previously. It stands to reason that factor, namely edge diffraction, which contributes to focal shift in traditional reflectors is the same contributing factor for the focal shift in reflectarrays. Therefore for practical applications (in which reflectarrays are usually electrically large) this phenomenon of focal shift will apparently not be an issue.

Nevertheless, to verify this phenomenon of focal shift in reflectarrays and to further validate the feasibility of the receive-mode analysis, two reflectarrays were constructed and the gain measured for different feed positions along the feed axis. The gain is

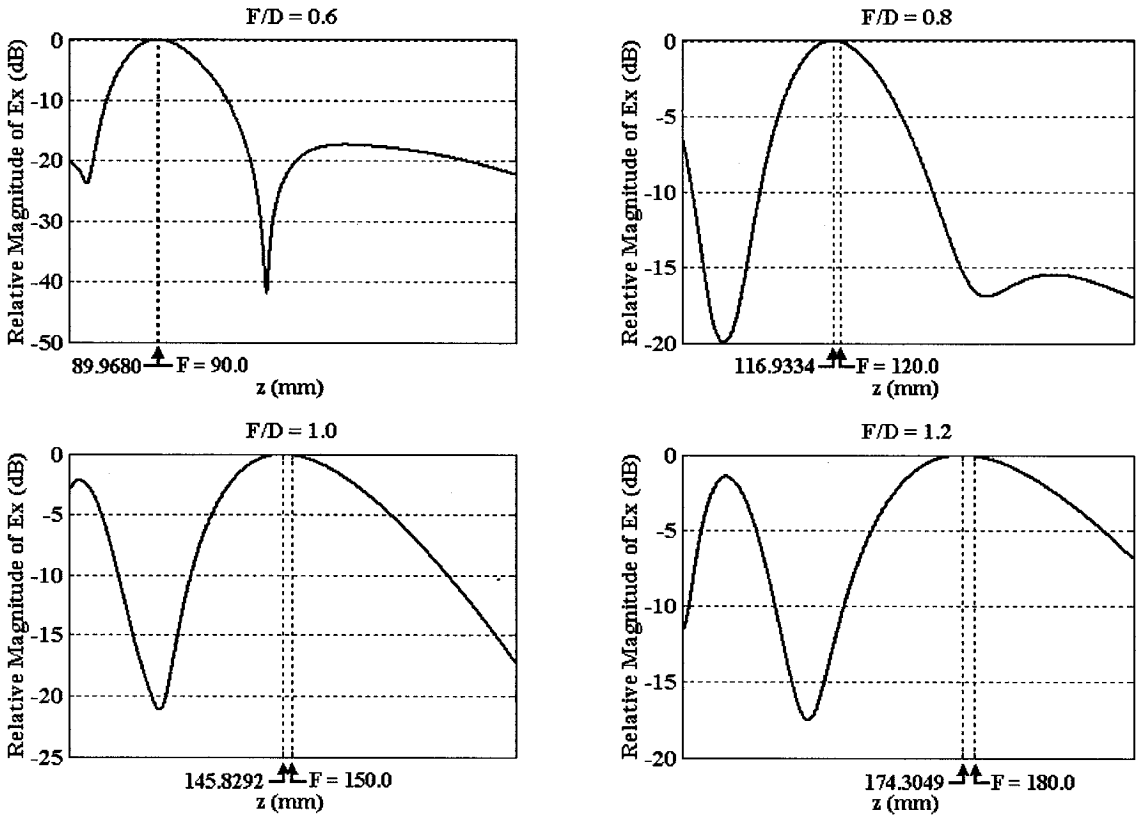

Figure 3.8: Near Field along Feed Axis ($D = 15\lambda$)

plotted normalized to the maximum measured gain value. Figures 3.11 and 3.12 show the measured results plotted over the simulated results from HFSS. In Figure 3.11 we have a $D = 10.2\lambda$ reflectarray with $F/D = 1.0$. We can see from the measured results that we have a good agrement with the simulated results. Another factor that must be noted is that the receive-mode analysis computes the reflected near-field at *points* along a line. In other words the receive-mode analysis is telling us how the field varies as we move a point source feed along the feed axis. The measured results, however are for a waveguide probe feed with a finite aperture. To achieve more accurate measured results we would need to compute Robieux's integral [102]. This was not done because the purpose of the receive-mode analysis was simply to gain a better understanding of reflectarray operation and to validate new reflectarray design, as we will see in the next chapter. What these measured results show is

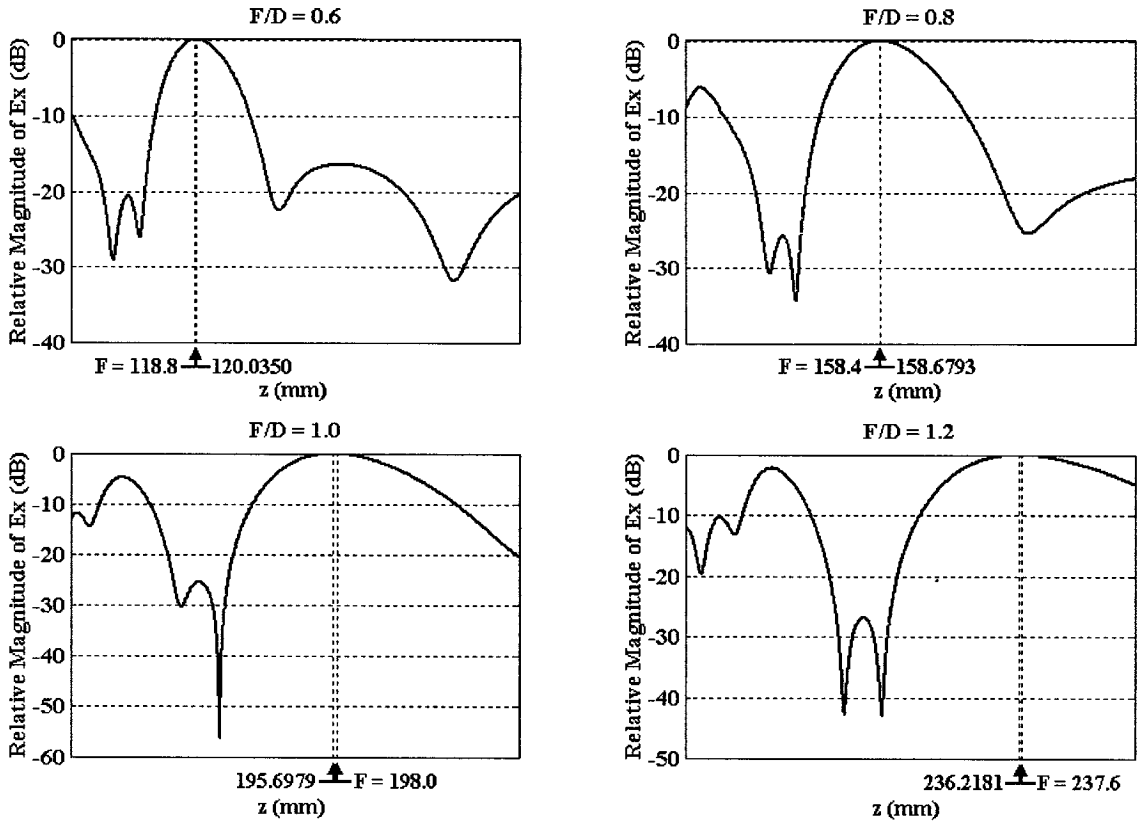

Figure 3.9: Near Field along Feed Axis ($D = 19.8\lambda$)

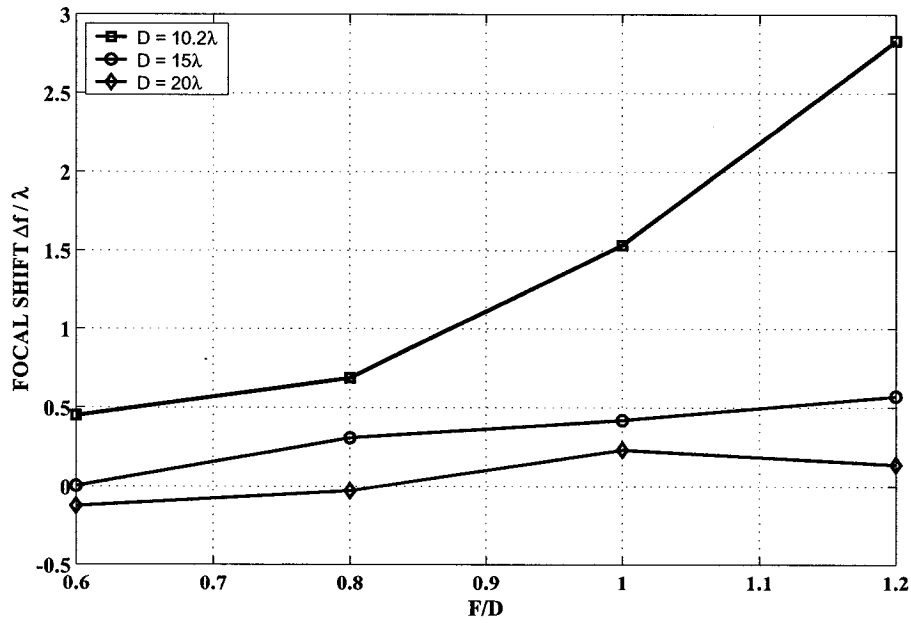

Figure 3.10: Focal Shift (Δ F) as Functions of F for Various Aperture Sizes

Table 3.1: Focal Shift for Various Reflectarray Sizes and F/D Ratios

Reflectarray Size $\lambda = 10mm$	F/D Ratio	Design Focal Location F(mm)	Maximum Field Location (mm)	Focal Shift (mm)
10.2λ	0.6	61.2	56.7113	4.4887
10.2λ	0.8	81.6	74.7450	6.8550
10.2λ	1.0	102.0	86.7173	15.2827
10.2λ	1.2	122.4	94.1588	28.2412
15.0λ	0.6	90.0	89.9680	0.0320
15.0λ	0.8	120.0	116.9334	3.0666
15.0λ	1.0	150.0	145.8292	4.1708
15.0λ	1.2	180.0	174.3049	5.6951
19.8λ	0.6	118.8	120.0350	-1.2350
19.8λ	0.8	158.4	158.6793	-0.2793
19.8λ	1.0	198.0	195.6979	2.3021
19.8λ	1.2	237.6	236.2181	1.3819

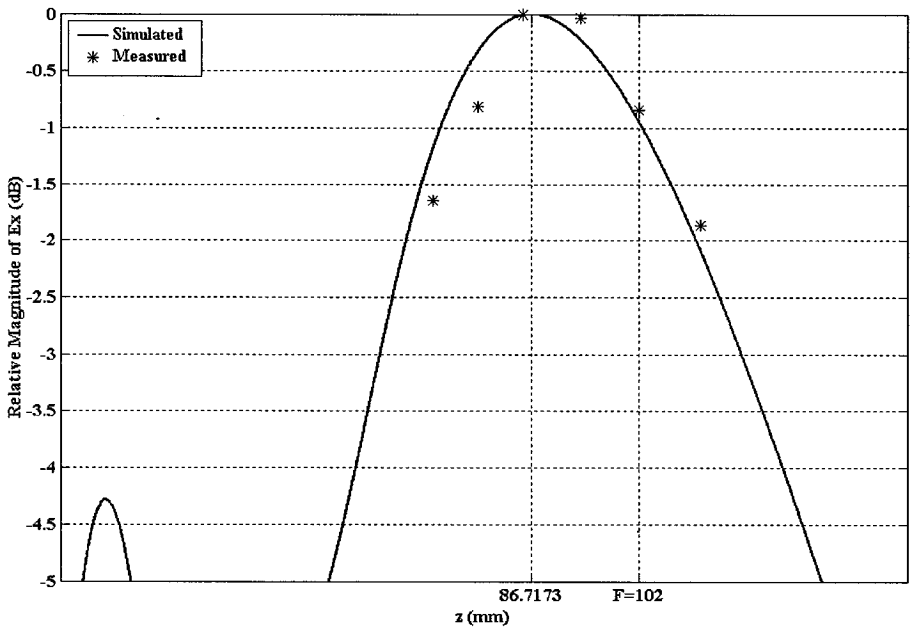

Figure 3.11: Measured Focal Shift - $D = 10.2\lambda$, $F/D = 1.0$

that the receive-mode analyses performed using HFSS are a good prediction tool for reflectarray designs. In Figure 3.12 we have a $D = 15\lambda$ reflectarray with $F/D = 1.0$. In this plot we see that as we move the feed away from the reflectarray, past the design

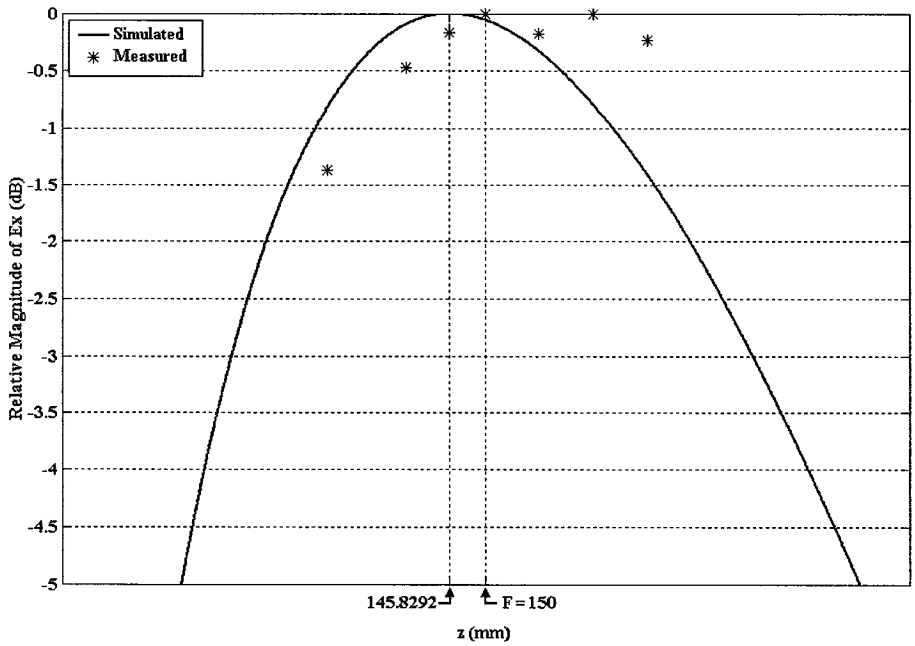

Figure 3.12: Measured Focal Shift - $D = 15\lambda$, $F/D = 1.0$

feed point F, the measured results do not follow the simulated curve. However, as we move the feed along the feed axis, towards the reflectarray we see good agreement with the simulated results. Ideally it would have been beneficial to collect measured results for points further away from the reflectarray than those that were taken. However, the measurement jig used had a restricted range of movement. It stands to reason that if were able to move the feed further away we would see the measured gain drop.

3.3 Gaussian Beam Interpretation

Another interesting aspect of the receive-mode analysis is that we can use the results for a Gaussian beam interpretation of the reflected wave. This type of interpretation can be used in determining ideal feed placement to maximize the received power. To perform a Gaussian beam interpretation of the reflected field we must examine the field transverse to the direction of propagation [104]. In the cases we are considering, propagation is along the z-axis. Therefore the field will be plotted along the x-axis(E-plane) and y-axis(H-plane). We will examine the transverse fields at four distinct locations, namely $z = z_{MAX}$, $z = F$, $z = z_{3dB}^{-}$ and $z = z_{3dB}^{+}$. In Figure 3.13 we see these locations in terms of the reflected near-field along the z-axis and Figure 3.14 shows these locations schematically. In Figure 3.15 and 3.16 we

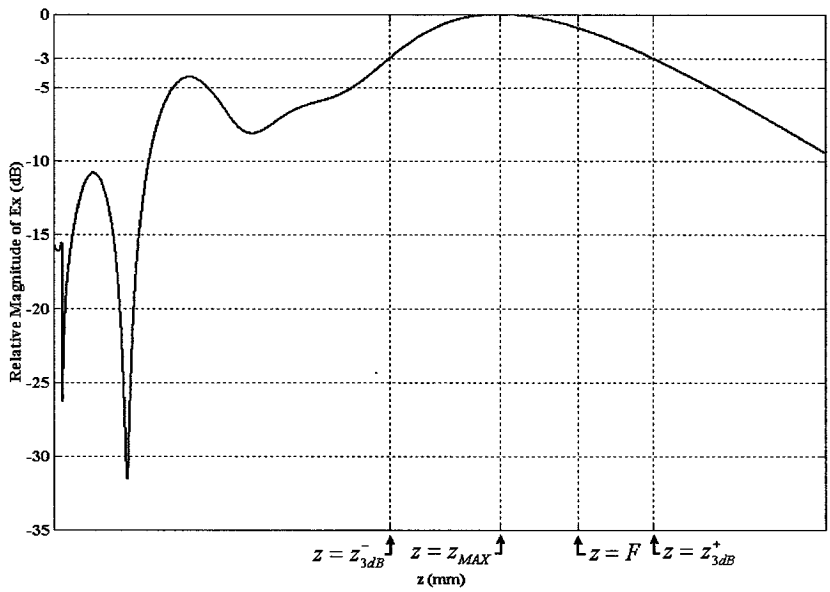

Figure 3.13: Reflected Near Field along Feed Axis - $D = 10.2\lambda$, $F/D = 1.0$

have the reflected field plotted in the E and H plane at the four locations of interest for a 10.2λ reflectarray with an $F/D = 1.0$. In this Gaussian beam interpretation we are interested in two specific quantities. First is the beam radius. The beam

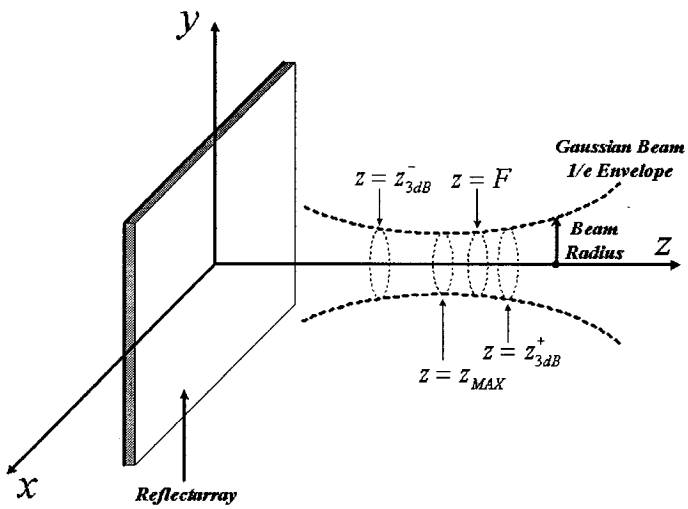

Figure 3.14: Schematic Representation of a Gaussian Beam

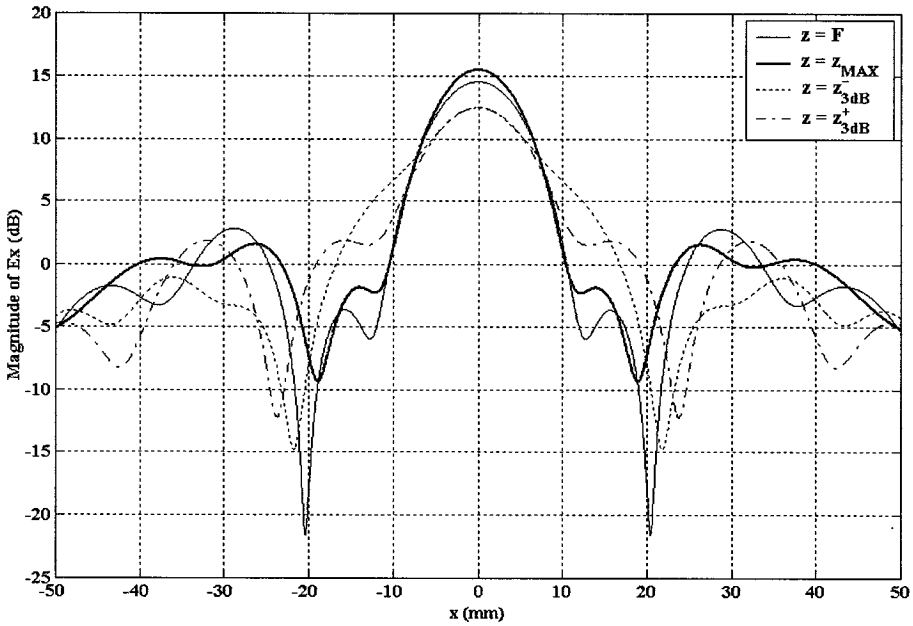

Figure 3.15: Reflected Near Field Along Transverse Axis (E-plane)

radius is the width of the beam, plotted along a line transverse to the direction of propagation, where its value has decayed from the peak value by e^{-1}, or in dB by $10log(e^{-1})$. Figure 3.14 shows schematically how the beam radius of a Gaussian beam varies as you move along the direction of propagation. The beam radii for the fields plotted in Figures 3.15 and 3.16 are given in Table 3.2. In Table 3.2 we can see

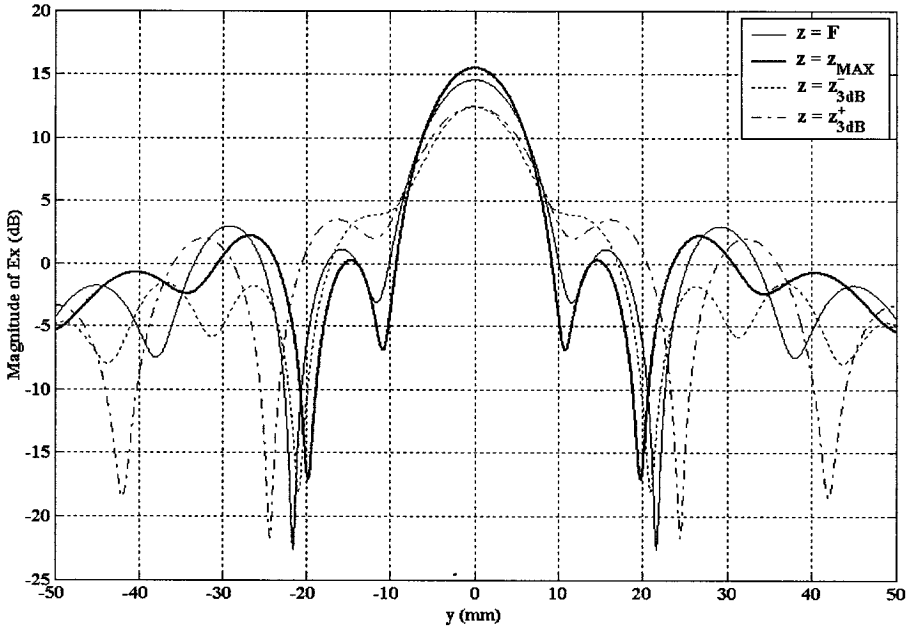

Figure 3.16: Reflected Near Field Along Transverse Axis (H-plane)

Table 3.2: Gaussian Beam Radius

Location along z-axis	E-plane Beam Radius (mm)	H-plane Beam Radius (mm)
$z = F$	6.3017	6.0465
$z = z_{MAX}$	5.8424	5.5363
$z = z_{3dB}^{-}$	7.0465	6.0465
$z = z_{3dB}^{+}$	6.9650	6.7099

that the Gaussian beam is at its narrowest at $z = z_{MAX}$ (where the beam radius is the beam waist) and the beam radius gets wider as you move away from $z = z_{MAX}$, as depicted in Figure 3.14. Ideally the beam radius at $z = z_{3dB}^{-}$ should be equal to the beam radius at $z = z_{3dB}^{+}$; this would be the case if we had the lowest order Gaussian beam [104]. We can clearly see from Figures 3.15 and 3.16 and the values of the beam radii in Table 3.2 that the field reflected by the reflectarray includes higher order Gaussian beams.

We can next have a look at the beam waist (at $z = z_{MAX}$) for the various reflectarray

sizes we are considering, versus F/D. This is plotted in Figure 3.17. From Figure 3.17

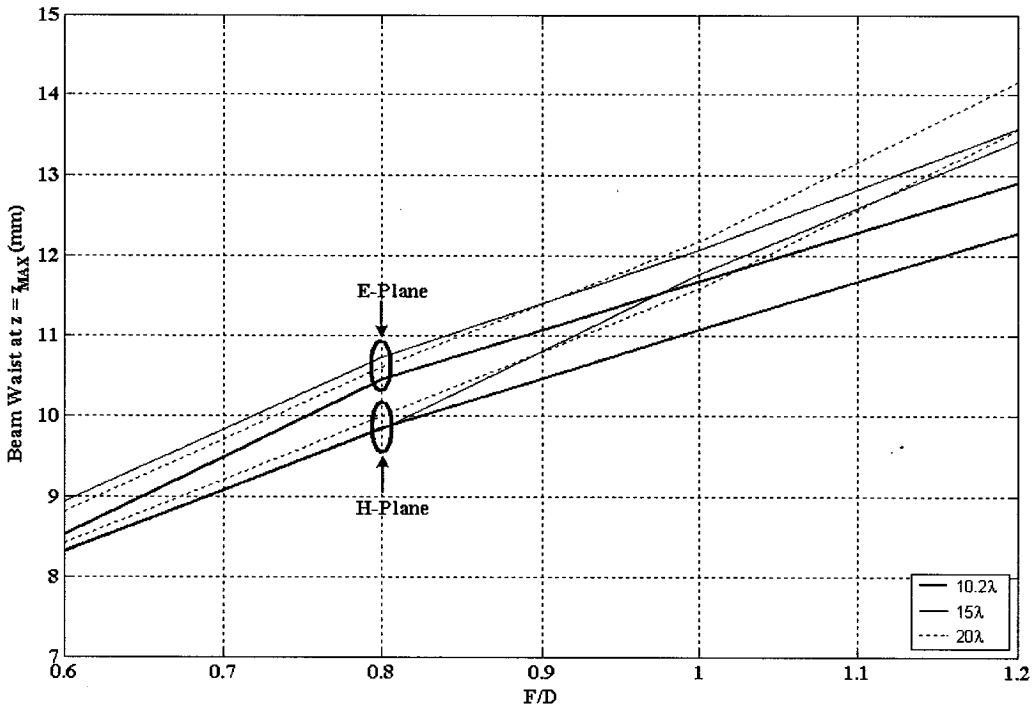

Figure 3.17: Beam Waist at $z = z_{MAX}$ versus F/D

we can see that the Gaussian beam is elliptical due to the larger beam waist in one plane versus the other. Also we can see how the beam waist varies with different F/D values, as F/D get larger the beam waist get larger almost linearly.

The next quantity of interest is how the phase varies within the beam radius. Typically the phase front of the field transverse to the direction of propagation is curved except at the beam waist where the phase front becomes flat. The phase fronts on either side of the beam waist have opposite and increasing curvatures. This is show, schematically, in Figure 3.18. In Figure 3.19 we see the curvature of the phase front for the reflected wave of the 10.2λ reflectarray, with $F/D = 1.0$ analyzed using HFSS, for the four specific points mention previously, namely $z = z_{MAX}$, $z = F$, $z = z_{3dB}^{-}$ and $z = z_{3dB}^{+}$. We can clearly see in Figure 3.19 that the phase front

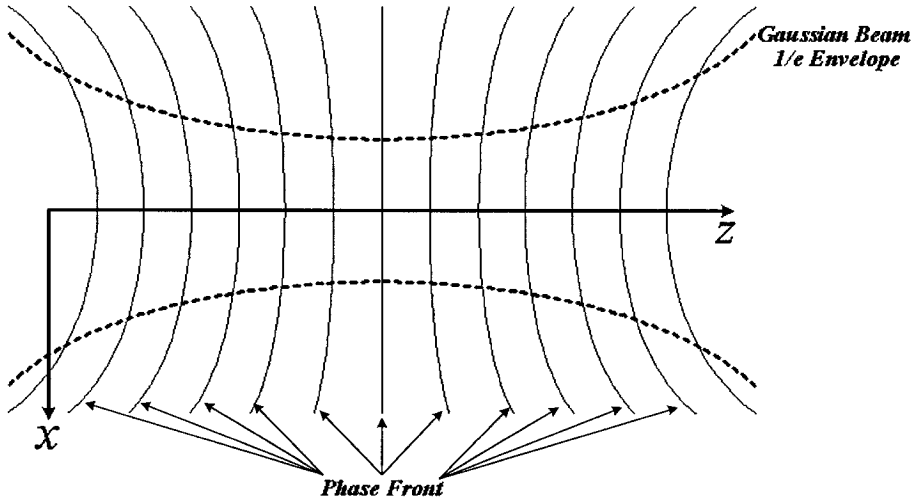

Figure 3.18: Gaussian Beam Phase Fronts

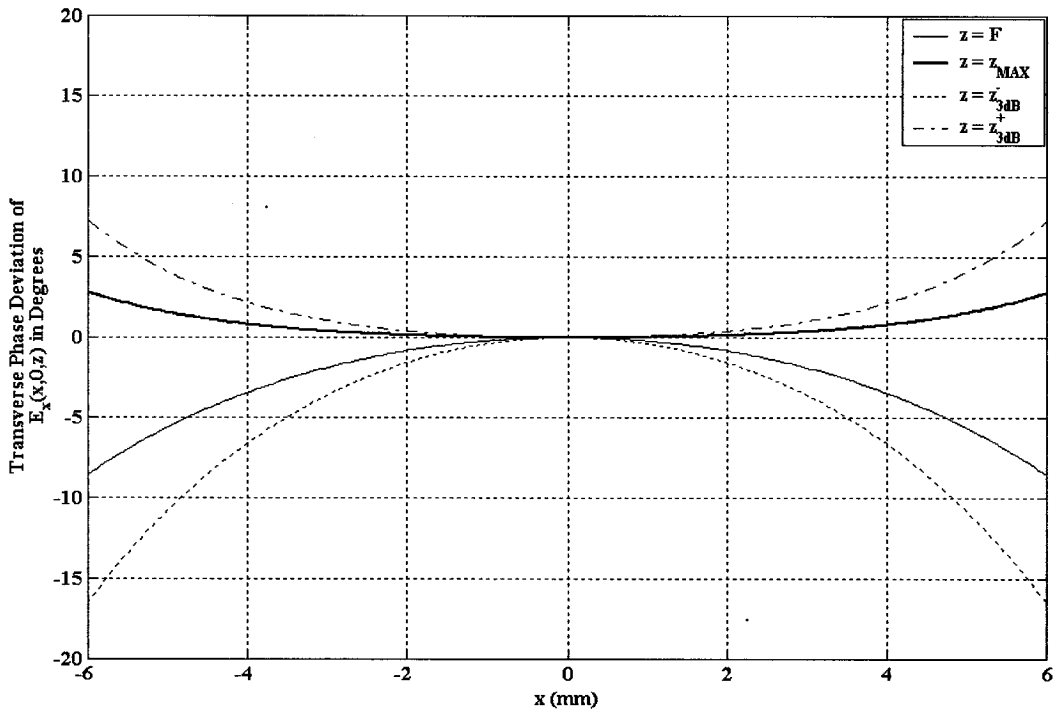

Figure 3.19: Phase of the Reflected Near Field Along Transverse Axis (E-plane)

is behaving as predicted. We can see that as we move away from the reflectarray the phase front is curved and as we move closer to $z = z_{MAX}$ the phase front flattens and after this point the curvature of the phase front returns.

Both these quantities, beam waist and phase distribution, could be used to design an optimum feed for the reflectarray. There exists design equations [104] to design a feed to achieve optimum coupling to the fundamental Gaussian Mode. The investigation of this type of optimum feed is outside the scope of this research.

3.4 Concluding Remarks

The major objective of this thesis is the development of a design procedure for multi-feed single-beam reflectarray antennas so that the antenna itself performs a spatial power combining action. It was expected that some additional means of interpreting the operation of reflectarrays would be needed during the research on such unconventional multi-feed single-beam types. Therefore, electromagnetic modelling of reflectarray operation in the receive mode, presented here for the first time, forms the subject of Chapter 3. Section 3.1 described the concept of receive mode analysis and immediately applied the approach to the operation of a conventional single-feed single-beam reflectarray (designed using the procedure from Section 2.5). The conventional single-feed single-beam case was considered since its operation in the receive mode was expected to be similar to that of a conventional paraboloidal reflector antenna. Thus it was possible to establish the validity of the receive mode analysis. Nevertheless, experimental validation was also given in Section 3.2, along with a discussion of the "focal shift" observed. Section 3.3 gives an interesting Gaussian beam interpretation of the focal region fields of the reflectarrays; although not essential to the work in this thesis it provides increased understanding of the antennas operation.

Chapter 4

THE DEVELOPMENT AND IMPLEMENTATION OF A DESIGN PROCEDURE FOR MULTI-FEED REFLECTARRAYS

4.1 Introduction

Recall that the goal of a reflectarray, as for a parabolic reflector, is to convert the phase of a wave with a spherical phase front, emitted by the feed, to a wave with a planar phase front. By reciprocity the reflectarray, if designed correctly, will convert the phase of an incident wave with a planar phase to a wave with a spherical phase front and focus the beam at the designed feed position. Figure 4.1 illustrates this point.

This chapter considers, for the first time, the design of multi-feed single-beam reflectarray antennas for use as integrated antenna/power-combiner devices. The mathematical analysis that allows the design procedure of Section 2.5 to be applied to such multi-feed single-beam reflectarray antennas is described in Section 4.2. Section 4.3 will give a very complete description of the implementation of the procedure to the two-feed case. This includes a receive-mode analysis of the two-feed antenna

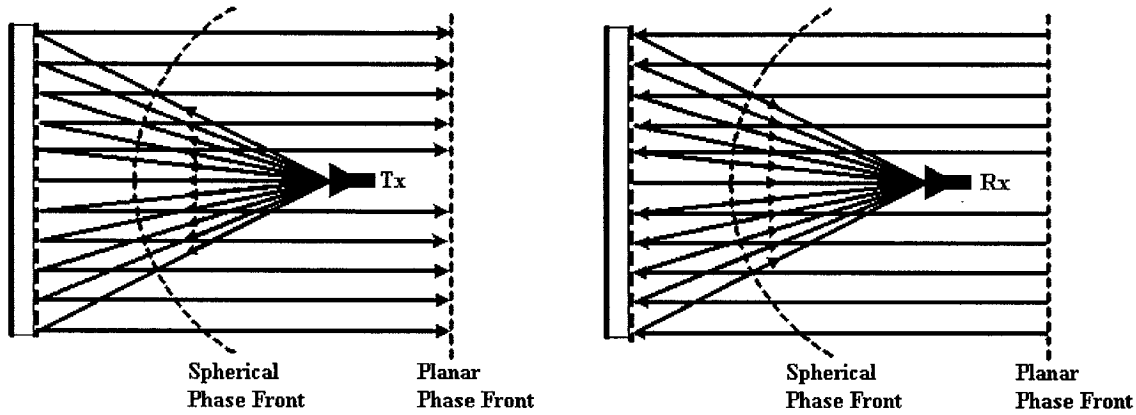

Figure 4.1: Phase Conversion of a Reflectarray

which clearly shows that an incoming plane wave is indeed focused to two separate feed locations, and is fundamentally different to single-feed single-beam antennas. Experimental validation of the two-feed antenna will be given, and its measured performance carefully compared to predictions simply to validate the design procedure. Section 4.4 will then described the design, implementation, predicted performance, and measured performance of a four-feed single-beam reflectarray antenna/power-combiner. The radiation pattern performance, as well as the power combining efficiency, will be investigated. Section 4.5 concludes the chapter.

4.2 Design Procedure for Multi-Feed Reflectarrays

4.2.1 Combined Field Analysis

In order to design a multi-feed reflectarray, we need a new design equation that will allow us to determine the required phase correction needed at each element to achieve the desired phase conversion. For simplicity let us first consider a two-feed reflectarray, for which the geometry of the structure is shown in Figure 4.2. Let us now start by considering the field incident on the n^{th} patch due to the first feed only.

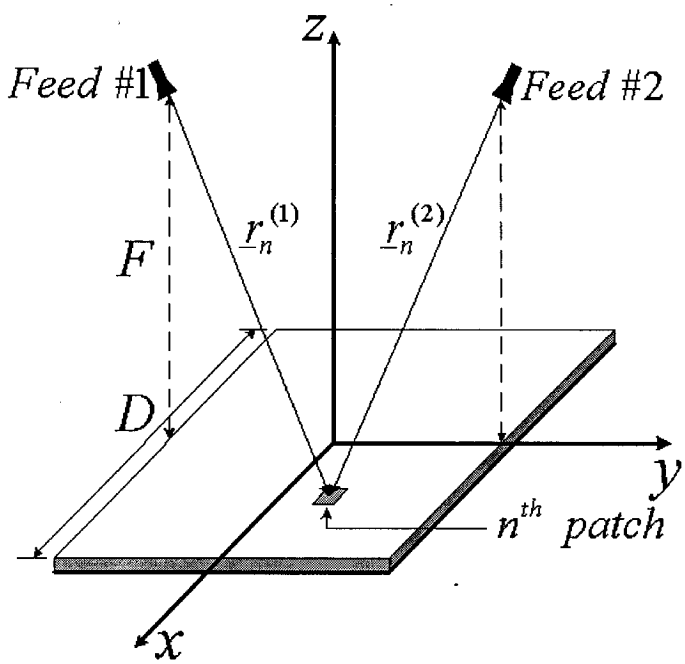

Figure 4.2: Geometry of a Two Feed Reflectarray

We can then write the reflected field as follows

$$E_1(\bar{r}_n^{(1)}) = |E_1(\bar{r}_n^{(1)})|e^{-j(k_o|\bar{r}_n^{(1)}|-\phi_n)} \tag{4.1}$$

Recall that ϕ_n is the phase of the reflection coefficient associated with the n^{th} patch, determined as explained in Section 2.5. The reflected field from the n^{th} patch in the presence of the second feed can be written as

$$E_2(\bar{r}_n^{(2)}) = |E_2(\bar{r}_n^{(2)})|e^{-j(k_o|\bar{r}_n^{(2)}|-\phi_n)} \tag{4.2}$$

Now the total reflected field at the n^{th} patch in the presence of both feeds can be written as

$$E_n^T = |E_1(\bar{r}_n^{(1)})|e^{-j(k_o|\bar{r}_n^{(1)}|-\phi_n)} + |E_2(\bar{r}_n^{(2)})|e^{-j(k_o|\bar{r}_n^{(2)}|-\phi_n)} \tag{4.3}$$

We can now decompose Equation (4.3) into its real and imaginary parts as follows:

$$E_n^T = |E_1(\bar{r}_n^{(1)})|cos(k_o|\bar{r}_n^{(1)}| - \phi_n) + |E_2(\bar{r}_n^{(2)})|cos(k_o|\bar{r}_n^{(2)}| - \phi_n)$$
$$-j|E_1(\bar{r}_n^{(1)})|sin(k_o|\bar{r}_n^{(1)}| - \phi_n) - j|E_2(\bar{r}_n^{(2)})|sin(k_o|\bar{r}_n^{(2)}| - \phi_n) \quad (4.4)$$

and hence write the phase of this total field

$$\angle E_n^T = tan^{-1}\left\{\frac{-|E_1(\bar{r}_n^{(1)})|sin(k_o|\bar{r}_n^{(1)}| - \phi_n) - |E_2(\bar{r}_n^{(2)})|sin(k_o|\bar{r}_n^{(2)}| - \phi_n)}{|E_1(\bar{r}_n^{(1)})|cos(k_o|\bar{r}_n^{(1)}| - \phi_n) + |E_2(\bar{r}_n^{(2)})|cos(k_o|\bar{r}_n^{(2)}| - \phi_n)}\right\} \quad (4.5)$$

We next assume that the feed is a point source, so that the patterns of the individual feeds is broad enough so that the angular dependance of their patterns can be ignored as far as the illumination of the reflectarray is concerned. Since we are considering the feeds as point sources we still have a $1/r$ decay (where r is the distance from the feed to the patch) of the magnitude of the fields. We can then write $|E_1(\bar{r}_n^{(1)})| = 1/|\bar{r}_n^{(1)}|$ and $|E_2(\bar{r}_n^{(2)})| = 1/|\bar{r}_n^{(2)}|$. Considering this we can the rewrite Equation (4.5) as

$$\angle E_n^T = tan^{-1}\left\{\frac{-\frac{1}{|\bar{r}_n^{(1)}|}sin(k_o|\bar{r}_n^{(1)}| - \phi_n) - \frac{1}{|\bar{r}_n^{(2)}|}sin(k_o|\bar{r}_n^{(2)}| - \phi_n)}{\frac{1}{|\bar{r}_n^{(1)}|}cos(k_o|\bar{r}_n^{(1)}| - \phi_n) + \frac{1}{|\bar{r}_n^{(2)}|}cos(k_o|\bar{r}_n^{(2)}| - \phi_n)}\right\} \quad (4.6)$$

We now have an equation which tells us the phase of the reflected field at each individual patch. In order to design a functioning reflectarray we must determine the value of ϕ_n at each patch that will make the phase of the total field, $\angle E_n^T$, constant for all patches. In other words we want a constant phase front at an aperture in front of the reflectarray. To do this, we use a numerical optimization routine that will attempt to set $\angle E_n^T = 0$ by finding the appropriate value of ϕ_n. The MATLAB routine *fsolve* was used to accomplish this task. Knowing the required values of ϕ_n for each n we can select the appropriate patch sizes by making use of the reflected phase from an infinite array of identical microstrip patches versus patch size curve of the type in Figure 2.11. Note that the selection of the appropriate patch size

was done by using the *spline* function in MATLAB in order to interpolate the data points in Figure 2.11.

The above procedure, which obtained a design equation for a two-feed reflectarray can easily be expanded for any number of feeds. Equation (4.7) is the general combined field formula to design a reflectarray with M feeds:

$$\angle E_n^T = tan^{-1}\left\{\sum_{m=1}^{M}\frac{-\frac{1}{|\bar{r}_n^{(m)}|}sin(k_o|\bar{r}_n^{(m)}| - \phi_n)}{\frac{1}{|\bar{r}_n^{(m)}|}cos(k_o|\bar{r}_n^{(m)}| - \phi_n)}\right\} \tag{4.7}$$

4.2.2 Radiation Pattern Analysis Using Array Theory

To validate these multi-feed designs one can use a receive-mode analysis as described in Chapter 3 and/or analyze it in an appropriate transmit mode as a planar array of microstrip patches (which it is). Considering the reflectarray in this latter manner allows us to use array theory to calculate the far-field pattern of the reflectarray. If we consider the geometry of a planar array [105] as seen in Figure 4.3, with

$$\bar{\mathbf{r}}_{\mathbf{mn}} = x_{mn}\hat{\mathbf{x}} + y_{mn}\hat{\mathbf{y}} + z_{mn}\hat{\mathbf{z}} \tag{4.8}$$

the array factor of this array, with I_{mn} the complex excitation of the mn^{th} element can be written as

$$AF(\theta,\phi) = \sum_{n=1}^{N}\sum_{m=1}^{M} I_{mn}e^{j\alpha_{mn}}e^{j\xi_{mn}} \tag{4.9}$$

where

$$\xi_{mn} = k_o\hat{\mathbf{r}}\cdot\bar{\mathbf{r}}_{\mathbf{mn}} = k_o[x_{mn}sin\theta cos\phi + y_{mn}sin\theta sin\phi] \tag{4.10}$$

$$\alpha_{mn} = -k_o[x_{mn}sin\theta_o cos\phi_o + y_{mn}sin\theta_o sin\phi_o] \tag{4.11}$$

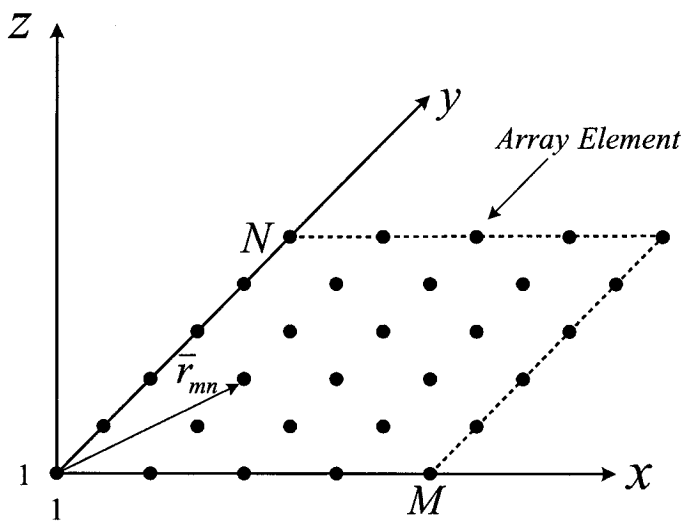

Figure 4.3: Planar Array Geometry

In (4.10) the (θ_o, ϕ_o) is the direction of the array main beam, and α_{mn} is the additional phase of the mn^{th} element required to achieve this beam direction. For the purpose of this research, we are considering all main beam directions to be at broadside so that $\theta_o = 0$, $\phi_o = 0$ and hence $\alpha = 0$. We can then write Equation (4.9) as

$$AF(\theta, \phi) = \sum_{n=1}^{N} \sum_{m=1}^{M} I_{mn} e^{jk_o(x_{mn} sin\theta cos\phi + y_{mn} sin\theta sin\phi)} \tag{4.12}$$

Recall from Figure 2.10 Chapter 2, which shows the geometry of a reflectarray, that the vector

$$\bar{r}_n = x_n \hat{\mathbf{x}} + y_n \hat{\mathbf{y}} \tag{4.13}$$

which is not the same as the $\bar{r}_n^{(i)}$ in Figure 4.2, locates the x and y coordinates of n^{th} patch. Using Equation (4.13) we can then rewrite the array factor in Equation (4.12) with a single index. This will give us the array factor of the reflectarray as

$$AF(\theta, \phi) = \sum_{n=1}^{N} I_n e^{jk_o(x_n sin\theta cos\phi + y_n sin\theta sin\phi)} \tag{4.14}$$

The term I_n in Equation (4.14) is the relative complex amplitude of the current excited on the n^{th} patch. If this current has a magnitude and phase it can be written as

$$I_n = A_n e^{j\beta_n} \tag{4.15}$$

Since we are considering a feed illuminating the individual patches of the reflectarray we can consider (albeit an approximation) that the excitation terms A_n and β_n as being proportional to the magnitude and phase of the reflected electric field at the n^{th} patch, respectively, or

$$I_n = |\bar{E}_n| e^{j\angle \bar{E}_n} \tag{4.16}$$

since we intend using the array theory to obtain relative pattern levels only. We can then write Equation (4.14) as

$$AF(\theta, \phi) = \sum_{n=1}^{N} |E_n| e^{jk_o(x_n sin\theta cos\phi + y_n sin\theta sin\phi) + j\angle E_n} \tag{4.17}$$

Now that we have determined an equation for the array factor, we can look at the element pattern for each element of the reflectarray. To do this first let us consider a single microstrip patch described in Figure 4.4. The far field radiation pattern for this microstrip patch is given to a good approximation by [106]

$$E_\theta^{patch}(\theta, \phi) = \frac{-sin(W_k)cos(L_k)}{W_k} \frac{cos\phi(\varepsilon_{eff} - sin^2\theta)}{\varepsilon_{eff} - sin^2\theta cos^2\phi} \tag{4.18}$$

$$E_\phi^{patch}(\theta, \phi) = \frac{sin(W_k)cos(L_k)}{W_k} \frac{\varepsilon_{eff} - cos\theta sin\phi}{\varepsilon_{eff} - sin^2\theta cos^2\phi} \tag{4.19}$$

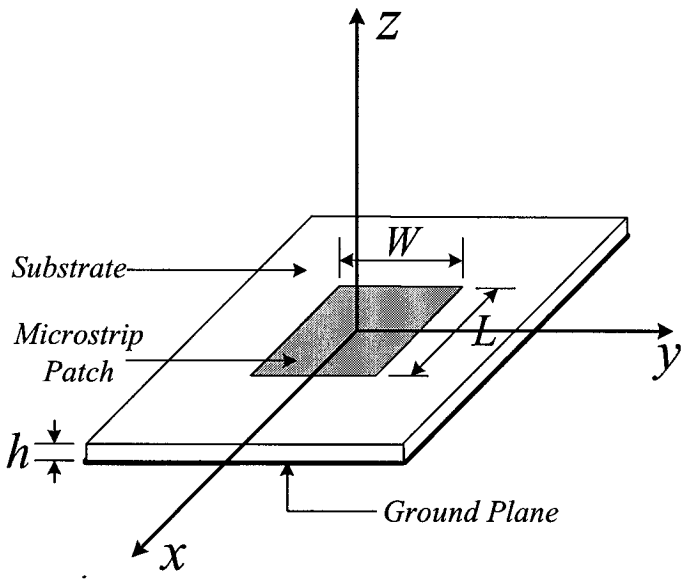

Figure 4.4: Microstrip Patch Geometry

where

$$\begin{aligned} \varepsilon_{eff} &= \frac{\varepsilon_r + 1}{2} + \frac{\varepsilon_r - 1}{2}\left(1 + 10\frac{h}{W}\right)^{-\frac{1}{2}} \\ W_k &= \frac{k_o W}{2} sin\theta sin\phi \\ L_k &= \frac{k_o(L + 2\Delta L)}{2} sin\theta cos\phi \end{aligned}$$

and

$$\Delta L = \frac{0.412h(\varepsilon_{eff} + 0.3)\left(\frac{W}{h} + 0.264\right)}{(\varepsilon_{eff} - 0.258)\left(\frac{W}{h} + 0.8\right)}$$

It should be noted that in the two principal planes (i.e. $\phi = 0°$ and $\phi = 90°$) we can use the total E-field as our element pattern and it is given by

$$E^{patch}(\theta, \phi) = \sqrt{[E_\theta^{patch}(\theta, \phi)]^2 + [E_\phi^{patch}(\theta, \phi)]^2} \tag{4.20}$$

Since our reflectarray is made up of patches of varying lengths L the element pattern at each patch will be different and it will be a function of L_n (i.e. the length of the n^{th} patch). With this in mind we can write the far-field pattern of the reflectarray using array theory as

$$E^{reflectarray}(\theta,\phi) = \sum_{n=1}^{N} E_n^{patch}(\theta,\phi,L_n)|E_n|e^{jk_o(x_n sin\theta cos\phi + y_n sin\theta sin\phi)+j\angle E_n} \quad (4.21)$$

The above equation will allow us to simulate the reflectarray to determine its far-field pattern prior to fabrication and testing. This is a useful tool especially if stringent criteria are required for the pattern of the reflectarray (ég. maximum allowed sidelobe levels).

4.3 Two-Feed Design

4.3.1 Initial Comments

The goal here is to design a reflectarray that will perform the spatial power combining of two feeds. In other words, we have a reflectarray structure that is being illuminated with two feeds, as seen in Figure 4.2. The reflectarray, if designed correctly, will correct the phase of the total field that is incident from both feeds on the reflectarray, to a wave with a uniform phase distribution over an aperture in front of the reflectarray. The reflectarray will then have one main beam at broadside with the combined power of both feeds. The design that we will be considering here is a 15.5λ square reflectarray at 30GHz with the main beam at broadside and an F/D ratio of 1. Again referring to Figure 4.2, with the reflectarray centered at the origin, the feeds would be located at $(x, y, z) = (0, \pm 7.75\lambda, 15.5\lambda)$ so that both are at a radial distance $r = 173.3mm$ from the coordinate origin. The feeds are placed in such a manner as to have an x-directed linearly polarized E-field. With a unit cell size of 5mm this

reflectarray has 961 elements, which are printed on 0.020" Rogers RO3003 substrate ($\varepsilon_r = 3.0$). With these design criteria in mind, we can proceed to the design of the microstrip patch elements. To accomplish this we will use the combined field design equation described in Section 4.2.1. Specifically we will make use of Equation (4.6) by setting $\angle E_n^T = 0$. As described earlier this equation will be solved using an optimization routine in MATLAB (*fsolve*). This routine attempts to make $\angle E_n^T$ equal to zero by selecting the ϕ_n appropriately. This was done, and $\angle E_n^T$ was found with a maximum error, over all the elements, of 9.2595×10^{-8} radians. With the optimization routine successfully executed we have the value of ϕ_n (i.e. required reflected phase) for each patch, we then use the curve obtained from EmPicasso simulations of the reflected phase from an infinite array of identical microstrip patches versus patch size, for a square unit cell size of 5mm, as seen in Figure 4.5. Note that the width of the patches is constant and equal to 3mm. Once all the patch sizes (L_n)

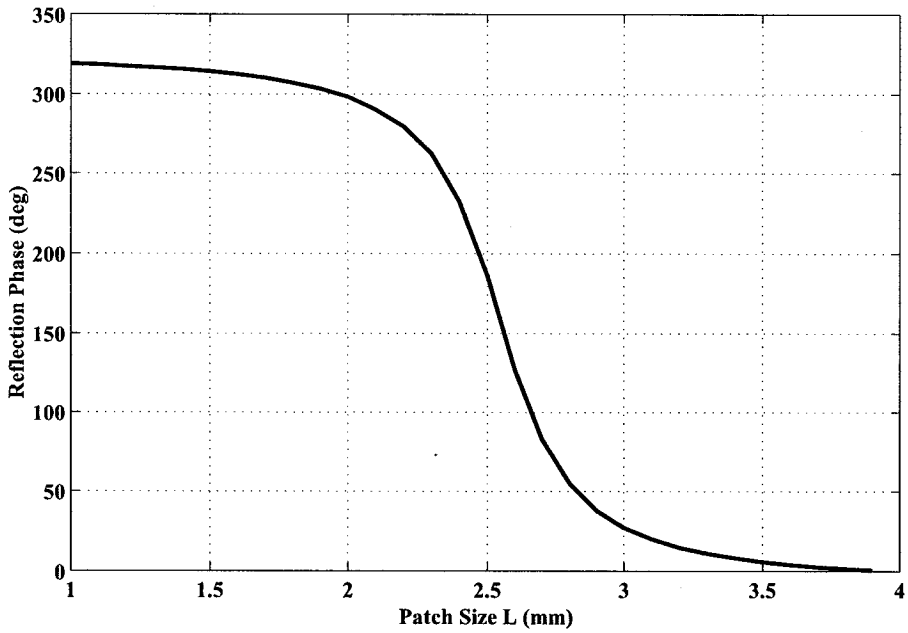

Figure 4.5: Reflected Phase from an Infinite Array of Identical Microstrip Patches versus Patch Size (L) for a 5mm Square Unit Cell and a Patch Width of 3mm

are determined from the required reflection phases (ϕ_n) we get the patch distribution

shown in Figure 4.6

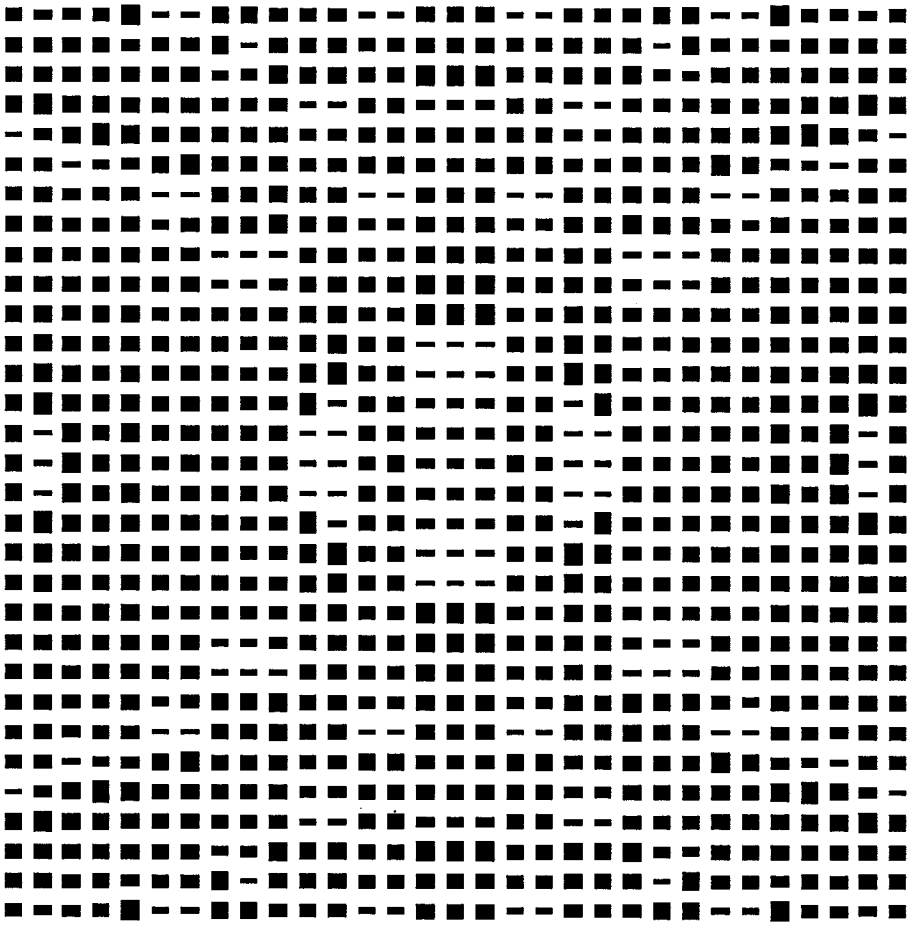

Figure 4.6: Distribution of Relative Patch Sizes for the Two-Feed Reflectarray

4.3.2 Receive Mode Analysis and Interpretation

As described in Chapter 3, we can use the receive mode analysis as a means of verifying the design. And as for the case of the single feed design of Chapter 3 we can exploit the quadrantal symmetry of the reflectarray design to alleviate the computational burden. In Figure 4.7 we see the quarter symmetry of the two feed reflectarray. The portion that is greyed out will not need to be simulated; instead the only portion to be simulated is the black quadrant of the reflectarray with symmetry planes placed appropriately. Once simulated we can use the post processing facility

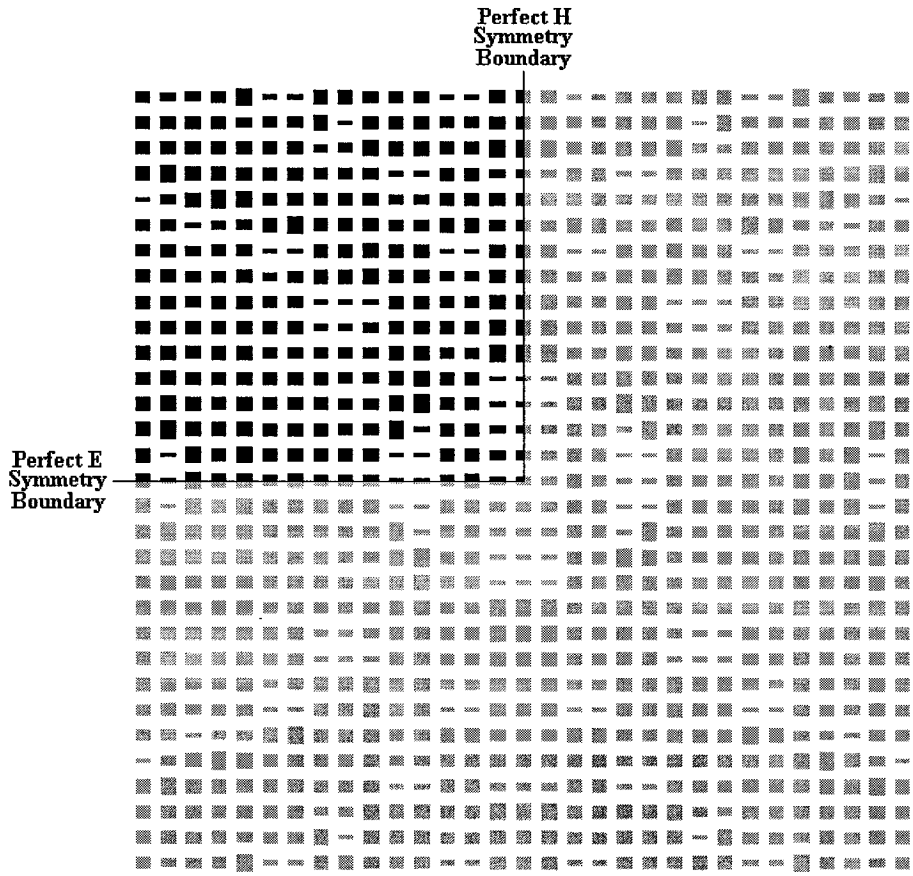

Figure 4.7: Symmetry of Patch Distribution for the Two-Feed Reflectarray

of HFSS to compute the reflected near field along lines of interest. Specifically we are interested in the behavior of the reflected field along lines that pass through the feed locations. We will then look at the reflected field along lines that start at the

origin (i.e. center of the reflectarray) and extend onto and past the location of the feeds as shown in Figure 4.8. Both lines will start at the origin, $(x, y, z) = (0, 0, 0)$ and extend to $(x, y, z) = (0, \pm 155mm, 310mm)$. The result of this calculation is

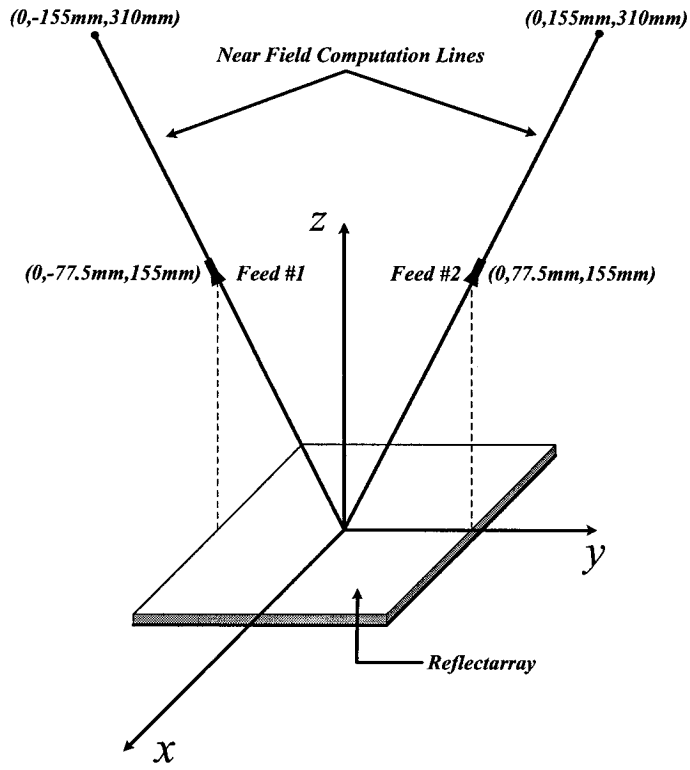

Figure 4.8: Reflected Near Field Computation Lines (Feed Lines)

shown in Figure 4.9. We can see from this graph that the reflected near field reaches a maximum near the feed locations assumed in the design procedure. It should be noted that, as was the case in the single feed designs where we observed a focal shift, we also see this phenomena in the two feed case. The maximum reflected field values occurs at $r = 165.9mm$ and not precisely at the feed locations ($r = 173.3mm$) assumed in the design procedure. Also note that the curves overlap each other precisely, demonstrating that the field reflected from the reflectarray towards each feed will be identical. To ensure that the simulation is actually working correctly we computed the reflected near field along other lines to see if there were any focusing effects. Specifically we will examine the reflected near field along a line that extends

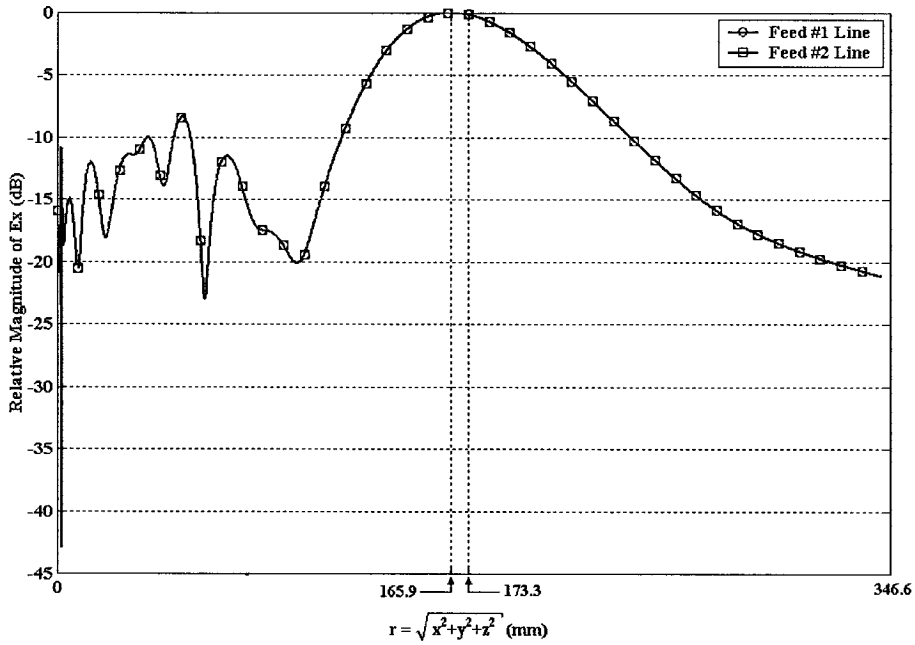

Figure 4.9: Reflected Near Field versus r = $\sqrt{x^2 + y^2 + z^2}$

from the origin along the z-axis; this would show us if there is any focusing effect along a line where a feed would be located if we had a center fed reflectarray. We will now also look at two other lines. These lines will start at the origin and will extend in the x-z plane (plane which is orthogonal to the plane containing the feeds). Alternatively these two lines will start at the origin $(x, y, z) = (0, 0, 0)$ and extend to $(x, y, z) = (\pm 155mm, 0, 310mm)$. Figure 4.10 demonstrates graphically these other lines of interest. We can see in Figure 4.11 the values of the reflected field plotted along the lines shown in Figure 4.10, relative to the reflected field along the lines which pass through the feed locations, namely the line shown in Figure 4.8. We can see here that near the focal region ($\simeq 173.3mm$) the reflected field at the design location of the feeds is significantly higher than along the other lines, shown in Figure 4.10. This result confirms that the combined field design equation for multi-feed reflectarrays, described at the start of this chapter, works as it should. It should be noted that in Figure 4.11 we see a peak in the field at $z = 77.675mm$ along the broadside axis line. It would appear that there is additional focusing at this location, however without

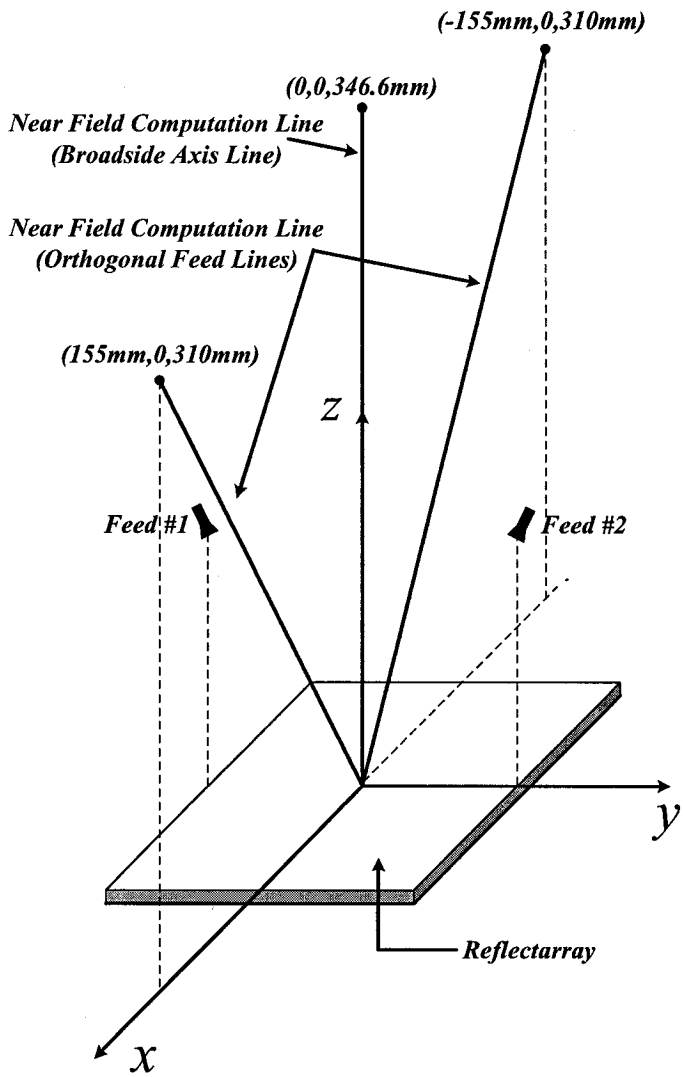

Figure 4.10: Reflected Near Field Computation Lines

knowing how the field behaves in a plane transverse to direction of propagation at this location (Gaussian Beam Analysis) it is not certain whether this focussing can be exploited. Also this peak, along the broadside axis, is much closer to the reflectarray and placing a feed there in order to exploit this focusing effect might cause secondary issues such as blockage and increased scattering.

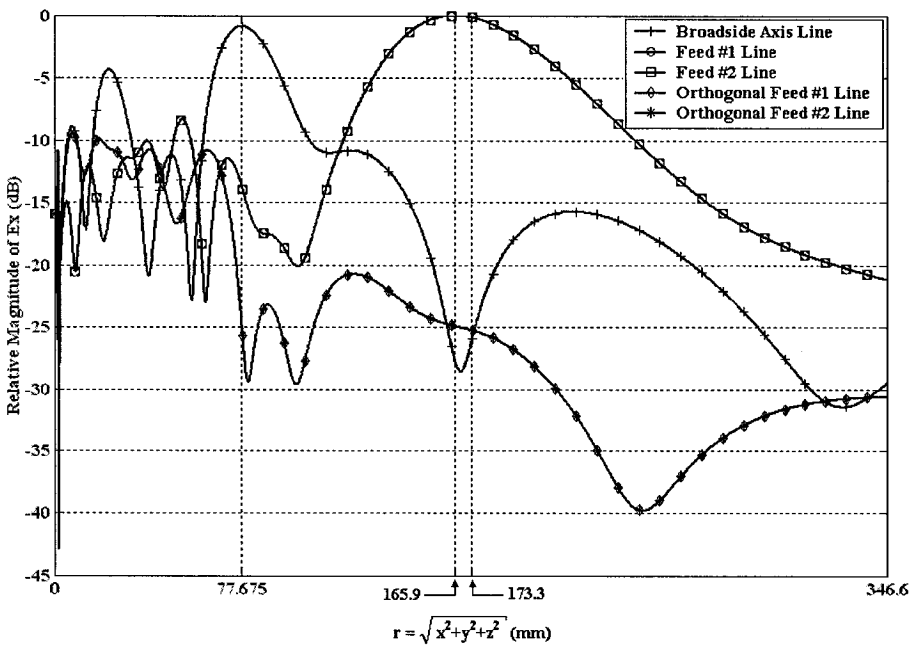

Figure 4.11: Reflected Near Field versus r = $\sqrt{x^2 + y^2 + z^2}$

4.3.3 Simulated Far-Field Patterns

The receive-mode analysis performed in the previous section provides a good indication that the two-feed reflectarray design will effectively focus and split the reflected field to the design location of the feeds. A transmit mode analysis will prove to be equally informative. We will thus further validate the design of the two-feed reflectarray by computing the far-field radiation pattern by making use of Equation (4.21) of Section 4.2.2. to confirm that we have a main beam at broadside and that there are no unexpected results (for example, multiple main beams or grating lobes). Recall that Equation (4.21) is given as

$$E^{reflectarray}(\theta,\phi) = \sum_{n=1}^{N} E_n^{patch}(\theta,\phi,L_n)|E_n|e^{jk_o(x_n sin\theta cos\phi + y_n sin\theta sin\phi)+j\angle E_n} \tag{4.22}$$

To evaluate this expression we need to determine $|E_n|$ and $\angle E_n$ for the elements of the two-feed reflectarray. Recall that $|E_n|$ and $\angle E_n$ are the magnitude and phase of the reflected electric field at the n^{th} patch respectively. In the case of the two-feed design this is a combination of the reflected fields due to the incident fields from the two feeds, as discussed in Section 4.2.1. In that section we derived an equation for the total reflected field (due to the two feeds), at the n^{th} patch, as (refer to Figure 4.2)

$$\begin{aligned} E_n^T = &\frac{1}{|\bar{r}_n^{(1)}|}cos(k_o|\bar{r}_n^{(1)}| - \phi_n) + \frac{1}{|\bar{r}_n^{(2)}|}cos(k_o|\bar{r}_n^{(2)}| - \phi_n) \\ &-j\frac{1}{|\bar{r}_n^{(1)}|}sin(k_o|\bar{r}_n^{(1)}| - \phi_n) - j\frac{1}{|\bar{r}_n^{(2)}|}sin(k_o|\bar{r}_n^{(2)}| - \phi_n) \end{aligned} \tag{4.23}$$

We can now write the magnitude and phase of this total field at the n^{th} patch as

$$|E_n^T| = \left[\left(\frac{1}{|\bar{r}_n^{(1)}|} cos(k_o|\bar{r}_n^{(1)}| - \phi_n) + \frac{1}{|\bar{r}_n^{(2)}|} cos(k_o|\bar{r}_n^{(2)}| - \phi_n) \right)^2 \right.$$
$$\left. + \left(-\frac{1}{|\bar{r}_n^{(1)}|} sin(k_o|\bar{r}_n^{(1)}| - \phi_n) - \frac{1}{|\bar{r}_n^{(2)}|} sin(k_o|\bar{r}_n^{(2)}| - \phi_n) \right)^2 \right]^{\frac{1}{2}} \tag{4.24}$$

$$\angle E_n^T = tan^{-1} \left\{ \frac{-\frac{1}{|\bar{r}_n^{(1)}|} sin(k_o|\bar{r}_n^{(1)}| - \phi_n) - \frac{1}{|\bar{r}_n^{(2)}|} sin(k_o|\bar{r}_n^{(2)}| - \phi_n)}{\frac{1}{|\bar{r}_n^{(1)}|} cos(k_o|\bar{r}_n^{(1)}| - \phi_n) + \frac{1}{|\bar{r}_n^{(2)}|} cos(k_o|\bar{r}_n^{(2)}| - \phi_n)} \right\} \tag{4.25}$$

We therefore have that $|E_n|$ and $\angle E_n$ from Equation (4.22) are given by $|E_n^T|$ and $\angle E_n^T$ respectively. Next let us consider the element pattern. Earlier in Section 4.2.2 we gave equations that will approximately give us the radiation pattern of a single rectangular patch as a function of θ, ϕ and the patch dimensions. Evaluating these expressions in the two principal planes (i.e. E-plane $\phi = 0°$ and H-plane $\phi = 90°$), for a constant width (W = 3mm) and for several length values (L = 1mm,2mm,3mm and 4mm) we get the radiation patterns seen in Figure 4.14. With this information, we can then evaluate the far-field radiation pattern, given by Equation (4.22), for the two-feed reflectarray. It should be noted that this pattern prediction is only approximate. There are several factors that we are not considering in this analysis, such as feed pattern angular dependance, blockage, finite ground and edge effects, and so on. However, as we will see, this analysis is nevertheless quite effective. This analysis was carried out using a routine written in MATLAB. In Figures 4.13 and 4.14 we see the predicted E-plane ($\phi = 0°$) and H-plane ($\phi = 90°$) patterns respectively. These patterns show that the reflectarray is functioning correctly, since we have a distinct main beam at broadside, as expected. Note that we have two large sidelobes at $\approx \pm 60°$ in the H-plane pattern. Initially these were thought to be grating lobes; however after further examination into the element spacing it was determined that these large sidelobes were entirely due to the phase distribution of

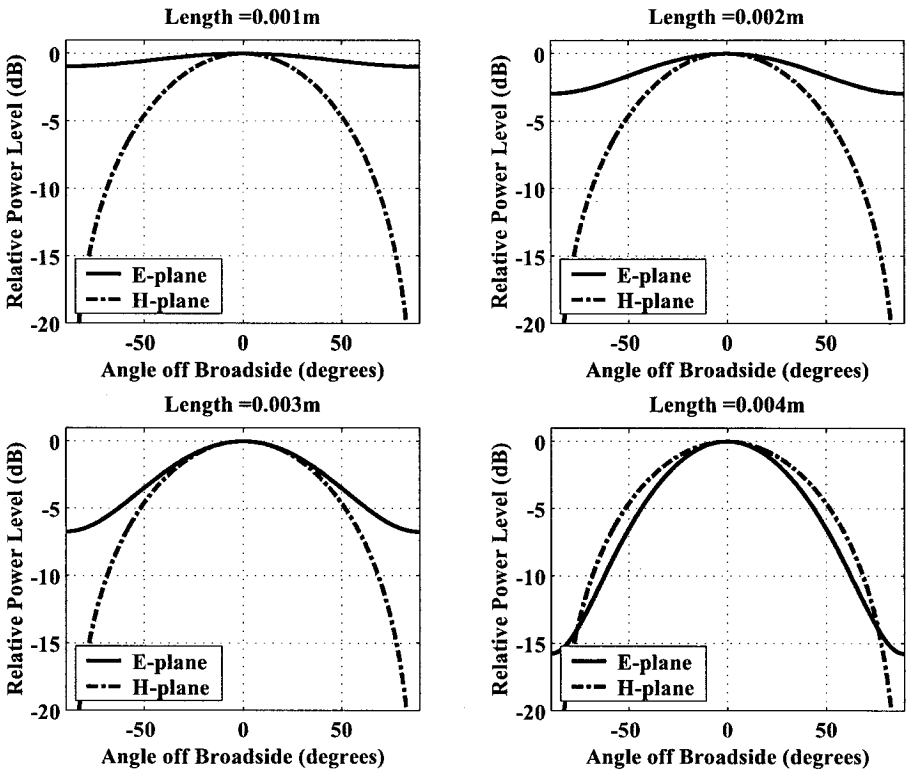

Figure 4.12: Far-Field Radiation Pattern of a Rectangular Microstrip Patch

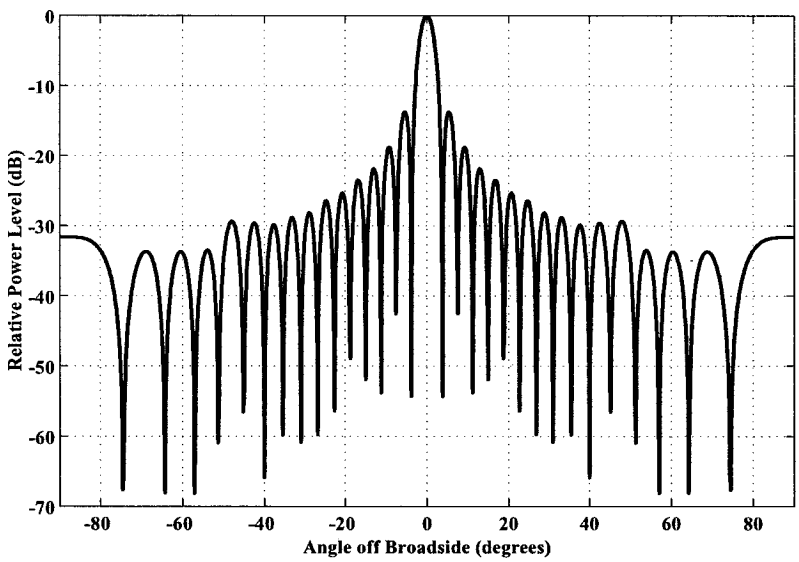

Figure 4.13: Predicted E-Plane Far-Field Radiation Pattern, Feeds Positioned at $(x, y, z) = (0, \pm 77.5mm, 155mm)$

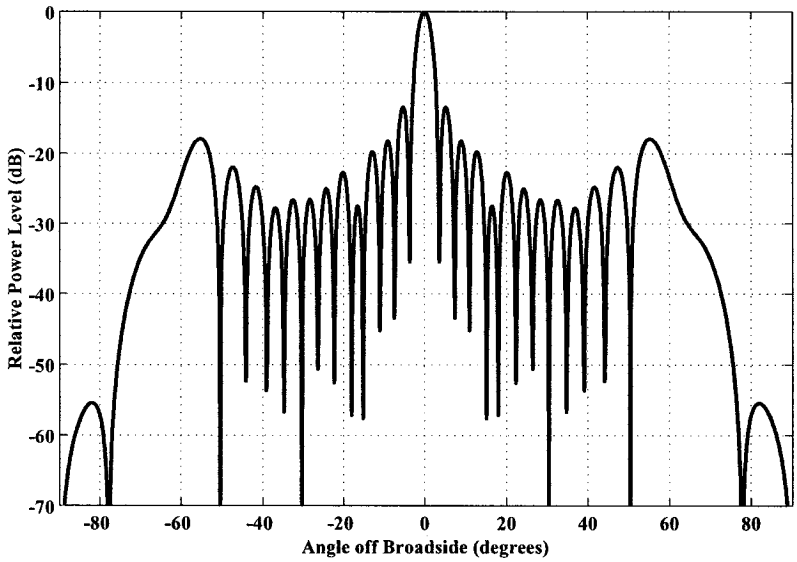

Figure 4.14: Predicted H-Plane Far-Field Radiation Pattern, Feeds Positioned at $(x, y, z) = (0, \pm 77.5mm, 155mm)$

the individual elements. This phase distribution is determined by the combined field analysis for the two-feed reflectarray design. If we wanted to lower the sidelobes by changing the element sizes (and thus their phases) without having to change the feed positions, we would end up with a reflectarray that was not optimally combining the fields from both feeds.

It is noted that by changing the location of the feeds and redesigning the reflectarray in consequence of these new feed locations, we could lower these sidelobes. For instance, Figures 4.15 and 4.16 show the principal plane patterns for a reflectarray with the feeds positioned at $(x, y, z) = (0, -77.5mm, 155mm)$ and $(x, y, z) = (-77.5mm, 0, 155mm)$; these feeds are in orthogonal planes relative to each other).

Nevertheless, in the remainder of this section we continue the discussion of the analysis of the two-feed reflectarray with the feeds positioned

at $(x, y, z) = (0, \pm 77.5mm, 155mm)$. To further validate the approximate array

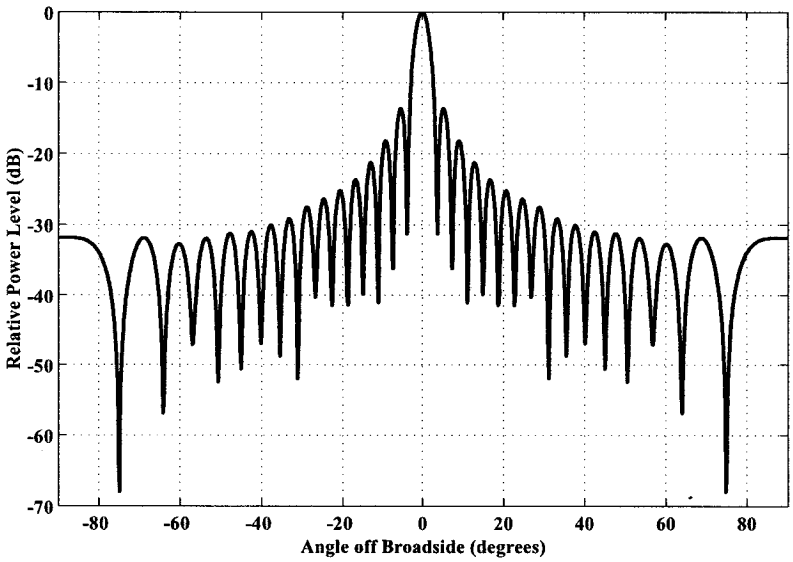

Figure 4.15: Predicted E-Plane Far-Field Radiation Pattern, Feeds Positioned at $(x, y, z) = (0, -77.5mm, 155mm)$ and $(x, y, z) = (-77.5mm, 0, 155mm)$

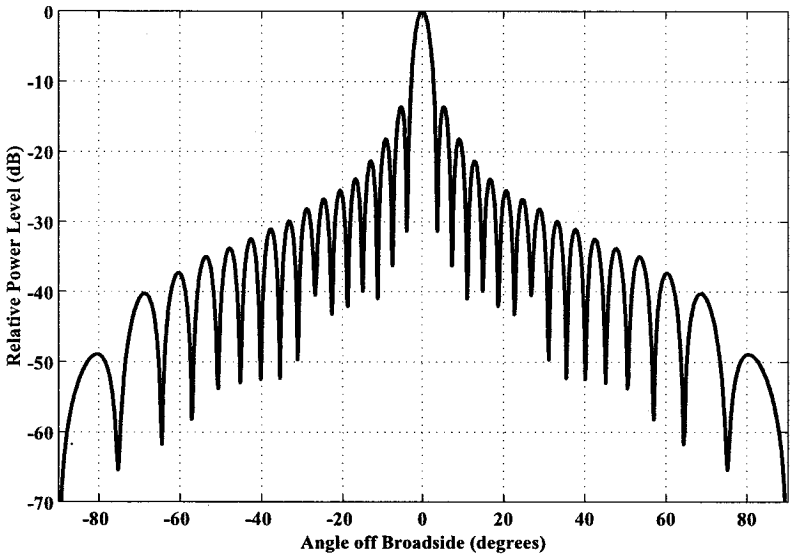

Figure 4.16: Predicted H-Plane Far-Field Radiation Pattern, Feeds Positioned at $(x, y, z) = (0, -77.5mm, 155mm)$ and $(x, y, z) = (-77.5mm, 0, 155mm)$

analysis under discussion, it was used to compute the half power beam width, which was found to be 3.24°. Using an approximate formula [107] for the half power

beam width of a rectangular aperture in free space with a uniform distribution we get $HPBW = 50.6°/(D/\lambda) = 50.6°/(15.5\lambda/\lambda) = 3.27°$. These results closely match each other, further validating the reflectarray design and its analysis using the approximate array theory. With the combination of the receive-mode analysis and the transmit mode pattern prediction using the approximate array theory we can then proceed more confidently to the fabrication of the two-feed spatial power combining reflectarray.

4.3.4 Implementation and Experimental Validation

For the purpose of experimental measurements the received power at each feed was combined using a 3dB power splitter with appropriate lengths of semi-ridged coaxial cables. The test setup is shown schematically in Figure 4.17. In order to perform accurate and informative measurements the entire test setup must be characterized. Figures 4.18 and 4.19 show the magnitude of the S-parameters measured between port#1 and port#2, and port#1 and port#3, respectively from 29-31GHz. Ideally, with a perfect power splitter, lossless semi-ridged coaxial cable and no discontinuity effects, we should see an equal power split between both feeds. In other words the insertion loss between port#1 and port#2, and port#1 and port#3 (i.e. S21 and S31) should both be -3dB (i.e. equal power split). We can see from Figures 4.18 and 4.19 that we have a large ripple and that at 30GHz we don't have precisely -3dB for the insertion loss of both paths. Specifically, the insertion loss terms S21 and S31 are -4.78dB and -4.86dB, respectively. We thus have an excess loss in the path to feed#1 of -1.78dB and in the path to feed#2 of -1.86dB. This excess loss in the feed paths corresponds to (on average) a 1.81db loss in the gain of the antenna. We next need to characterize the phase imbalance between the two paths. In an ideal situation we would want 0° phase difference between the paths, because the

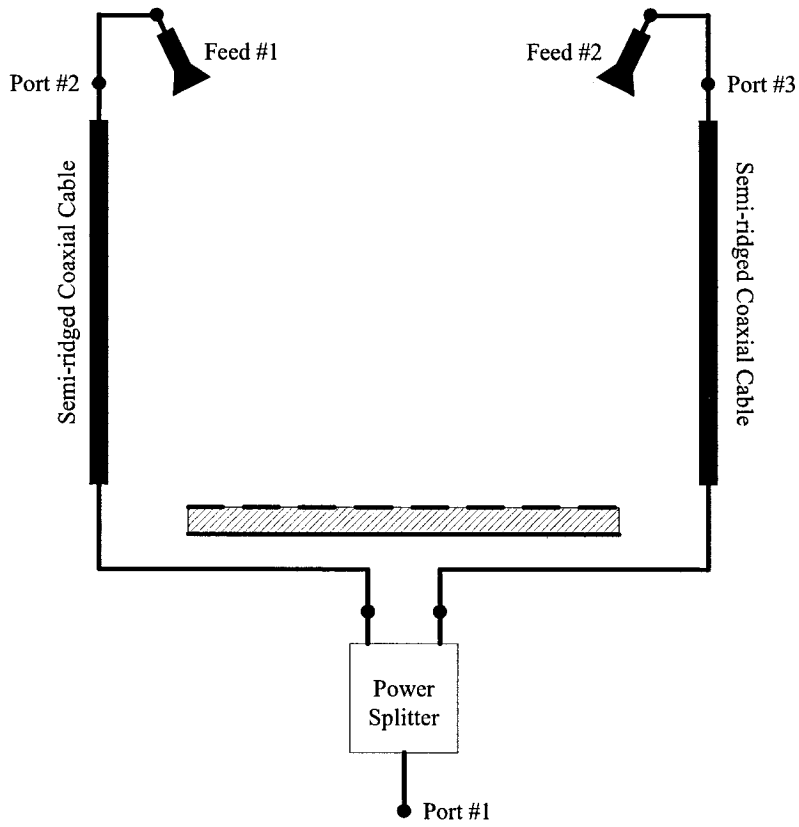

Figure 4.17: Schematic of Reflectarray Feed Arrangement Used for Experimental Work

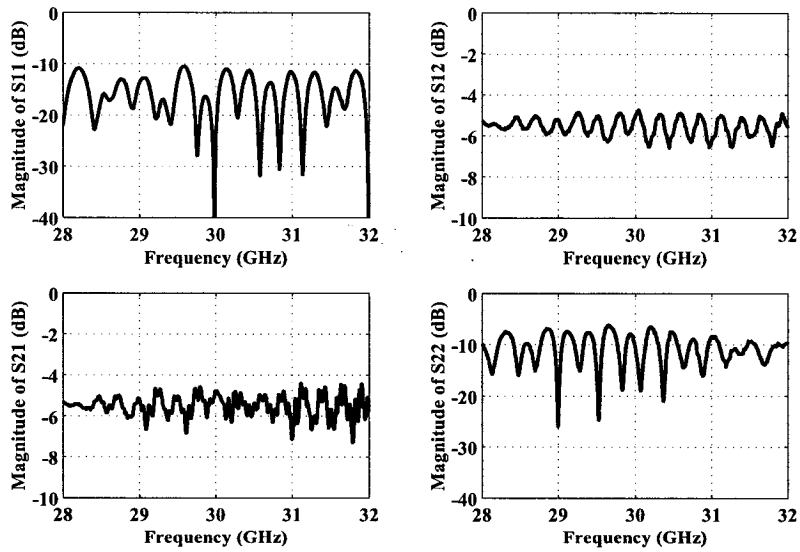

Figure 4.18: Magnitude of S-parameters between port#1 and port#2

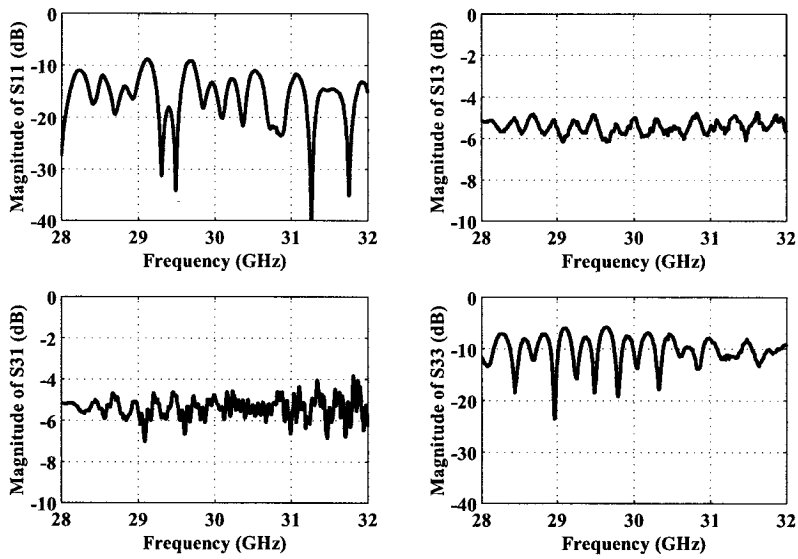

Figure 4.19: Magnitude of S-parameters between port#1 and port#3

combined field analysis described earlier assumes that we have a phase match between the feeds. The phase imbalance between the S21 and S31 was measured and found to be 21.58°. To translate this phase imbalance into a loss in directivity we used the array analysis described in Section 4.3.3 to determine how much loss in directivity we would get if one of the feeds had an excess phase of 21.58°. It was also found that this phase imbalance contributed to a decrease in directivity of 0.149dB. It should be noted that along with a drop in directivity due to the phase imbalance, with this imbalance between the two feeds the computed pattern also exhibits a squint in the main beam of 0.07° . This result shows that the directivity of the reflectarray is fairly tolerant of a phase imbalance. Specifically this tolerance of the phase imbalance was examined computationally and the results are summarized in Table 4.1. Clearly, from Table 4.1 we see that for a very large phase imbalance we would have some significant losses in directivity. However, for an imbalance of up to 40° we only have a loss in directivity of less that 0.5dB; for some applications this could be acceptable. Next we consider the losses due to the input reflection coefficient. We measured the reflection coefficient of the test setup, shown in Figure 4.17, with the feeds connected and

Table 4.1: Phase Imbalance Tolerance

Phase Imbalance	Loss in Directivity	Beam Squint
0°	0.0000dB	0.00°
10°	0.0012dB	0.03°
20°	0.1060dB	0.07°
30°	0.2447dB	0.10°
40°	0.4039dB	0.14°
50°	0.7370dB	0.18°
60°	1.1631dB	0.22°
70°	1.6054dB	0.27°
80°	2.1992dB	0.32°
90°	2.8502dB	0.38°

the magnitude of S11 (input reflection coefficient) is seen plotted in Figure (4.20) versus frequency, from 29GHz to 31GHz. At 30GHz we have an input reflection

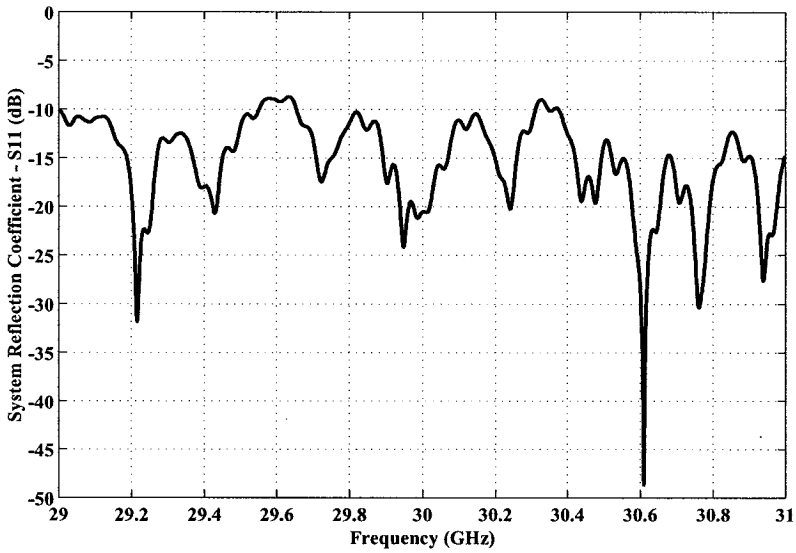

Figure 4.20: Input Reflection Coefficient - S11

coefficient equal to -20.55dB, which translates to a reflection loss of 0.04dB. In order to take all the above-mentioned loss contributions into account we must thus add $1.81dB + 0.149dB + 0.04dB = 1.999dB$ to the peak measured realized gain in order to be able to obtain an accurate number for the directivity, and hence the aperture efficiency. Figures 4.21 and 4.22 show the measured antenna patterns in the two

principal planes. The peak gain for this antenna was measured to be 26.17dBi. If

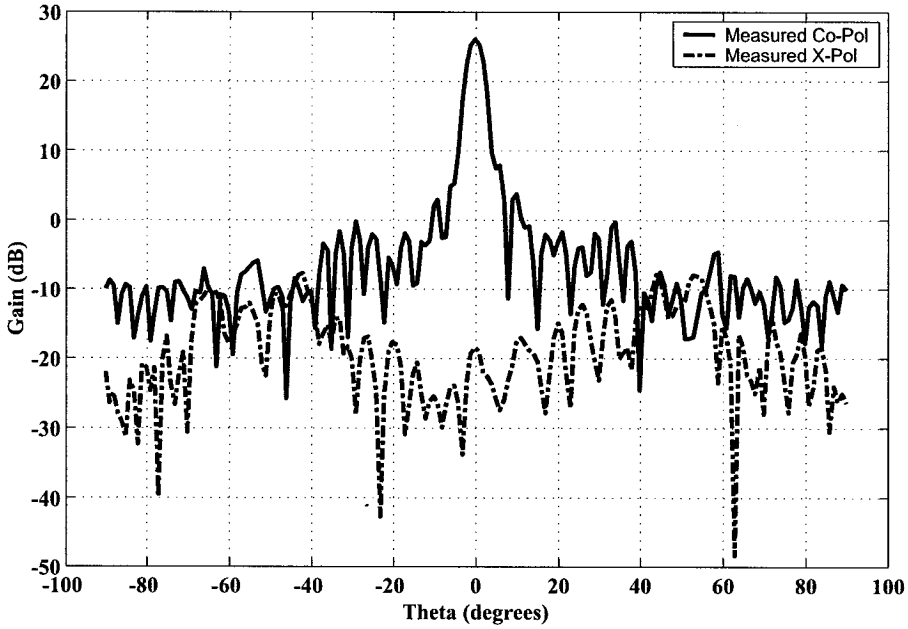

Figure 4.21: Measured E-Plane Far-Field Radiation Pattern

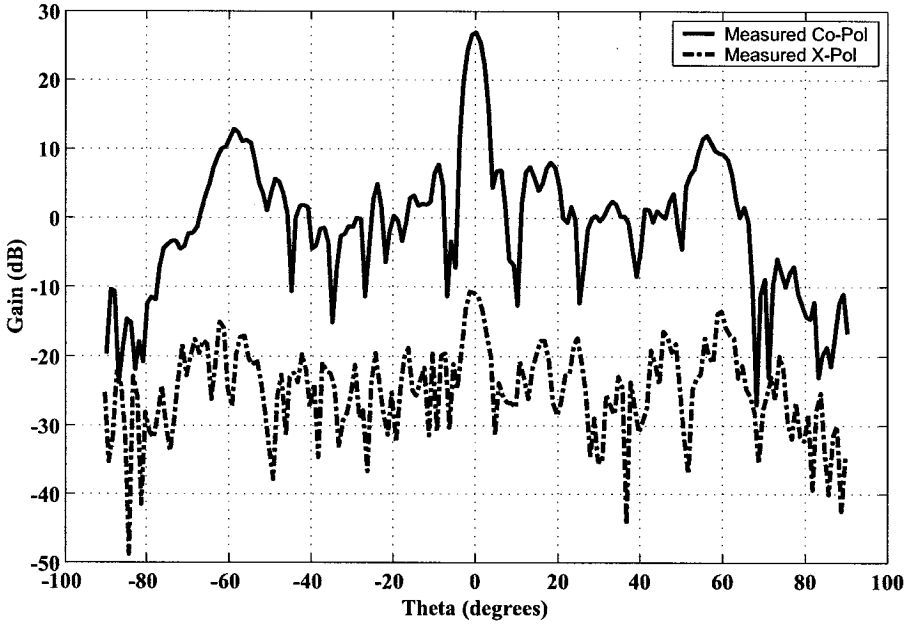

Figure 4.22: Measured H-Plane Far-Field Radiation Pattern

we now add the above 1.999dB we get a corrected gain of 28.17dBi. This yields a 21.73% aperture efficiency, which is fairly low. Recall that in Figure 4.11 that there

appeared to be additional focusing on the broadside axis line when we performed the receive-mode analysis of this reflectarray. This apparent additional focusing might explain the low aperture efficiency of this reflectarray.

To verify that our predicted pattern from the previous Section, using array theory, matches the measured pattern we can normalize the measured pattern and plot it on top of the predicted pattern. Figures 4.23 and 4.24 shows the comparison of the measured and predicted far field patterns, in the two principal planes. We can

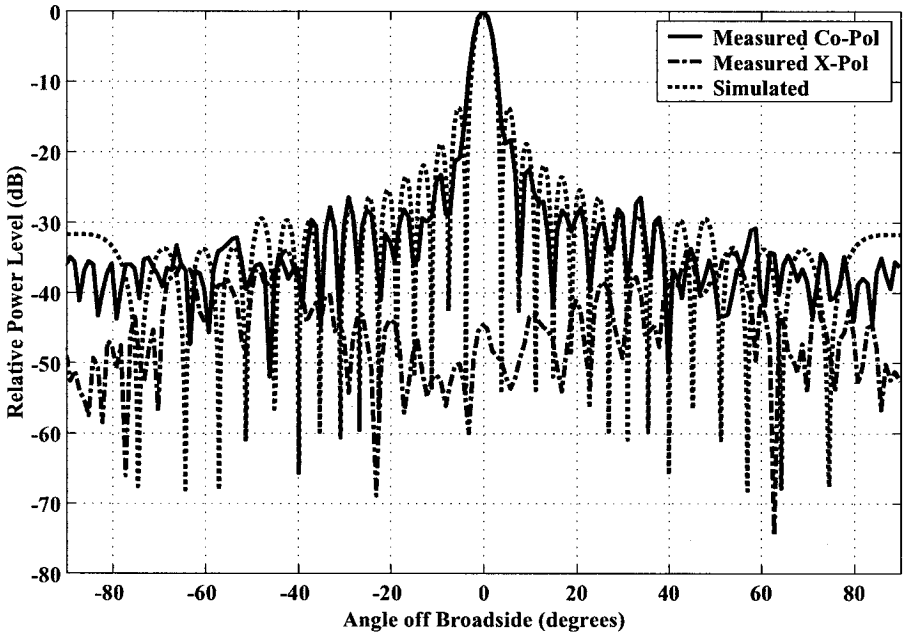

Figure 4.23: Normalized E-Plane Far-Field Radiation Pattern

clearly see the the pattern prediction technics, using the approximate array theory, predicts the far-field patterns quite well.

Even though the reflectarray was designed for proper operation with both feeds in use, the performance was also examined with only feed#1 present (and feed#2

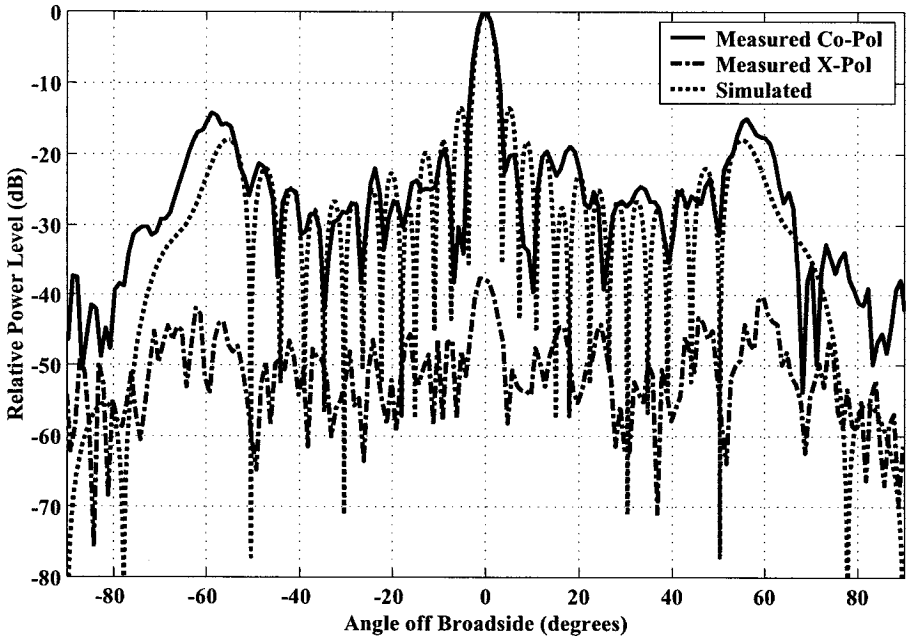

Figure 4.24: Normalized H-Plane Far-Field Radiation Pattern

removed). Under these conditions the total field at the n^{th} patch is

$$E_n^T = \frac{1}{|\bar{r}_n^{(1)}|} cos(k_o|\bar{r}_n^{(1)}| - \phi_n) - j\frac{1}{|\bar{r}_n^{(1)}|} sin(k_o|\bar{r}_n^{(1)}| - \phi_n) \tag{4.26}$$

We can write the magnitude and the phase of this field as

$$|E_n^T| = \left[\left(\frac{1}{|\bar{r}_n^{(1)}|} cos(k_o|\bar{r}_n^{(1)}| - \phi_n) \right)^2 + \left(-\frac{1}{|\bar{r}_n^{(1)}|} sin(k_o|\bar{r}_n^{(1)}| - \phi_n) \right)^2 \right]^{\frac{1}{2}} \tag{4.27}$$

and

$$\angle E_n^T = tan^{-1} \left\{ \frac{-\frac{1}{|\bar{r}_n^{(1)}|} sin(k_o|\bar{r}_n^{(1)}| - \phi_n)}{\frac{1}{|\bar{r}_n^{(1)}|} cos(k_o|\bar{r}_n^{(1)}| - \phi_n)} \right\} \tag{4.28}$$

We can then use this magnitude and phase in Equation (4.21) to predict the pattern of this reflectarray configuration. Figure 4.25 shows the measured normalized H-plane radiation pattern with only feed#1 present, as well as the simulated far-field pattern in the single feed configuration. We can see that there are high wide-angle lobes in

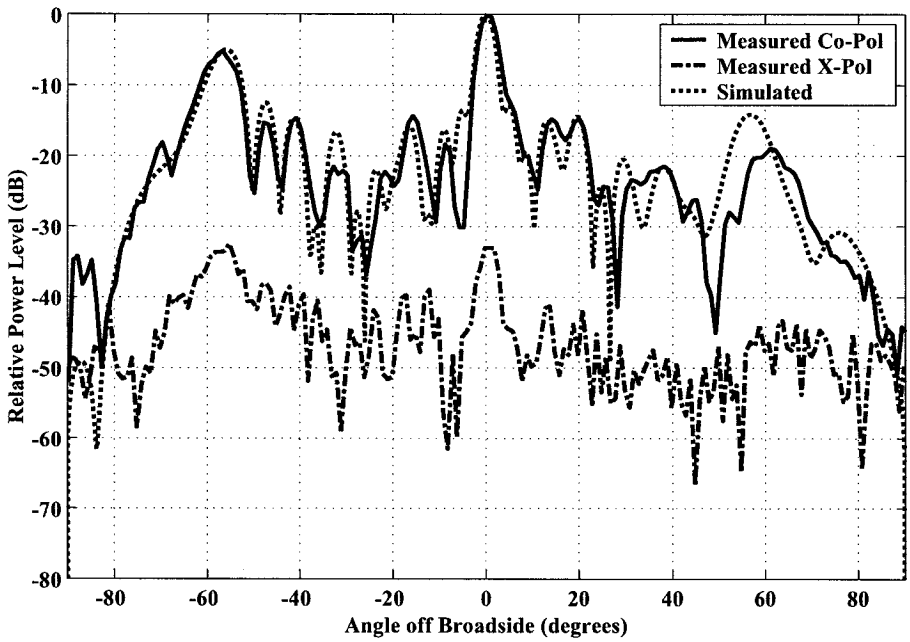

Figure 4.25: Normalized H-Plane Far-Field Radiation Pattern (Single-Feed)

the vicinity of $\pm 60^{(\circ)}$, and that their presence is correctly predicted. There are no such lobes either predicted or measured in the E-plane pattern, and thus these are not shown. Similar results are of course found when only feed#2 illuminates the reflectarray and feed#1 is removed. It is clear from this result for the "incomplete" antenna (i.e. one feed only) that the design procedure and approximate array theory "captures" the principal physical phenomena involved.

The evaluation of the two-feed design just discussed was intended to validate the new design procedure of Section 4.2. This has been achieved. A complete evaluation of the device as an antenna/power-combiner will be done in Section 4.4, which considers a four-feed design.

4.4 Four-Feed Design

4.4.1 Initial Comments

We will now expand multi-feed reflectarrays, for spatial power combining, to a design with 4 feeds. We then have a reflectarray structure that is being illuminated with four feeds, as seen in Figure 4.26. The reflectarray, if designed correctly, will correct

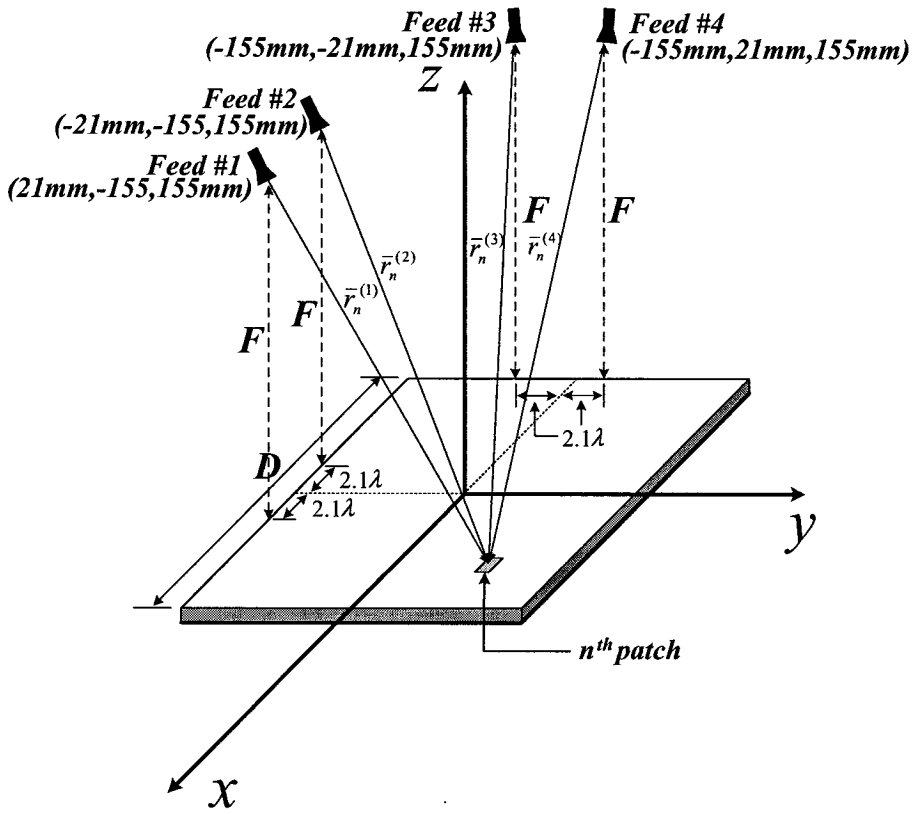

Figure 4.26: Geometry of a Four-Feed Reflectarray

the phase of the field incident on the reflectarray from the four feeds. The reflectarray will be designed to have a single main beam at broadside with the combined power of all four feeds. The design that we will be considering here is a 15.5λ square reflectarray at 30GHz with the main beam at broadside and an F/D ratio of 1. Figure 4.26 shows that the reflectarray is centered at the origin; the feeds are located at $(x, y, z) = (\pm 2.1\lambda, -7.75\lambda, 15.5\lambda)$ and $(x, y, z) = (-7.75\lambda, \pm 2.1\lambda, 15.5\lambda)$. The feeds are placed in such a manner as to have an x-directed linearly polarized E-field.

With a unit cell size of 5mm this reflectarray has 961 elements, which are printed on 0.020" Rogers RO3003 substrate ($\varepsilon_r = 3.0$). With these design criteria in mind, we can proceed to the design of the microstrip patch elements. To accomplish this we will use the general combined field design equation described in Section 4.2.1. Specifically we will make use of Equation (4.7). Evaluating this equation with $M = 4$ yields the equation

$$\angle E_n^T = tan^{-1}\left\{\frac{-\frac{1}{|\bar{r}_n^{(1)}|}sin(k_o|\bar{r}_n^{(1)}| - \phi_n) - \frac{1}{|\bar{r}_n^{(2)}|}sin(k_o|\bar{r}_n^{(2)}| - \phi_n)}{\frac{1}{|\bar{r}_n^{(1)}|}cos(k_o|\bar{r}_n^{(1)}| - \phi_n) + \frac{1}{|\bar{r}_n^{(2)}|}cos(k_o|\bar{r}_n^{(2)}| - \phi_n)} \right.$$
$$\left. \frac{-\frac{1}{|\bar{r}_n^{(3)}|}sin(k_o|\bar{r}_n^{(3)}| - \phi_n) - \frac{1}{|\bar{r}_n^{(4)}|}sin(k_o|\bar{r}_n^{(4)}| - \phi_n)}{\frac{1}{|\bar{r}_n^{(3)}|}cos(k_o|\bar{r}_n^{(3)}| - \phi_n) + \frac{1}{|\bar{r}_n^{(4)}|}cos(k_o|\bar{r}_n^{(4)}| - \phi_n)}\right\} \tag{4.29}$$

As was the case in the two-feed design, the equation formed by setting (4.29) equal to zero will be solved using an optimization routine in MATLAB (*fsolve*). $\angle E_n^T$ was found with a maximum error, over all the elements, of 1.2107×10^{-7} radians, the optimization routine providing the values of ϕ_n (i.e. required reflected phase). We then use the curve in Figure 4.5 to determine the patch sizes. The patch distribution shown in Figure 4.27 is obtained for the four-feed reflectarray.

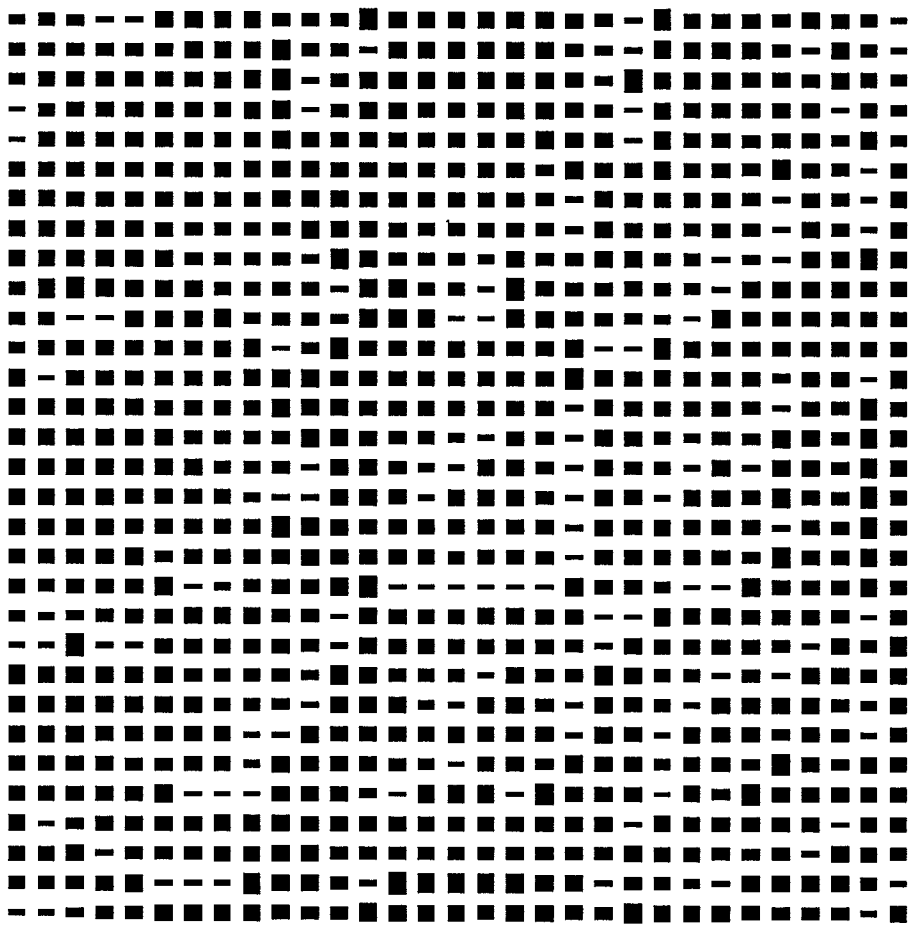

Figure 4.27: Distribution of Relative Patch Sizes for the Four-Feed Reflectarray

4.4.2 Receive Mode Analysis and Interpretation

We will again make use of the receive-mode analysis described in Chapter 3. However, we can see in Figure 4.27 that there is no symmetry that can be exploited to reduce the solution time of this structure. In order to solve this structure we had to use a unix workstation to simulate the entire structure; a structure of this electrical size could not be solved on a PC. The structure was solved and again we used HFSS's post processor to compute the near field along lines of interest. As was the case for the two feed reflectarray, the lines along which we are specifically interested to compute the reflected near field start at the origin, pass through each of the feed locations, and extend beyond them. In other words the lines will all start at $(x, y, z) = (0, 0, 0)$ and extend to $(x, y, z) = (\pm 42mm, -155mm, 310mm)$ and $(x, y, z) = (-155mm, \pm 42mm, 310mm)$. Figure 4.28 shows the computed reflected near field along these lines. As was done in the two feed case we will look at

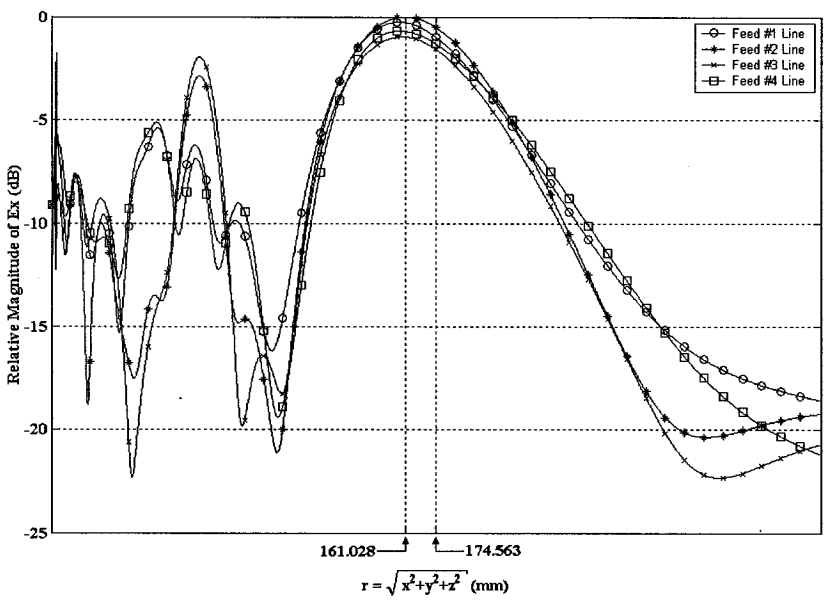

Figure 4.28: Reflected Near Field versus r = $\sqrt{x^2 + y^2 + z^2}$

the near field along additional lines to ensure that there is no apparent focusing

along any other lines. For this we will look at 4 lines orthogonal to the four "feed lines" detailed above. Namely, the additional lines will have their origin at $(x, y, z) = (0, 0, 0)$ and extend to $(x, y, z) = (\pm 42mm, 155mm, 310mm)$ and $(x, y, z) = (155mm, \pm 42mm, 310mm)$. In addition to these four "orthogonal" lines we will also look at the field along the broadside axis (the z-axis). The computed reflected near fields along these lines are plotted in Figure 4.29, normalized to the peak value of the feed lines. We can see from Figure 4.29 that there is no obvious

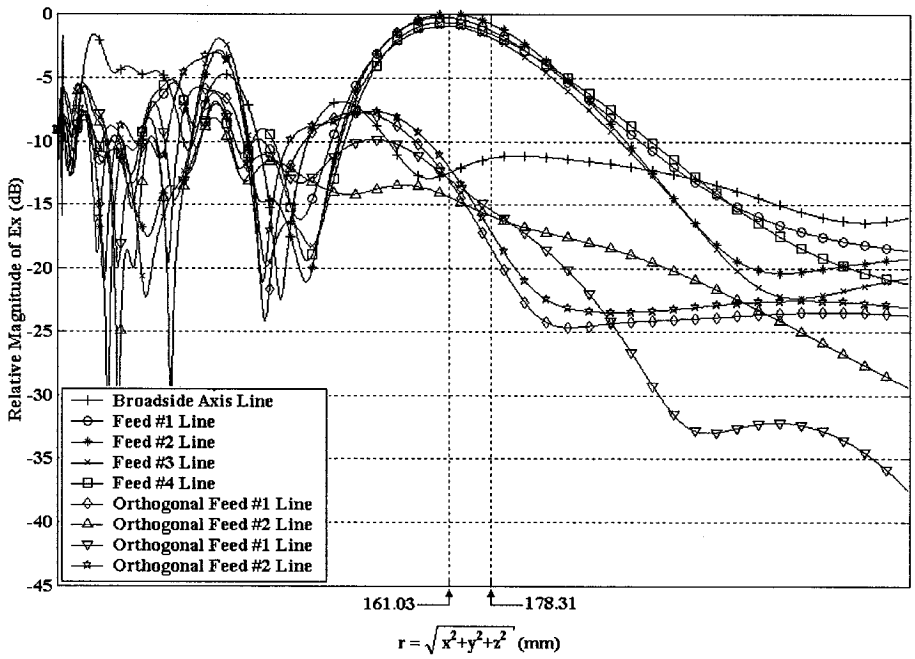

Figure 4.29: Reflected Near Field versus r = $\sqrt{x^2 + y^2 + z^2}$

focusing along any of the lines that do not pass through the location of a feed. It should be noted that, as opposed to the two-feed case where the computed reflected field along the lines that passed through the feed locations were equal, in the four-feed case we see a slight difference in the level of the field between the four lines that pass through the feed locations. It is believed that this is due to the asymmetry of the four-feed reflectarray design. However the receive-mode analysis has revealed a distinct focusing near the location of the four feeds. These results suggest that there

is no design flaws with the four-feed design.

4.4.3 Simulated Far-Field Patterns

As was done in the two feed case, we will make use of the approximate array theory to plot a predicted far-field pattern for this reflectarray. We will again make use of Equation (4.21) from Section 4.2.2. The reflected field at the n^{th} patch for a reflectarray with four feeds is given by

$$\begin{aligned} E_n^T = & \frac{1}{|\bar{r}_n^{(1)}|}cos(k_o|\bar{r}_n^{(1)}| - \phi_n) + \frac{1}{|\bar{r}_n^{(2)}|}cos(k_o|\bar{r}_n^{(2)}| - \phi_n) \\ & \frac{1}{|\bar{r}_n^{(3)}|}cos(k_o|\bar{r}_n^{(3)}| - \phi_n) + \frac{1}{|\bar{r}_n^{(4)}|}cos(k_o|\bar{r}_n^{(4)}| - \phi_n) \\ & -j\frac{1}{|\bar{r}_n^{(1)}|}sin(k_o|\bar{r}_n^{(1)}| - \phi_n) - j\frac{1}{|\bar{r}_n^{(2)}|}sin(k_o|\bar{r}_n^{(2)}| - \phi_n) \\ & -j\frac{1}{|\bar{r}_n^{(3)}|}sin(k_o|\bar{r}_n^{(3)}| - \phi_n) - j\frac{1}{|\bar{r}_n^{(4)}|}sin(k_o|\bar{r}_n^{(4)}| - \phi_n) \end{aligned} \tag{4.30}$$

The magnitude and the phase of this field are therefore

$$\begin{aligned} |E_n^T| = & \left[\left(\frac{1}{|\bar{r}_n^{(1)}|}cos(k_o|\bar{r}_n^{(1)}| - \phi_n) + \frac{1}{|\bar{r}_n^{(2)}|}cos(k_o|\bar{r}_n^{(2)}| - \phi_n) \right. \right. \\ & \left. + \frac{1}{|\bar{r}_n^{(3)}|}cos(k_o|\bar{r}_n^{(3)}| - \phi_n) + \frac{1}{|\bar{r}_n^{(4)}|}cos(k_o|\bar{r}_n^{(4)}| - \phi_n) \right)^2 \\ & + \left(-\frac{1}{|\bar{r}_n^{(1)}|}sin(k_o|\bar{r}_n^{(1)}| - \phi_n) - \frac{1}{|\bar{r}_n^{(2)}|}sin(k_o|\bar{r}_n^{(2)}| - \phi_n) \right. \\ & \left. \left. -\frac{1}{|\bar{r}_n^{(3)}|}sin(k_o|\bar{r}_n^{(3)}| - \phi_n) - \frac{1}{|\bar{r}_n^{(4)}|}sin(k_o|\bar{r}_n^{(4)}| - \phi_n) \right)^2 \right]^{\frac{1}{2}} \end{aligned} \tag{4.31}$$

and

$$\angle E_n^T = tan^{-1}\left\{\frac{-\frac{1}{|\bar{r}_n^{(1)}|}sin(k_o|\bar{r}_n^{(1)}| - \phi_n) - \frac{1}{|\bar{r}_n^{(2)}|}sin(k_o|\bar{r}_n^{(2)}| - \phi_n)}{\frac{1}{|\bar{r}_n^{(1)}|}cos(k_o|\bar{r}_n^{(1)}| - \phi_n) + \frac{1}{|\bar{r}_n^{(2)}|}cos(k_o|\bar{r}_n^{(2)}| - \phi_n)} \right.$$
$$\left. \frac{-\frac{1}{|\bar{r}_n^{(3)}|}sin(k_o|\bar{r}_n^{(3)}| - \phi_n) - \frac{1}{|\bar{r}_n^{(4)}|}sin(k_o|\bar{r}_n^{(4)}| - \phi_n)}{\frac{1}{|\bar{r}_n^{(3)}|}cos(k_o|\bar{r}_n^{(3)}| - \phi_n) + \frac{1}{|\bar{r}_n^{(4)}|}cos(k_o|\bar{r}_n^{(4)}| - \phi_n)} \right\} \quad (4.32)$$

respectively. Again we have that $|E_n|$ and $\angle E_n$ from Equation (4.22) are given by (4.31) and (4.32) respectively. The element patterns will be the same as those described in the two-feed case in Section 4.3.3. Figures 4.30 and 4.31 show the computed patterns of this reflectarray in the principal planes, namely $\phi = 0°$ (E-Plane) and $\phi = 90°$ (H-Plane), respectively. It can be seen in Figures 4.30 and 4.31 that we

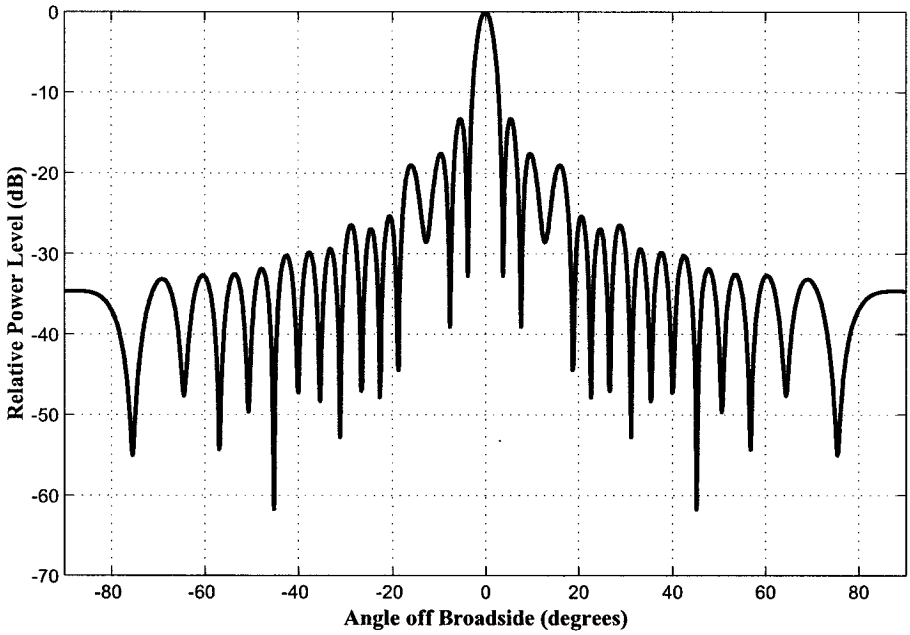

Figure 4.30: Predicted E-Plane Far-Field Radiation Pattern of the Four-Feed Reflectarray

do not have any large sidelobes in the vicinity of $\pm 60°$ as we had in the two-feed case. Indeed, recall that we showed in the two-feed case that by changing the position of the feeds we could eliminate these large sidelobes. This is what was done in the

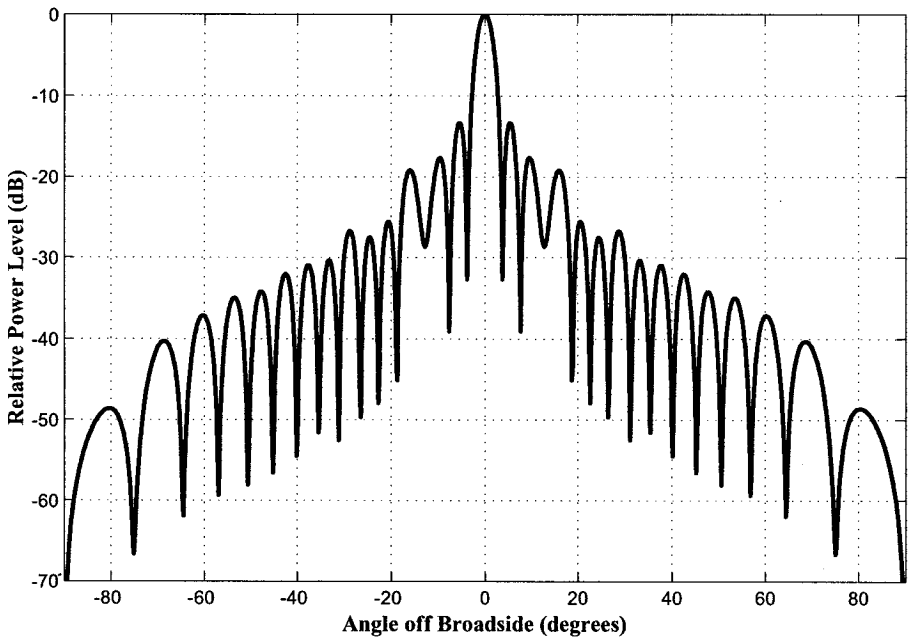

Figure 4.31: Predicted H-Plane Far-Field Radiation Pattern of the Four-Feed Reflectarray

four-feed case. Prior to selecting the feed positions we performed a study of the predicted radiation patterns and the feed positions that were selected yielded the radiation patterns with the lowest sidelobes.

4.4.4 Implementation and Experimental Validation

For the purpose of experimental measurements the received power at each feed was combined using a 4-way microstrip power splitter, as seen in Figure 4.32, with appropriate lengths of semi-ridged coaxial cables between the splitter ports and the feeds. The test setup is shown schematically in Figure 4.33. As was the case in the two feed reflectarray set up, the four feed reflectarrays feed network (i.e. microstrip power splitter and semi-ridged coax combination) must be characterized. A more precise characterization of the feed network was done in this four-feed case than was done in the two-feed case, since we wish to determine the combining efficiency of the reflectarray/spatial power-combiner. We use a scattering parameter analysis. By

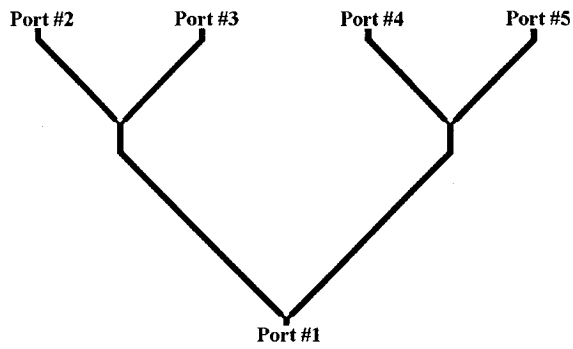

Figure 4.32: 4-Way Microstrip Power Splitter

definition, given the scattering matrix of the 5-port network (1 input port and 4 output ports) we may write:

$$\begin{aligned} b_1 &= S_{11}a_1 + S_{12}a_2 + S_{13}a_3 + S_{14}a_4 + S_{15}a_5 \\ b_2 &= S_{21}a_1 + S_{22}a_2 + S_{23}a_3 + S_{24}a_4 + S_{25}a_5 \\ b_3 &= S_{31}a_1 + S_{32}a_2 + S_{33}a_3 + S_{34}a_4 + S_{35}a_5 \\ b_4 &= S_{41}a_1 + S_{42}a_2 + S_{43}a_3 + S_{44}a_4 + S_{45}a_5 \\ b_5 &= S_{51}a_1 + S_{52}a_2 + S_{53}a_3 + S_{54}a_4 + S_{55}a_5 \end{aligned} \tag{4.33}$$

The scattering parameters S_{ij} were measured using a vector network analyzer. We have also measured the input reflection coefficient Γ_n (n=2,3,4,5) of each of the feed horns that are connected as "loads" at the output ports (ports 2,3,4,5) of the 5 port network in Figure 4.33 . We can then write:

$$\begin{aligned} a_2 &= \Gamma_2 b_2 \\ a_3 &= \Gamma_3 b_3 \\ a_4 &= \Gamma_4 b_4 \\ a_5 &= \Gamma_5 b_5 \end{aligned} \tag{4.34}$$

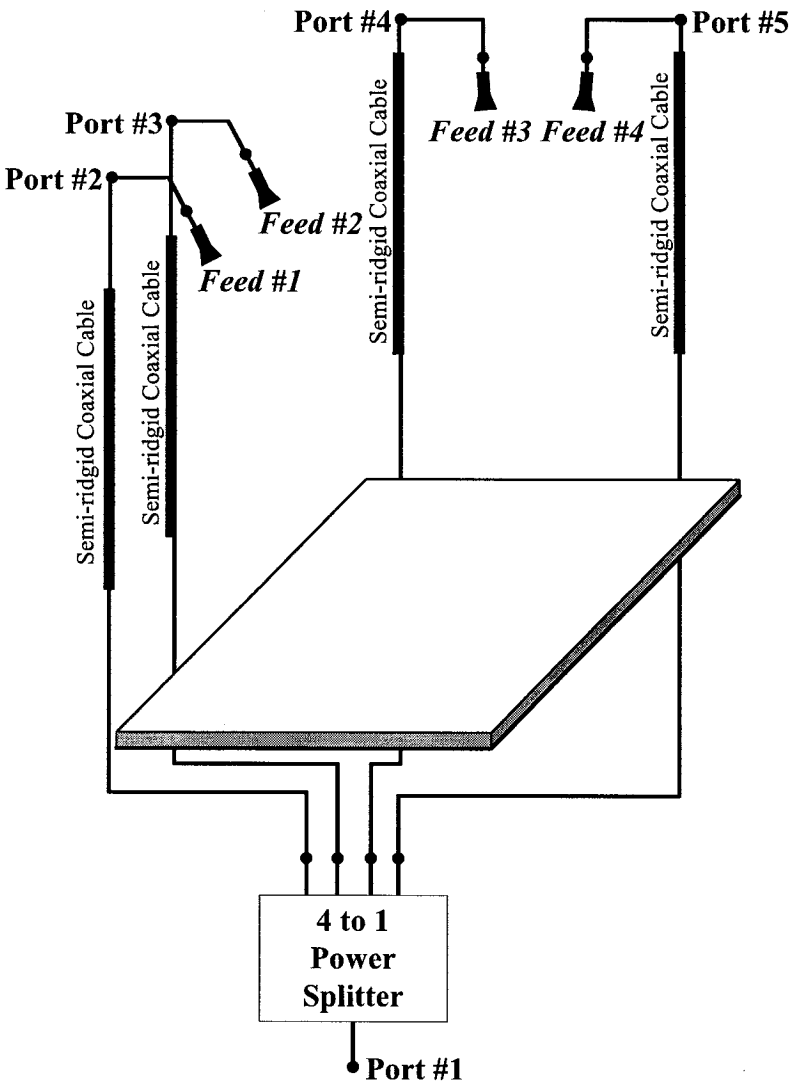

Figure 4.33: Schematic of Reflectarray Feed Arrangement Used for Experimental Work

We can now substitute Equations (4.34) into Equations (4.33) to get:

$$
\begin{aligned}
b_1 &= S_{11}a_1 + S_{12}\Gamma_2 b_2 + S_{13}\Gamma_3 b_3 + S_{14}\Gamma_4 b_4 + S_{15}\Gamma_5 b_5 \\
b_2 &= S_{21}a_1 + S_{22}\Gamma_2 b_2 + S_{23}\Gamma_3 b_3 + S_{24}\Gamma_4 b_4 + S_{25}\Gamma_5 b_5 \\
b_3 &= S_{31}a_1 + S_{32}\Gamma_2 b_2 + S_{33}\Gamma_3 b_3 + S_{34}\Gamma_4 b_4 + S_{35}\Gamma_5 b_5 \\
b_4 &= S_{41}a_1 + S_{42}\Gamma_2 b_2 + S_{43}\Gamma_3 b_3 + S_{44}\Gamma_4 b_4 + S_{45}\Gamma_5 b_5 \\
b_5 &= S_{51}a_1 + S_{52}\Gamma_2 b_2 + S_{53}\Gamma_3 b_3 + S_{54}\Gamma_4 b_4 + S_{55}\Gamma_5 b_5
\end{aligned}
\tag{4.35}
$$

We can now re-arrange Equations (4.35) as follows:

$$b_1 = S_{11}a_1 + S_{12}\Gamma_2 b_2 + S_{13}\Gamma_3 b_3 + S_{14}\Gamma_4 b_4 + S_{15}\Gamma_5 b_5 \tag{4.36}$$

$$(1 - S_{22}\Gamma_2)b2 = S_{21}a_1 + S_{23}\Gamma_3 b_3 + S_{24}\Gamma_4 b_4 + S_{25}\Gamma_5 b_5 \tag{4.37}$$

$$(1 - S_{33}\Gamma_2)b3 = S_{31}a_1 + S_{32}\Gamma_2 b_2 + S_{34}\Gamma_4 b_4 + S_{35}\Gamma_5 b_5 \tag{4.38}$$

$$(1 - S_{44}\Gamma_2)b4 = S_{41}a_1 + S_{42}\Gamma_2 b_2 + S_{43}\Gamma_3 b_3 + S_{45}\Gamma_5 b_5 \tag{4.39}$$

$$(1 - S_{55}\Gamma_2)b5 = S_{51}a_1 + S_{52}\Gamma_2 b_2 + S_{53}\Gamma_3 b_3 + S_{54}\Gamma_4 b_4 \tag{4.40}$$

Equations (4.37) to (4.40) can be further re-arranged as a set of four linear simultaneous equations with four unknowns b_2/a_1, b_3/a_1, b_4/a_1, b_5/a_1 as follows:

$$\begin{bmatrix} (1 - S_{22}\Gamma_2) & -S_{23}\Gamma_3 & -S_{24}\Gamma_4 & S_{25}\Gamma_5 \\ -S_{32}\Gamma_2 & (1 - S_{33}\Gamma_3) & -S_{34}\Gamma_4 & -S_{35}\Gamma_5 \\ -S_{42}\Gamma_2 & -S_{43}\Gamma_3 & (1 - S_{44}\Gamma_4) & -S_{45}\Gamma_5 \\ -S_{52}\Gamma_2 & -S_{53}\Gamma_3 & -S_{54}\Gamma_4 & (1 - S_{55}\Gamma_5) \end{bmatrix} \begin{bmatrix} b_2/a_1 \\ b_3/a_1 \\ b_4/a_1 \\ b_5/a_1 \end{bmatrix} = \begin{bmatrix} S_{21} \\ S_{31} \\ S_{41} \\ S_{51} \end{bmatrix} \tag{4.41}$$

After substituting the complex numerical values of the scattering parameters and the horn reflection coefficients in (4.41) the set of equations was solved to give

$$\begin{aligned} b_2/a_1 &= 0.3280e^{-j^*171.255^\circ} \\ b_3/a_1 &= 0.3102e^{j^*75.8931^\circ} \\ b_4/a_1 &= 0.3165e^{j^*168.5534^\circ} \\ b_5/a_1 &= 0.3246e^{-j^*145.6260^\circ} \end{aligned} \tag{4.42}$$

Now that the b_n/a_1 (n=2,3,4,5) are known, the input reflection coefficient at port #1 is obtained from Equation (4.36) as:

$$\Gamma_{IN} = b_1/a_1 = S_{11} + S_{12}\Gamma_2(b_2/a_1) + S_{13}\Gamma_3(b_3/a_1) + S_{14}\Gamma_4(b_4/a_1) + S_{15}\Gamma_5(b_5/a_1) \tag{4.43}$$

Now that we know these quantities (i.e. Γ_{IN} and b_n/a_1) we can determine how much power is reflected at the input (port #1) of the reflectarray and how much power will be dissipated by the 4-way microstrip power splitter and the semi-ridged coaxial cables. This information will allow us to correct the measured realized gain of the antenna as it was done in the two-feed reflectarray, by removing the effects of the power splitter excess loss and the mismatch that it causes. To do this we must define some important quantities, the first two being the incident power at port#1 given by:

$$P_{INC} = |a_1|^2/2 \tag{4.44}$$

and the reflected power at the input port (port #1)

$$P_{REF} = |b_1|^2/2 = |\Gamma_{IN}|^2 P_{INC} \tag{4.45}$$

Now the power accepted by the antenna (i.e. feed horn and reflectarray combination) is given by:

$$P_{Accepted}^{Actual} = \left\{ \sum_{n=2}^{5} |b_n/a_1|^2 \right\} P_{INC} \tag{4.46}$$

This accounts for the non-zero reflection coefficient Γ_{IN} and the power dissipated by the microstrip power splitter and semi-ridged coaxial cables. If the splitter/coax combination was matched (i.e. $\Gamma_{IN} = 0$), and there was no power dissipated in the splitter/coax, combination the accepted power would be

$$P_{Accepted}^{Ideal} = P_{INC} \tag{4.47}$$

If we take a ratio of the actual accepted power to that of the ideal case, we will be able to determine what must be added to the measured gain in order to account for

the splitter/coax combination losses and mismatch. We then get:

$$\frac{P_{Accepted}^{Actual}}{P_{Accepted}^{Ideal}} = \left\{ \sum_{n=2}^{5} |b_n/a_1|^2 \right\} \tag{4.48}$$

If we use the b_n/a_1 (n=2,3,4,5) values that were determined earlier and given in Equations (4.42) we get

$$10 * Log \left\{ \sum_{n=2}^{5} |b_n/a_1|^2 \right\} = -3.8786 dB \tag{4.49}$$

We must thus add 3.8786dB to the measured realized gain value for the four-feed reflectarray to account for the mismatch and the losses of the splitter/coax combination.

The measured realized gain of course includes the effects of the non-zero relative phases at the outputs of the splitter/coax combination. This phase imbalance serves to decrease the gain from the value that would have been achieved had these ports (and hence the four feeds) been in phase. In order to estimate the gain loss due to the phase imbalance we will compare the level of the radiation pattern computed with all four feeds fed in phase to that with the feeds having the imperfect phases determined in expression (4.42). Since we are only altering the relative phases of the feeds in the above comparison and not the feed excitation amplitudes, the difference between the pattern levels (i.e. the electric field values) is equivalent to the difference in the true directivities in the two instances.

Figure 4.34 shows the normalized measured radiation pattern of the four-feed antenna. Also shown is the predicted normalized radiation pattern for the case where the relative feed phases from (4.42) are used. The presence of a relatively high predicted near-in sidelobe on the side of the main lobe clearly does not match that of the measured patterns. It would appear that the relative phases at the

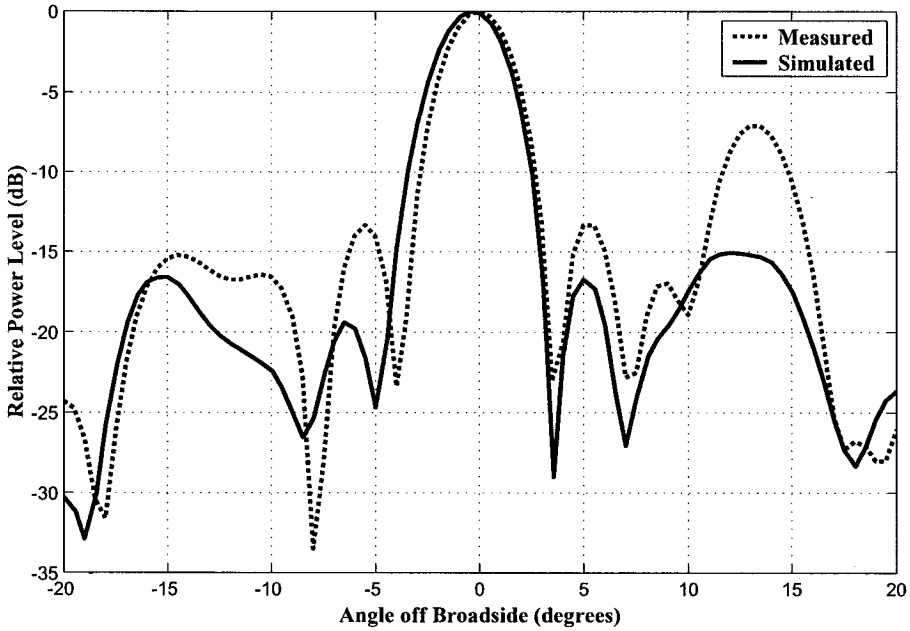

Figure 4.34: Normalized E-Plane Far-Field Radiation Pattern with Phase Imbalance from (4.42)

outputs of the power divider (and hence the four feeds) are not as different as expressions (4.42) would indicate. It must be remembered that the computed phases in expressions (4.42) were done using the measured input reflection coefficients of the feeds, but do not include coupling between the feeds. Although such coupling is very low (approximately -35dB for adjacent feeds in an E-plane array, -53dB for adjacent feeds in an H-plane array and -54dB for feeds in orthogonal positions), it would appear that it causes the final actual relative phases of the four feeds to be much closer than the values in (4.42). There is also an additional factor that could contribute to the variation in the phase imbalance and it is that when the coaxial cables are connected to the feed horns the additional flexing in the semi-ridged cables, at 30GHz, could cause a change in the phase at the splitter/coax output. In order to obtain a more realistic estimate of the actual phase imbalance we have adjusted the relative phases of the four feeds so as to obtain a better "match" between the measured and computed normalized radiation patterns over

the angular range ±20°. This has been done by considering these phases to be four variables that are used to minimize the square of the difference between the measured and computed patterns at each angle within the above range; it has been implemented using a numerical minimization routine. The resulting relative phases are 152.7337°,93.5604°,165.4613°,110.8066°. A comparison between the measured and computed normalized radiation patterns, which contains the "extracted" relative phases, is now shown in Figure 4.35. The agreement is clearly much better. The

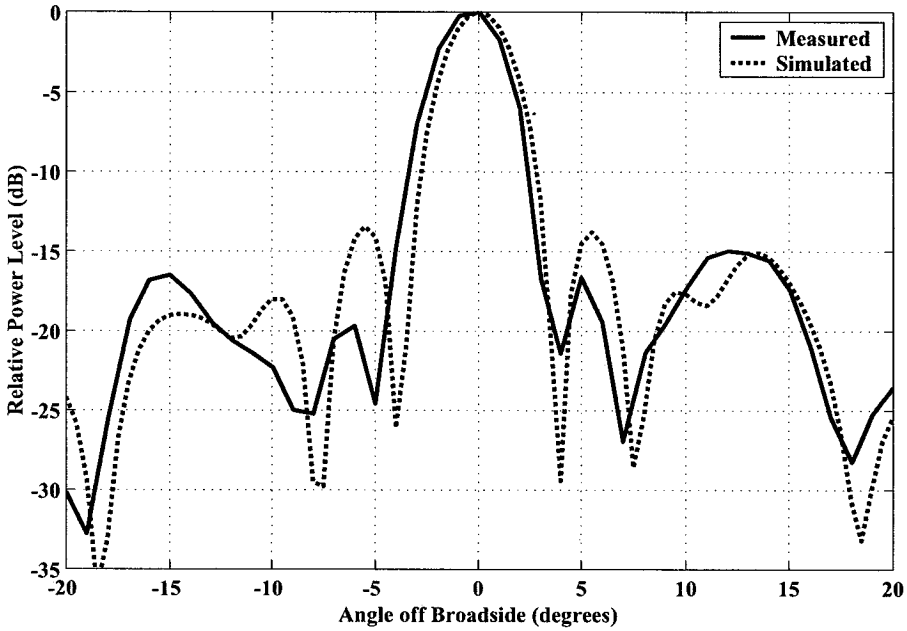

Figure 4.35: Normalized E-Plane Far-Field Radiation Pattern with "Extracted" Relative Phases

computed radiation pattern (not normalized) using the above "extracted" relative phases is now compared to the computed radiation pattern (not normalized) and the difference in the levels of the pattern peak is found to be 0.9419dB. This is an indication of the correction that must be added to the measured gain to compensate for the phase imbalance.

We will now look at the measured patterns for the four-feed reflectarray. Figures 4.36

and 4.37 show the complete measured E-plane and H-plane patterns of the four-feed reflectarray, respectively. The measured realized gain for this antenna was 25.64dBi.

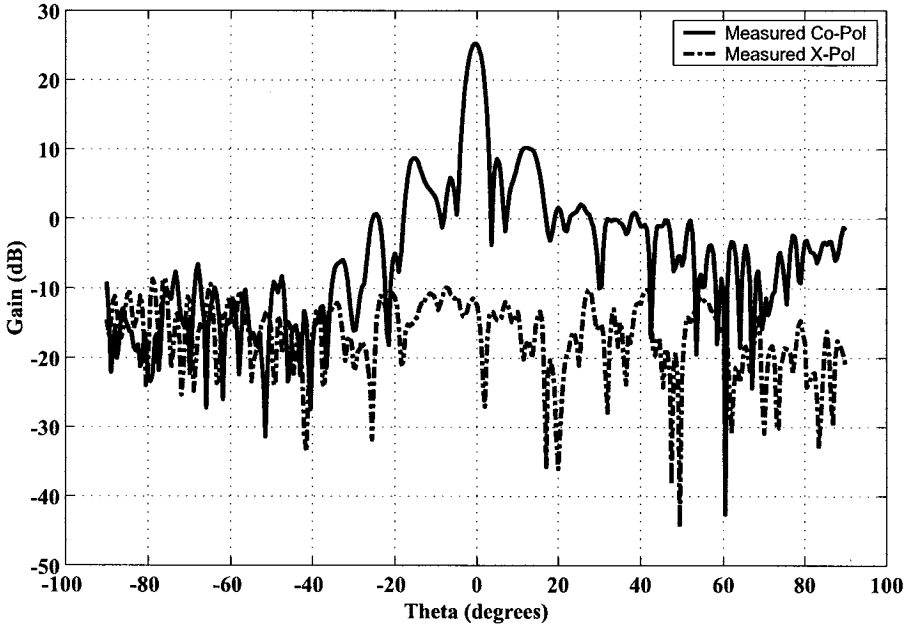

Figure 4.36: Measured E-Plane Far-Field Radiation Pattern

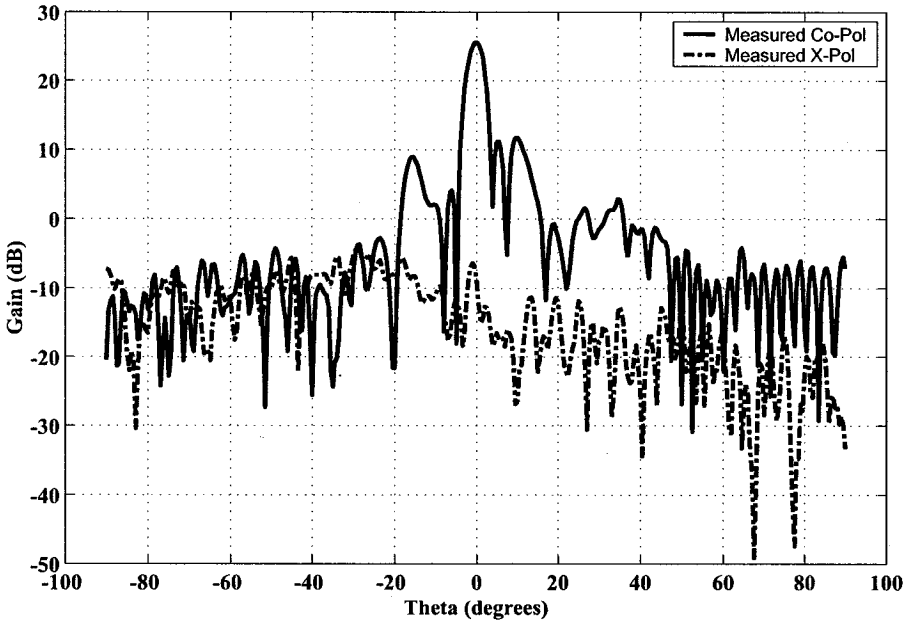

Figure 4.37: Measured H-Plane Far-Field Radiation Pattern

We can now correct this gain for the losses in the splitter/coax combination that

was calculated earlier and the decrease in gain due to the phase imbalance. We then get a corrected gain for the antenna of 25.64dB + 3.8786dB + 0.9419dB = 30.46dBi. This gives us an aperture efficiency of 36.82%. One thing to notice about the measured patterns is that there is a clear asymmetry in the patterns; this is due to blockage by the test setup. Figure 4.38 shows the actual test setup used. We can see from this setup that the arms holding the feeds, the feeds themselves and the semi-ridged coaxial cable will all cause blockage and scattering that will affect the far-field radiation pattern. To verify that our predicted pattern with the

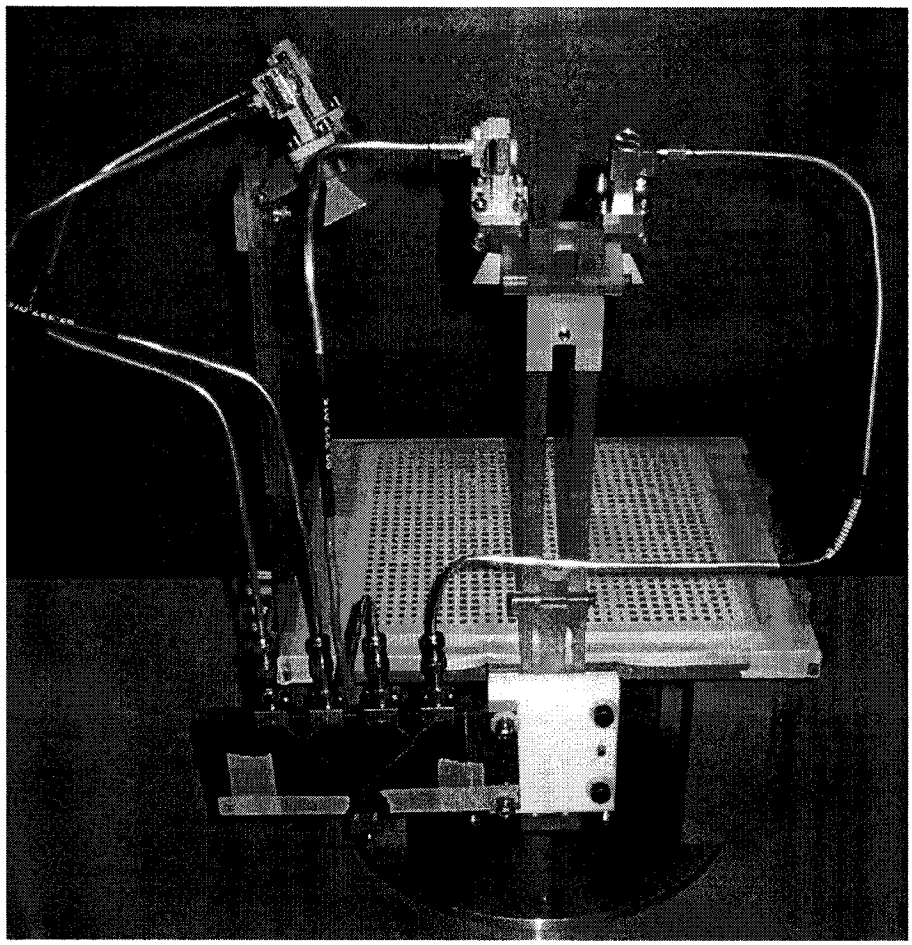

Figure 4.38: Four-Feed Reflectarray Test Setup

"extracted" relative phase imbalance, using the approximate array theory, matches the measure pattern we can normalize the measured patterns and plot them on top

of the associated predicted patterns. Figures 4.39 and 4.40 show this comparison in the two principal planes. We can clearly see the the pattern prediction techniques,

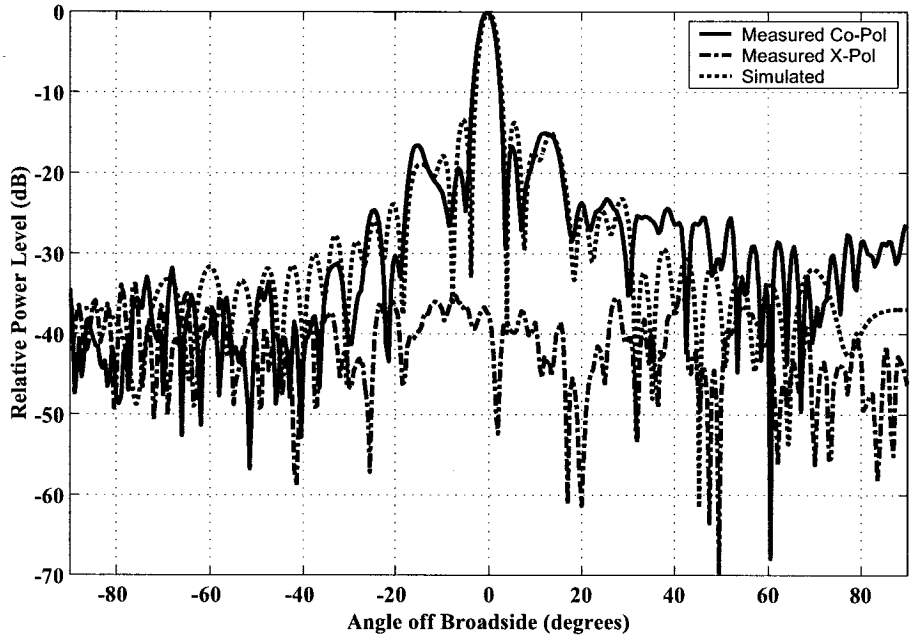

Figure 4.39: Normalized E-Plane Far-Field Radiation Pattern

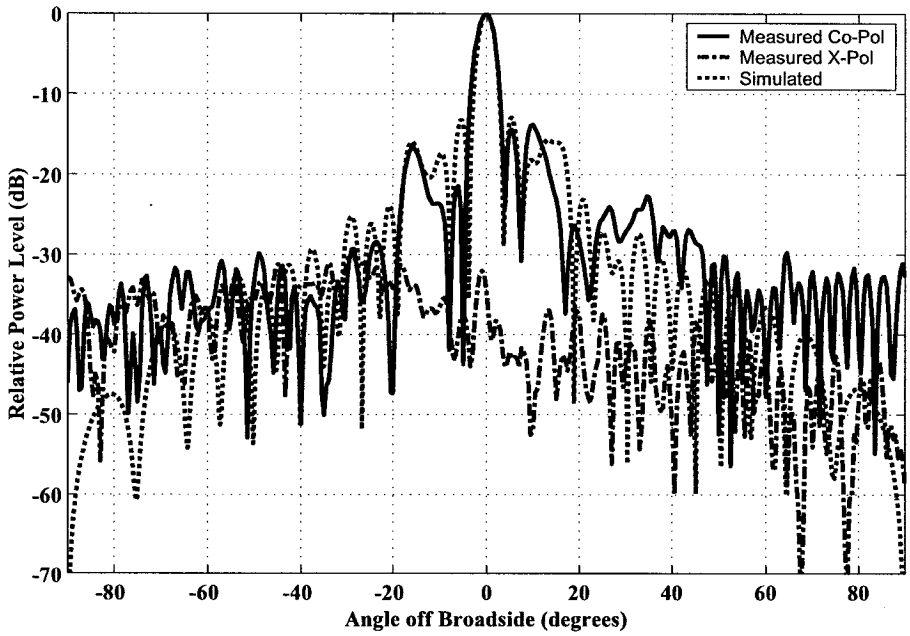

Figure 4.40: Normalized H-Plane Far-Field Radiation Pattern

using array theory, accurately predicts the far-field patterns, especially with regards to the beam-width of the main beam.

The next and final step in this examination of this design is to determine how well the reflectarray combines the power from the four feeds. We must determine a combining efficiency number to this reflectarray. To do this we consider a single feed reflectarray, where the feed is positioned so that the spillover and taper efficiencies are much the same as each of the four feeds of the four-feed reflectarray. Ideally if we had 100% combining efficiency for the four-feed reflectarray, the gain would be the same as that of the single feed case. This statement can be made because we know that all the other factors that will affect the gain, and most importantly the spillover and taper efficiencies are identical between the four-feed reflectarray and the single feed reflectarray with the feed positioned in one of the positions of the four-feed reflectarray. A single feed reflectarray was designed with the feed positioned at $(x, y, z) = (2.1\lambda, -7.75\lambda, 15.5\lambda)$ or the same position as Feed#1 in the four-feed reflectarray shown in Figure 4.26. All other design parameters for this single feed reflectarray are the same as that of the four-feed reflectarray. This single feed reflectarray was measured and the realized gain was found to be 31.04dBi. The input reflection coefficient was measured and it was equal to -25.58dB, which translates to a reflection loss of 0.01dB. The gain of the single feed reflectarray is then corrected to 31.05dbi. The combining efficiency is then given by:

$$\eta_c = \frac{G_{4Feeds}}{G_{1Feed}} = \frac{10^{\frac{30.46}{10}}}{10^{\frac{31.05}{10}}} = 87.3\% \tag{4.50}$$

Various current configurations of spatial power combiners [108–112] quote combining efficiencies ranging from 70-90%.

In [6] the author defines combining efficiency as

$$\eta_c = \frac{P_o}{NP_{oa}} \tag{4.51}$$

If we apply (4.51) to the present cconfiguration, then P_o (the power at the output of each feed horn) and P_{oa} (the power transmitted by the reflectarray), are as shown in terms of the $N = 4$ feed reflectarray in Figure 4.41. If we fed each horn of the

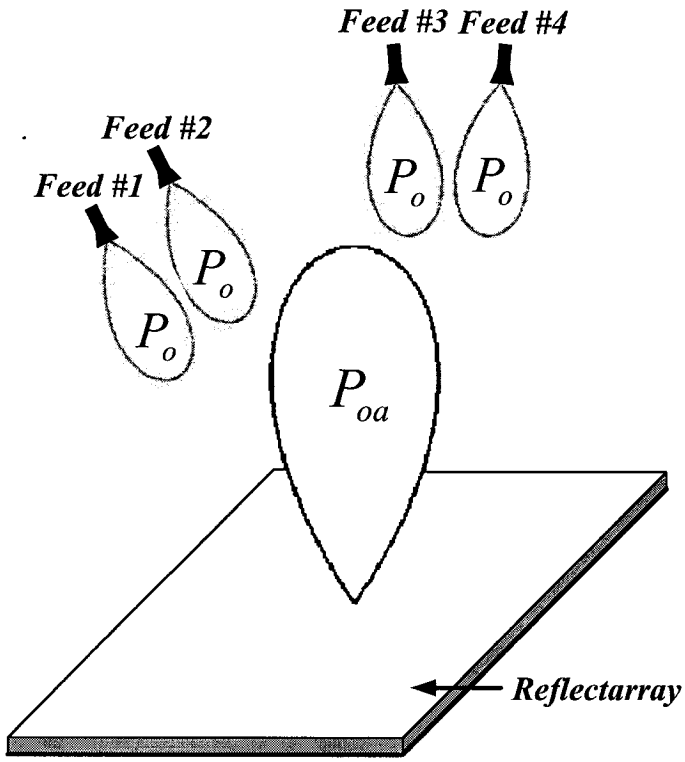

Figure 4.41: Four-Feed Combining System

four-feed reflectarray with 0.25 watts the power transmitted by the reflectarray would then be 0.873 watts.

4.5 Concluding Remarks

This chapter contains the most important original contributions of this thesis. The work was first done for the two-feed case and then for the four-feed case. The mathematical analysis that allows the design procedure of Section 2.5 to be applied to multi-feed single-beam reflectarray antennas was described in Section 4.2. Section 4.3 gave a very complete description of the implementation of the procedure to the two-feed case. A receive-mode analysis of this two-feed antenna was discussed and shown to interestingly indicate the difference between such reflectarrays and the conventional single-feed ones that were reviewed in Section 2.3. Experimental validation of the designed antenna was given, and its measured performance carefully compared to predictions. The design procedure having been validated, Section 4.4 then described the design, implementation, predicted performance, and measured performance of a four-feed single-beam reflectarray antenna. The radiation pattern performance, as well as the power combining efficiency, were shown to be excellent.

Chapter 5

GENERAL CONCLUSIONS

The principal contributions of this thesis are as follows:

- A complete design procedure for multi-feed single-beam reflectarrays has been developed for the first time.
- The above design procedure has been experimentally validated through its use in the design of multi-feed reflectarrays for use as integrated antenna/power-combiners. The power combining efficiency of a four-feed device has been shown to be excellent.
- A method for the receive mode analysis of reflectarray antennas has been devised and applied. This does not appear to have been described elsewhere. It has been shown how this can be used to understand the focusing action of the reflectarray. An interesting Gaussian beam interpretation of the focal region fields has been shown to be possible.

Portions of this work have already been described in the publications [113] and [114].

There are a number of issues whose investigation in future work would move the reflectarray/power-combiner concept closer to its final overall goal. Firstly, it is

necessary to determine how well four or more solid-state sources, one at each of the feeds, could be synchronized. This is the manner in which it is intended that the antenna/power-combiner operate. Secondly, the feeds used in this research were pyramidal horns. The use of microstrip patches as feeds, would enable the entire antenna to be produced using printed technology. The use of microstrip patches as feeds would allow a greater number of feeds due to their small size and low-profile. One issue with increasing number of feeds is to keep the spacing large enough to avoid coupling between the feeds and properly illuminate the reflectarray. Finally an investigation into the apparent additional focusing seen when performing the receive mode analysis, specifically in the two feed case as seen in Figure 4.11, should be investigated.

Bibliography

[1] D.G.Berry, R.G.Malech, and W.A.Kennedy. "The Reflectarray Antenna". *IEEE Trans. Antennas and Propagat.*, Vol.11(No.6):pp.645–651, November 1963.

[2] R.E. Munson, H. Haddad, and J. Hanlen. "Microstrip reflectarray antenna for satellite communication and RCS enhancement or reduction". U.S. Patent 4 684 952, August 1987.

[3] R.A. York and Z.B. Popovic. *Active and Quasi-Optical Array for Solid-State Power Combining.* New York: Wiley, 1996.

[4] M.P. DeLisio and R.A. York. "Quasi-Optical and Spatial Power Combining". *IEEE Trans. Microwave Theory Tech.*, Vol.50(No.3):pp.929–936, March 2002.

[5] M. Gouker. "Toward Standard Figures-of-Merit for Spatial and Quasi-Optical Power-Combined Arrays". *IEEE Trans. Microwave Theory Tech.*, Vol.43(No.7):pp.1614–1617, July 1995.

[6] R.A. York. "Some Considerations for Optimal Efficiency and Low Noise in Large Power Combiners". *IEEE Trans. Microwave Theory Tech.*, Vol.49(No.8):pp.1477–1482, August 2001.

[7] J. Montgomery. "Scattering by an infinite periodic array of microstrip elements". *IEEE Trans. Antennas and Propagat.*, Vol.26(No.6):pp.850–854, November 1978.

[8] J. Huang. "Microstrip Reflectarray". In *IEEE Int. Symp. Antenna Propagat.*, volume 2, pages pp.612–615, June 1991.

[9] J. Huang and R.J. Pogorzelski. "A Ka-Band Microstrip Reflectarray with Elements Having Variable Rotation Angles". *IEEE Trans. Antennas and Propagat.*, Vol.46(No.5):pp.650–656, May 1998.

[10] T.A. Metzler. "Stub loaded microstrip reflectarrays". In *IEEE Int. Symp. Antenna Propagat.*, volume 1, pages pp.574–577, June 1995.

[11] D.M.Pozar, S.D.Targonski, and H.D.Syrigos. "Design of Millimeter Wave Microstrip Reflectarrays". *IEEE Trans. Antennas and Propagat.*, Vol.45(No.2):pp.287–295, February 1997.

[12] S.D. Targonski, D.M. Pozar, and H.D. Syrigos. "Analysis and design of millimeter wave microstrip reflectarrays". In *IEEE Int. Symp. Antenna Propagat.*, volume 1, pages pp.578–581, June 1995.

[13] S.D. Targonski and D.M. Pozar. "Analysis and design of a microstrip reflectarray using patches of variable size". In *IEEE Int. Symp. Antenna Propagat.*, volume 3, pages pp.1820–1823, June 1994.

[14] D.M. Pozar and T.A. Metzler. "Analysis of a reflectarray antenna using microstrip patches of variable size". *Electron. Lett.*, Vol.29(No.8):pp.657–658, April 1993.

[15] S. Datthanasombat, A. Jr. Prata, P. Brown, O. Quintero, S. Spitz, and E. Rodriguez. "Spiral microstrip patch element for reflectarrays". In *IEEE Int. Symp. Antenna Propagat.*, volume 3, pages pp.721–724, July 2001.

[16] C. Han and K. Chang. "Ka-band reflectarray using ring elements". *Electron. Lett.*, Vol.39(No.6):pp.491–493, March 2003.

[17] N. Misran, R. Cahill, and V.F. Fusco. "Concentric split ring element for dual frequency reflectarray antennas". *Electron. Lett.*, Vol.39(No.25):pp.1776–1777, December 2003.

[18] J.A. Encinar. "Design of two-layer printed reflectarrays for bandwidth enhancement". In *IEEE Int. Symp. Antenna Propagat.*, volume 2, pages pp.1164–1167, July 1999.

[19] K.Y. Sze and L. Shafai. "Hat-shaped patches for line-source-fed microstrip reflectarray". *Electron. Lett.*, Vol.37(No.15):pp.937–939, July 2001.

[20] M. Bozzi, S. Germani, and L. Perregrini. "Performance comparison of different element shapes used in printed reflectarrays". In *IEEE Int. Symp. Antenna Propagat.*, volume 3, pages pp.294–297, June 2003.

[21] S. Germain, M. Bozzi, and L. Perregrim. "Analysis and performance comparison of printed reflectarrays". In *33rd European Microwave Conference*, volume 2, pages pp.523–526, October 2003.

[22] D.M. Pozar and S.D. Targonski. "A microstrip reflectarray using crossed dipoles". In *IEEE Int. Symp. Antenna Propagat.*, volume 2, pages pp.1008–1011, June 1998.

[23] M.E. Bialkowski and H.J. Song. "Dual linearly polarized reflectarray using aperture coupled microstrip patches". In *IEEE Int. Symp. Antenna Propagat.*, volume 3, pages pp.486–489, July 2001.

[24] D.I. Wu, R.C. Hall, and J. Huang. "Dual-frequency microstrip reflectarray". In *IEEE Int. Symp. Antenna Propagat.*, volume 4, pages pp.2128–2131, June 1995.

[25] J.A. Encinar. "Design of a dual frequency reflectarray using microstrip stacked patches of variable size". *Electron. Lett.*, Vol.32(No.12):pp.1049–1050, June 1996.

[26] J.A. Encinar. "Design of two-layer printed reflectarrays using patches of variable size". *IEEE Trans. Antennas and Propagat.*, Vol.49(No.10):pp.1403–1410, October 2001.

[27] J.A. Encinar and J.A. Zornoza. "Broadband design of three-layer printed reflectarrays". *IEEE Trans. Antennas and Propagat.*, Vol.51(No.7):pp.1662–1664, July 2003.

[28] J.A. Zornoza and M.E. Bialkowski. "Australia and New Zealand satellite coverage using a microstrip patch reflectarray". *Microw. and Optical Tech. Lett.*, Vol.37(No.5):pp.321–325, June 2003.

[29] J.A. Encinar and J.A. Zornoza. "Three-Layer Printed Reflectarrays for Contoured Beam Space Applications". *IEEE Trans. Antennas and Propagat.*, Vol.52(No.5):pp.1138–1148, May 2004.

[30] A. Zornoza, J.A. Encinar, and M.E. Bialkowski. "A double-layer microstrip reflectarray design to obtain Australia and New Zealand footprint". In *IEEE Int. Symp. Antenna Propagat.*, volume 3, pages pp.310–313, June 2003.

[31] N. Misran, R. Cahill, and V. Fusco. "Reflection phase response of microstrip stacked ring elements". *Electron. Lett.*, Vol.38(No.8):pp.356–357, April 2002.

[32] D.-C. Chang and M.-C.Huang. "Microstrip Reflectarray Antenna with Offset Feed". *Electron. Lett.*, Vol.28(No.16):pp.1498–1491, July 1992.

[33] R.D. Javor, X.-D. Wu, and K. Chang. "Offset-feed microstrip reflectarray antenna". *Electron. Lett.*, Vol.30(No.17):pp.1363–1365, August 1994.

[34] H. Deguchi, N. Takagi, M. Tsuji, and H. Shigesawa. "Microstrip reflectarray with offset feed for improving effective aperture area". In *IEEE Int. Symp. Antenna Propagat.*, volume 3, pages pp.290–293, June 2003.

[35] S.D. Targonski and D.M. Pozar. "Minimization of beam squint in microstrip reflectarrays using an offset feed". In *IEEE Int. Symp. Antenna Propagat.*, volume 2, pages pp.1326–1329, July 1996.

[36] D. Pilz and W. Menzel. "Folded reflectarray antenna". *Electron. Lett.*, Vol.34(No.9):pp.832–833, April 1998.

[37] W. Menzel, D. Pilz, and M. Al-Tikriti. "60 GHz triple folded reflector antenna". *Electron. Lett.*, Vol.38(No.19):pp.1075–1076, September 2002.

[38] C.-P. Chiu and S.-J. Chung. "A new millimeter-wave folded microstrip reflectarray antenna with beam steering". In *IEEE Int. Symp. Antenna Propagat.*, volume 3, page pp.140, June 2002.

[39] D.M. Pozar. "Bandwidth of reflectarrays". *Electron. Lett.*, Vol.39(No.21):pp.1490–1491, October 2003.

[40] S.M. Duffy and S.D. Targonski. "Comparison of two flat reflector-type designs for dual-polarization, dual-band operation". In *IEEE Int. Symp. Antenna Propagat.*, volume 2, pages pp.288–291, July 2001.

[41] D.G. Kurup, M. Himdi, and A. Rydberg. "Design of an unequally spaced reflectarray". *IEEE Antenna and Wireless Propagat. Lett.*, Vol.2(No.1):pp.33–35, 2003.

[42] J. Huang. "A High-Gain Circularly Polarized Ka-Band Microstrip Reflectarray". *Microw. and Optical Tech. Lett.*, Vol.14(No.3):pp.163–166, February 1997.

[43] M.R. Chaharmir, J. Shaker, M. Cuhaci, and A. Sebak. "Circularly polarised reflectarray with cross-slot of varying arms on ground plane". *Electron. Lett.*, Vol.38(No.24):pp.1492–1493, November 2002.

[44] B. Strassner, C. Han, and K. Chang. "Circularly polarized reflectarray with microstrip ring elements having variable rotation angles". *IEEE Trans. Antennas and Propagat.*, Vol.52(No.4):pp.1122–1125, April 2004.

[45] M.R. Chaharmir, J. Shaker, and M. Cuhaci. "Development of a dual band circularly polarized microstrip reflectarray". In *33rd European Microwave Conference*, volume 3, pages pp.1075–1078, October 2003.

[46] D.-C. Chang and M.-C.Huang. "Multiple-polarization microstrip reflectarray antenna with high efficiency and low cross-polarization". *IEEE Trans. Antennas and Propagat.*, Vol.43(No.8):pp.829–834, August 1995.

[47] R.D. Javor, X.-D. Wu, and K. Chang. "Dual polarisation of microstrip reflectarray antenna". *Electron. Lett.*, Vol.30(No.13):pp.1018–1019, June 1994.

[48] J. Shaker and M. Cuhaci. "A novel dual orthogonal polarisation planar reflector for LMCS applications". In *IEEE Vehicular Technology Conf.*, volume 3, pages pp.1943–1945, 1999.

[49] F.-C.E. Tsai and M.E. Bialkowski. "Designing a 161-element Ku-band microstrip reflectarray of variable size patches using an equivalent unit cell waveguide approach". *IEEE Trans. Antennas and Propagat.*, Vol.51(No.10):pp.2953–2962, October 2003.

[50] M.E. Bialkowski and F.-C.E. Tsai. "A unit cell waveguide model of a reflectarray formed by microstrip patches and slots". *Microw. and Optical Tech. Lett.*, Vol.36(No.3):pp.206–210, February 2003.

[51] F. Venneri, G. Angiulli, and G. Di Massa. "Experimental evalustion of the phase of the field scattered by microstrip patches for reflect-array design". *Microw. and Optical Tech. Lett.*, Vol.34(No.3):pp.163–164, August 2002.

[52] A. Robinson and M. Bialkowski. "Polarization-independent planar amplifier array". *Microw. and Optical Tech. Lett.*, Vol.20(No.6):pp.380–384, March 1999.

[53] Y. Zhuang, J. Litva, C. Wu, and K.-L. Wu. "Modelling studies of microstrip reflectarrays". *IEE Proc. Microw. Antennas Propag.*, Vol.142(No.1):pp.78–80, February 1995.

[54] Y. Zhuang, K.-L. Wu, C. Wu, and J. Litva. "Microstrip reflectarrays: Full-wave analysis and design scheme". In *IEEE Int. Symp. Antenna Propagat.*, volume 3, pages pp.1386–1389, July 1993.

[55] S.R. Rengarajan. "A study of the characteristics of microstrip reflectarrays as a function of the number and type of basis functions". In *IEEE Int. Symp. Antenna Propagat.*, volume 3, pages pp.302–305, June 2003.

[56] K.W. Lam and C.H. Chang. "Parallel computation in microstrip reflectarray". In *IEEE Int. Symp. Antenna Propagat.*, volume 2, pages pp.810–813, July 2001.

[57] F.-C.E. Tsai and M.E. Bialkowski. "Designing a multi-layer microstrip reflectarray with the use of an unit cell waveguide approach". In *IEEE Int. Symp. Antenna Propagat.*, volume 3, pages pp.306–309, June 2003.

[58] F.-C.E. Tsai and M.E. Bialkowski. "A unit cell waveguide approach to designing multi-layer reflectarrays of variable size patches". In *IEEE Int. Symp. Phased Array Sys. and Technology*, pages pp.476–481, October 2003.

[59] F.-C.E. Tsai and M.E. Bialkowski. "An equivalent unit cell waveguide approach to designing of multilayer microstrip reflectarrays". In *IEEE Int. Symp. Antenna Propagat.*, volume 3, page pp.148, June 2002.

[60] E. Girard, R. Moulinet, R. Gillard, and H. Legay. "An FDTD optimization of a circularly polarized reflectarray unit cell". In *IEEE Int. Symp. Antenna Propagat.*, volume 3, page pp.136, June 2002.

[61] S. Costanzo, F. Venneri, C. Di Massa, and C. Angiulli. "A synthesis algorithm for microstrip reflectarrays design". In *IEEE Int. Symp. Antenna Propagat.*, volume 1, pages pp.796–799, June 2003.

[62] D.M. Pozar, S.D. Targonski, and R. Pokuls. "A shaped-beam microstrip patch reflectarray". *IEEE Trans. Antennas and Propagat.*, Vol.47(No.7):pp.1167–1173, July 1999.

[63] R.E. Zicht, M. Mussetta, M. Tovaglieri, P. Pirinoli, and M. Orefice. "Frequency response of a new genetically optimized microstrip reflectarray". In *IEEE Int. Symp. Antenna Propagat.*, volume 1, pages pp.173–176, June 2003.

[64] S. Costanzo, F. Venneri, G. Di Massa, and G. Angiulli. "Synthesis of microstrip reflectarrays as planar scatterers for SAR interferometry". *Electron. Lett.*, Vol.39(No.3):pp.266–267, February 2003.

[65] M. Bozzi and L. Perregrini. "Element shape optimization of planar periodic structures". In *IVth Int. Cong. on Antenna Theory and Techniques*, volume 2, pages pp.453–458, Sept 2003.

[66] J.A. Zornoza and M.E. Bialkowski. "Design of a shaped beam multi-layer microstrip reflectarray with Australia and New Zealand coverage pattern". In *IEEE Int. Symp. Phased Array Sys. and Technology*, pages pp.488–493, October 2003.

[67] R.E. Zich, M., M. Tovaglieri, P. Pirinoli, and M. Orefice. "Genetic optimization of microstrip reflectarrays". In *IEEE Int. Symp. Antenna Propagat.*, volume 3, page pp.128, June 2002.

[68] K.Y. Sze and L. Shafai. "Analysis of phase variation due to varying patch length in a microstrip reflectarray". In *IEEE Int. Symp. Antenna Propagat.*, volume 2, pages pp.1134–1137, June 1998.

[69] J. Huang. "Capabilities of printed reflectarray antennas". In *IEEE Int. Symp. on Phased Array Sys. and Technology*, pages pp.131–134, October 1996.

[70] K.Y. Sze and L. Shafai. "Substrate thickness in a microstrip reflectarray". In *Asia-Pacific Microwave Conference*, volume 1, pages pp.146–149, December 1999.

[71] K.M. Shum, Q. Xue, C.H. Chan, and K.M. Luk. "Gain enhancement of microstrip reflectarray incorporating a PBG structure". In *IEEE Int. Symp. Antenna Propagat.*, volume 1, pages pp.350–353, July 2000.

[72] M.R. Chaharmir, J. Shaker, M. Cuhaci, and A. Sebak. "Reflectarray with variable slots on ground plane". *IEE Proc. Microw. Antennas Propag.*, Vol.150(No.6):pp.436–439, December 2003.

[73] G. Cung, G.H. Huff, and J.T. Bernhard. "Ground plane edge serrations for improved performance of microstrip active reflectarray elements". *Antenna and Wireless Propag. Lett.*, Vol.2(No.22):pp.334–336, 2003.

[74] H. Legay, B. Pinte, M. Charrier, A. Ziaei, E. Girard, and R. Gillard. "A steerable reflectarray antenna with mems controls". In *IEEE Int. Symp. Phased Array Sys. and Technology*, pages pp.494–499, October 2003.

[75] K.W. Lam, K.F. Chan, K.M. Shum, and C.H. Chan. "Study and analysis of planar microstrip reflectarray with photonic band gap structure". In *IEEE Int. Symp. Antenna Propagat.*, volume 3, pages pp.152–155, June 2002.

[76] M.R. Chaharmir, J. Shaker, M. Cubaci, and A. Sebak. "Reflectarray with slots of varying length on ground plane". In *IEEE Int. Symp. Antenna Propagat.*, volume 3, page pp.144, June 2002.

[77] R.W. Clark, G.H. Huff, and J.T. Bernhard. "An integrated active microstrip reflectarray element with an internal amplifier". *IEEE Trans. Antennas and Propagat.*, Vol.51(No.5):pp.993–999, May 2003.

[78] M.E. Bialkowski and H.J. Song. "Investigations into a power-combining structure using a reflectarray of dual-feed aperture-coupled microstrip patch antennas". *IEEE Trans. Antennas and Propagat.*, Vol.50(No.6):pp.841–849, June 2002.

[79] M.E. Bialkowski, A.W. Robinson, and H.J. Song. "Design, development, and testing of X-band amplifying reflectarrays". *IEEE Trans. Antennas and Propagat.*, Vol.50(No.8):pp.1065–1076, August 2002.

[80] M.E. Bialkowski, H.J. Song, K.-M. Luk, and C.-H. Chan. "Theory of an active transmit/reflect array of patch antennas operating as a spatial power combiner". In *IEEE Int. Symp. Antenna Propagat.*, volume 4, pages pp.764–767, July 2001.

[81] R. Clark, H. Pan, and J.T. Bernhard. "Microstrip antenna elements with internal amplifier slots for spatial power combining reflectarray applications". In *IEEE Int. Symp. Antenna Propagat.*, volume 3, pages pp.1248–1251, July 2000.

[82] L. Boccia, F. Venneri, G. Amendola, and G. DiMassa. "Experimental investigation of a varactor loaded reflectarray antenna". In *IEEE MTT-S Int. Microwave Symp. Digest*, volume 1, pages pp.2–7, June 2002.

[83] A.W. Robinson and M.E. Bialkowski. "An X-band active microstrip reflectarray". In *Asia Pacific Microwave Conference Proceedings*, volume 3, pages pp.925–928, December 1997.

[84] H.J. Song and M.E. Bialkowski. "Spatial power combiner using an active reflectarray of dual-feed aperture coupled microstrip patch antennas". In *IEEE Int. Symp. Antenna Propagat.*, volume 4, pages pp.768–771, July 2001.

[85] L. Boccia, F. Venneri, G. Amendola, and G. DiMassa. "Application of varactor diodes for reflectarray phase control". In *IEEE Int. Symp. Antenna Propagat.*, volume 3, page pp.132, June 2002.

[86] N. Misran, R. Cahill, and V.F. Fusco. "RCS reduction technique for reflectarray antennas". *Electron. Lett.*, Vol.39(No.23):pp.1630–1632, November 2003.

[87] F. Venneri, S. Costanzo, G. Di Massa, and G. Angiulli. "Investigation of printed reflectarrays as permanent scatterers in SAR interferometry". *Microw. and Optical Tech. Lett.*, Vol.37(No.1):pp.18–20, April 2003.

[88] J. Huang and A. Feria. "A 1-m X-band inflatable reflectarray antenna". *Microw. and Optical Tech. Lett.*, Vol.20(No.2):pp.97–99, January 1999.

[89] J. Huang and A. Feria. "Inflatable microstrip reflectarray antennas at X and Ka-band frequencies". In *IEEE Int. Symp. Antenna Propagat.*, volume 3, pages pp.1670–1673, July 1999.

[90] J. Huang. "The development of inflatable array antennas". *IEEE Antennas and Propagat. Magazine*, Vol.43(No.4):pp.44–50, August 2001.

[91] J. Huang, A. Feria, and M. Lou. "The development of inflatable array antennas". In *IEEE Aerospace Conf. Proc.*, volume 5, pages pp.59–65, March 2000.

[92] J. Huang, V.A. Feria, and H. Fang. "Improvement of the three-meter Ka-band inflatable reflectarray antenna". In *IEEE Int. Symp. Antenna Propagat.*, volume 1, pages pp.122–125, July 2001.

[93] M. Zawadzki and J. Huang. "Integrated RF antenna and solar array for spacecraft application". In *IEEE Int. Proc. Phased Array Sys. and Technology*, pages pp.239–242, May 2000.

[94] J. Huang and M. Zawadzki. "Antennas integrated with solar arrays for space vehicle applications". In *Vth Int. Symp. on Antennas, Propag. and EM Theory*, pages pp.86–89, August 2000.

[95] A.J. Zaman and R.Q. Lee. "A spherical to plane wave transformation using a reflectarray". In *IEEE Int. Symp. Antenna Propagat.*, volume 2, pages pp.1284–1287, July 1997.

[96] A.W. Robinson, M.E. Bialkowski, and H.J. Song. "A Passive Reflect-Array with Dual-Feed Microstrip Patch Elements". *Microw. and Optical Tech. Lett.*, Vol.23(No.5):pp.295–299, December 1999.

[97] A.W. Robinson, M.E. Bialkowski, and H.J. Song. "A 137 Element Active Reflect-Array with Dual-Feed Microstrip Patch Elements". *Microw. and Optical Tech. Lett.*, Vol.26(No.3):pp.147–151, August 2000.

[98] S-W. Lee, G. Zarrillo, and C-L. Law. "Simple Formulas for Transmission Through Periodic Metal Grids or Plates". *IEEE Trans. Antennas and Propagat.*, Vol.30(No.5):pp.904–909, September 1982.

[99] A.A. Oliner and R.G. Malech. *"Microwave Scanning Antennas"*, chapter "Mutual coupling in infinte scanning arrays". Academic Press, 1966.

[100] EMAG Technologies Inc., 1340 Eisenhower Place, Ann Arbor, Michigan 48108. *EMPiCASSO.*

[101] Ansoft Corporation, Four Station Square, Suite 200, Pittsburgh, PA 15219-1119, USA. *$HFSS^{TM}$ (High Frequency Structure Simulator).*

[102] T.S.M.MaClean. *Principles of Antennas : Wire and Aperture.* Cambridge University Press, 1986.

[103] H.Ling, S.W.Lee, P.T.C.Lam, and W.V.T.Rusch. "Focal Shifts in Parabolic Antennas". *IEEE Trans. Antennas and Propagat.*, Vol.33:pp.744–748, July 1985.

[104] P.F. Goldsmith. *Quasioptical Systems: Gaussian Beam Quasioptical Propogation and Applications.* Wiley - IEEE Press, 1997.

[105] W.L.Stutzman and G.A.Thiele. *Antenna Theory and Desing.* John Wiley and Sons, Inc., 1998.

[106] K. Hirasawa and M. Haneishi. *Analysis, Design and Measurement of Small and Low-Profile Antennas.* Artech House, Norwood, MA, 1992.

[107] C.A.Balanis. *Antenna Theory: Analysis and Design.* Harper and Row, 1982.

[108] N-S. Cheng, A. Alexanian, M.G. Case, D.B. Rensch, and R.A. York. "40-W CW Broad-Band Spatial Power Combiner Using Dense Finline Arrays". *IEEE Trans. Microwave Theory Tech.*, Vol.47(No.7):pp.1070–1076, July 1999.

[109] R. Bashirullah and A. Mortazawi. "A Slotted-Waveguide Power Amplifier for Spatial Power-Combining Applications". *IEEE Trans. Microwave Theory Tech.*, Vol.48(No.7):pp.1142–1147, July 2000.

[110] S. Yang and V.F. Fusco. "Combination Dielectric Resonator, Power Combiner, and Antenna". *IEEE Trans. Microwave Theory Tech.*, Vol.48(No.9):pp.1516–1521, September 2000.

[111] S.M. Duffy and M.A. Gouker. "High Combining-Efficiency X-Band Spatial Power-Combined Array Using a Multilayered Packaging Architecture". *IEEE Trans. Microwave Theory Tech.*, Vol.48(No.10):pp.1769–1771, October 2000.

[112] S. Pajić and Z.B. Popović. "An Efficient X-Band 16-Element Spatial Combiner of Switched-Mode Power Amplifiers". *IEEE Trans. Microwave Theory Tech.*, Vol.51(No.7):pp.1863–1870, July 2003.

[113] F. Arpin, D.A. McNamara, J. Shaker, and A. Ittipiboon. "A Receive-Mode Analysis of Reflectarray Antennas". In *Proceeding of the ANTEM Symposium*, Ottawa, Canada, July 2004.

[114] F. Arpin, J. Shaker, and D.A.McNamara. "Multi-Feed Single-Beam Power-Combining Reflectarray Antenna". *Electron. Lett.*, Vol.40(No.17):pp.1035–1037, August 2004.

List of Figures

List of Tables